Supporting Information

for

Methyl Scanning and Revised Binding Mode of 2-Pralidoxime, an Antidote for Nerve Agent Poisoning

Adriana Gambino, James C. Burnett, and Kazunori Koide*

Department of Chemistry, University of Pittsburgh

219 Parkman Avenue, Pittsburgh, Pennsylvania 15260, United States

koide@pitt.edu

General Synthetic Techniques

All reactions were carried out with solvents and reagents obtained from commercial sources and were used without further purification unless noted. Moisture-sensitive reactions were performed under an inert atmosphere using a nitrogen line with standard Schlenk techniques unless otherwise stated. Unless specifically stated, the temperature of a water bath during the evaporation of organic solvents using a rotary evaporator was 40 ± 5 °C. All syringes in this study were dried in an oven at 80 °C and stored in a desiccator over Drierite©. All reactions were monitored by thin-layer chromatography (TLC) carried out on 0.25-mm Merck silica gel plates (60F-254) using UV light (254 nm) for visualization or with 2.4% phosphomolybdic acid, 1.4% phosphoric acid, and 5% sulfuric acid in water with heat as a developing agent.

Solvents used for NMR spectroscopy were purchased from Cambridge Isotope Laboratories and $CDCl_3$ was stored over anhydrous K_2CO_3. NMR spectra were recorded on a Bruker Advance spectrometer at 300 megahertz (MHz) or 400 MHz. The chemical shifts are given in parts per million (ppm) on a delta (δ) scale. The solvent peak was used a reference value, for ^{1}H NMR: $CHCl_3$ = 7.27 ppm, DMSO = 2.50 ppm; for ^{13}C NMR: $CDCl_3$ = 77.00 ppm, DMSO-d_6 = 49.10 ppm. The following abbreviations are used to indicate the multiplicities:

s = singlet; d = doublet; t = triplet; q = quartet; dd = doublet of doublets; app = apparent; m = multiplet; br = broad. Melting points were obtained using a DigiMelt MPA160. Infrared (IR) spectra were collected using a Nicolet IR200 FT-IR spectrometer. Samples for acquiring IR spectra were prepared as a thin film on KBr plate by dissolving the compound in CH_2Cl_2 and then evaporating the CH_2Cl_2. High-resolution mass spectra were recorded on a VG 7070 spectrometer. Ultraviolet-visible (UV-Vis) spectra were collected using an HP 8453 UV-Visible spectroscopy system.

Abbreviations

http://pubs.acs.org/paragonplus/submission/joceah/index.html

General Biological Procedures

Ellman's reagent (5,5'-dithiobis(2-nitrobenzoic acid)) (DTNB) was purchased from Acros Organics and used as received. S-acetylthiocholine iodide (ATCh) was purchased from Alfa Aesar and used as received. Paraoxon, human acetylcholinesterase (recombinant, expressed in HEK293 cells, lyophilized powder, ≥1,000 units/mg protein) (hAChE) and acetylcholinesterase from *Electrophorus electricus* (electric eel) Type VI-S (200-1,000 units/mg protein) (eel AChE) were purchased from Sigma-Aldrich. Absorbance was measured at 405 nm in 3 min intervals in a Modulus II Microplate Multimode Reader. The time point for the absorbance measurement was chosen as the time at which the samples containing 600 μM 2-PAM stopped increasing in absorbance. The background absorbance value was defined as the average of the absorbance values of the samples containing the inhibited eel AChE and no reactivator. The background absorbance was subtracted from all samples. The data were plotted using GraphPad Prism 8 software. Data for each reactivator were plotted with the data for 2-PAM as a reference.

Ellman's Assay using hAChE: A solution of 1.20 mM reactivator in 100 mM phosphate pH 7.4 buffer (100 μL) was added to the wells of a clear 96-well plate. 100 mM Phosphate pH 7.4 buffer (50 μL) was added to the wells as the diluent, and two-fold serial dilutions of the reactivator were performed; the total volume of reactivator in the wells following the dilution was 50 μL. 1.02 mM DTNB in 100 mM phosphate pH 7.4 buffer (19.5 μL) and 1.36 mM ATCh in 100 mM phosphate pH 7.4 buffer (19.5 μL) were transferred to the wells with the reactivator solutions.

Separately, 100 U/mL hAChE in 20 mM Tris pH 7.4 buffer (10 μL per well) was inhibited with 200 μM paraoxon dissolved in isopropanol (1 μL per well). An additional aliquot of 100 U/mL hAChE (40 μL) was mock inhibited with isopropanol (4 μL). After incubating for 10 min at 25 °C, the inhibited enzyme solution (11 μL) was added to the wells containing the reactivator solution. The mock-inhibited (i.e., uninhibited) enzyme (11 μL) was added to wells containing 0 μM reactivator. Absorbance was measured in 3 min intervals in a Modulus II Microplate

Multimode Reader (Promega). The time point for the absorbance measurement was chosen as the time at which the samples containing 600 μM 2-PAM stopped increasing in absorbance. The background absorbance value was defined as the average of the absorbance values of the samples containing the inhibited hAChE and no reactivator. The background absorbance was subtracted from all samples. The data were plotted using GraphPad Prism 8 software. Data for each reactivator were plotted with the data for 2-PAM as a reference.

Ellman's Assay using eel AChE: A solution of 1.20 mM reactivator in 100 mM phosphate pH 7.4 buffer (100 μL) was added to the wells of a clear 96-well plate. 100 mM Phosphate pH 7.4 buffer (50 μL) was added to the wells as the diluent, and two-fold serial dilutions of the reactivator were performed; the total volume of reactivator in the wells following the dilution was 50 μL. 1.02 mM DTNB in 100 mM phosphate pH 7.4 buffer (19.5 μL) and 1.36 mM ATCh in 100 mM phosphate pH 7.4 buffer (19.5 μL) were transferred to the wells with the reactivator solutions.

Separately, 10 U/mL eel AChE in 20 mM Tris pH 7.4 buffer (10 μL per well) was inhibited with 0.2% v/v paraoxon dissolved in isopropanol (1 μL per well). An additional aliquot of 10 U/mL eel AChE (40 μL) was mock inhibited with isopropanol (4 μL). After incubating for 10 min at 25 °C, the inhibited enzyme solution (11 μL) was added to the wells containing the reactivator solution. The mock-inhibited (i.e., uninhibited) (11 μL) was added to wells containing 0 μM reactivator. Absorbance was measured in 3 min intervals in a Modulus II Microplate Multimode Reader (Promega). The time point for the absorbance measurement was chosen as the time at which the samples containing 600 μM 2-PAM stopped increasing in absorbance. The background absorbance value was defined as the average of the absorbance values of the samples containing the inhibited eel AChE and no reactivator. The background absorbance was subtracted from all samples. The data were plotted using GraphPad Prism 8 software. Data for each reactivator were plotted with the data for 2-PAM as a reference.

Inhibition of acetylcholinesterase by the reactivator: A solution of either 0 or 1.2 mM reactivator in 100 mM phosphate pH 7.4 buffer (50 μL) was added to the wells. 0 or 100 U/mL hAChE in 20 mM Tris pH 7.4 buffer (10 μL) was added to the reactivators. The solutions were incubated at 24 °C for 10 min. A solution containing 500 μM DTNB and 650 μM ATCh in 100 mM pH 7.4 phosphate buffer (40 μL) was added to the wells, and the absorbance was measured at 405 nm in 3 min intervals in a Modulus II Microplate Multimode Reader. The background absorbance value was defined as the average of the absorbance values of the samples without hAChE or reactivator. The background absorbance was subtracted from all samples. The data were plotted using GraphPad Prism 8 software.

A solution of either 0 or 1.2 mM reactivator in 100 mM phosphate pH 7.4 buffer (50 μL) was added to the wells. 0 or 10 U/mL eel AChE in 20 mM Tris pH 7.4 buffer (10 μL) was added to the reactivators. The solutions were incubated at 24 °C for 10 min. A solution containing 500 μM DTNB and 650 μM ATCh in 100 mM pH 7.4 phosphate buffer (40 μL) was added to the wells, and the absorbance was measured at 405 nm in 3 min intervals

in a Modulus II Microplate Multimode Reader. The background absorbance value was defined as the average of the absorbance values of the samples without eel AChE or reactivator. The background absorbance was subtracted from all samples. The data were plotted using GraphPad Prism 8 software.

General Computational Methods

All molecular modeling was performed on a Linux workstation (Dell T7600) equipped with a three-dimensional (3-D) monitor. Insight II (2005) (Dassault Systèmes BIOVIA, San Diego, CA), Discovery Studio 2018 (Dassault Systèmes BIOVIA, San Diego, CA), and Maestro 2016-1 (Maestro, Schrödinger, LLC, New York, NY) were used to build, energy refine, and inspect models, and for docking studies. The cff91 force field was used during all stages of model energy refinement. The HINT program (eduSoft LC, La Jolla, CA) was used to evaluate the quality of the models via the quantitation of intermolecular contacts. The HINT parameter settings used during the studies: steric term = Lennard-Jones 6–12 (for cff91 compatibility); lone pair vector focusing = 10; and distance dependence atom-atom interactions = exp (1/*r*). Figures were generated using Pymol (the PyMOL Molecular Graphics System, Version 2.0 Schrödinger, LLC).

Synthesis

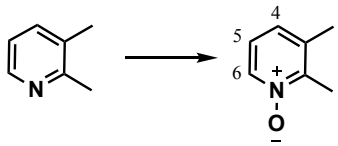

Preparation of 2,3-dimethylpyridine 1-oxide: 2,3-Dimethylpyridine *1*-oxide was synthesized following the literature protocol found at *Chem.-Eur. J.* **2014,** *20*, 559: A 500-mL pear-shaped flask was charged with 2,3-lutidine (10.7 mL, 100 mmol) at 23 °C under an open atmosphere. Aqueous 0.6 M K_2CO_3 (50 mL), *t*-BuOH (50 mL), MeCN (8.0 mL, 150 mmol, 1.5 equiv), 30% aqueous H_2O_2 (60 mL, 500 mmol, 5 equiv), and 2,2,2-trifluoroacetophenone (1.4 mL, 10 mmol, 10 mol %) were added sequentially in one portion, and the reaction mixture continued to stir at 23 °C under an open atmosphere for 24 h. After this period, H_2O (50 mL) was added, and the resulting reaction mixture was allowed to stir for 6 h at 23 °C under an open atmosphere. The reaction mixture was extracted with CH_2Cl_2 (4 × 50 mL) using a separatory funnel. The combined organic layers were dried over anhydrous Na_2SO_4, filtered, and concentrated *in vacuo*. The crude residue was purified by flash chromatography (60 to 100% EtOAc in hexanes) on silica gel (250 mL) to afford 2,3-dimethylpyridine 1-oxide as a white solid (8.56 g, 70% yield).

Data for 2,3-dimethylpyridine 1-oxide: ^{1}H NMR (400 MHz, 293 K, $CDCl_3$): δ 8.16 (br d, J = 6.0 Hz, 1H, 6-H), 7.06–6.99 (m, 2H, 4-H and 5-H), 2.51 (s, 3H, -CH_3), 2.34 (s, 3H, -CH_3). The ^{1}H NMR spectrum for 2,3-dimethylpyridine 1-oxide was consistent with that in the literature.[1]

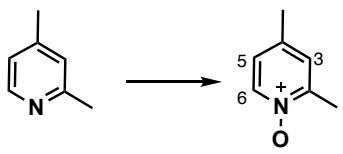

Preparation of 2,4-dimethylpyridine 1-oxide: 2,4-Dimethylpyridine 1-oxide was synthesized following the literature protocol found at *Chem.-Eur. J.* **2014,** *20*, 559: A 500-mL pear-shaped flask was charged with 2,4-lutidine (4.8 mL, 44.8 mmol) at 23 °C under an open atmosphere. Aqueous 0.6 M K_2CO_3 (22 mL), *t*-BuOH (22

mL), MeCN (3.5 mL, 67 mmol, 1.5 equiv), 30% aqueous H_2O_2 (27.0 mL, 135 mmol, 3 equiv), and 2,2,2-trifluoroacetophenone (620 μL, 4.48 mmol, 10 mol %) were added sequentially in one portion, and the reaction mixture continued to stir at 23 °C under an open atmosphere for 27 h. After this period, H_2O (25 mL) was added, and the resulting reaction mixture was allowed to stir for 2 h at 23 °C under an open atmosphere. The reaction mixture was extracted with CH_2Cl_2 (4 × 30 mL) using a separatory funnel. The combined organic layers were dried over anhydrous Na_2SO_4, filtered, and concentrated *in vacuo*. The crude residue was purified by flash chromatography (60 to 100% EtOAc in hexanes) on silica gel (110 mL) to afford 2,4-dimethylpyridine 1-oxide as a yellow oil (3.56 g, 65% yield).

Data for 2,4-dimethylpyridine 1-oxide: ^{1}H NMR (400 MHz, 293 K, $CDCl_3$): δ 8.05 (d, J = 6.6 Hz, 1H, 6-H), 6.97 (s, 1H, 3-H), 6.85 (d, J = 6.6 Hz, 1H, 5-H), 2.38 (s, 3 H, -CH_3), 2.20 (s, 3H, -CH_3). The ^{1}H NMR spectrum for 2,4-dimethylpyridine 1-oxide was consistent with those in the literature.[2]

Preparation of 2,5-dimethylpyridine 1-oxide: 2,5-Dimethylpyridine 1-oxide was synthesized following the literature protocol found at *Chem.-Eur. J.* **2014,** *20*, 559: A 500-mL pear-shaped flask was charged with 2,5-lutidine (10.7 mL, 100 mmol) at 23 °C under an open atmosphere. Aqueous 0.6 M K_2CO_3 (50 mL), *t*-BuOH (50 mL), MeCN (8.0 mL, 150 mmol, 1.5 equiv), 30% aqueous H_2O_2 (60 mL, 500 mmol, 5 equiv), and 2,2,2-trifluoroacetophenone (1.4 mL, 10 mmol, 10 mol %) were added sequentially in one portion, and the reaction mixture continued to stir at 23 °C under an open atmosphere for 24 h. After this period, H_2O (50 mL) was added, and the resulting reaction mixture was allowed to stir for 6 h at 23 °C under an open atmosphere. The reaction mixture was extracted with CH_2Cl_2 (4 × 50 mL) using a separatory funnel. The combined organic layers were dried over anhydrous Na_2SO_4, filtered, and concentrated *in vacuo*. The crude residue was purified by flash chromatography (60 to 100% EtOAc in hexanes) on silica gel (250 mL) to afford 2,5-dimethylpyridine 1-oxide as a white solid (8.47 g, 69% yield).

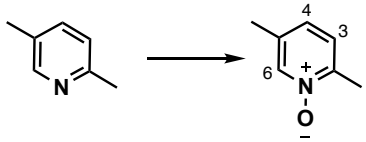

Data for 2,5-dimethylpyridine 1-oxide: ^{1}H NMR (300 MHz, 293 K, $CDCl_3$): δ = 8.09 (s, 1H, 6-H), 7.09 (d, J = 8.1 Hz, 1H, 4-H), 6.97 (d, J = 8.1 Hz, 1H, 3-H), 2.43 (s, 3 H, -CH_3), 2.23 (s, 3H, -CH_3). The ^{1}H NMR spectrum for 2,5-dimethylpyridine 1-oxide was consistent with those in the literature.[1]

Preparation of 2,6-dimethylpyridine 1-oxide: 2,6-Dimethylpyridine 1-oxide was synthesized following the literature protocol found *Chem.-Eur. J.* **2014,** *20*, 559: A 500-mL pear-shaped flask was charged with 2,6-lutidine (10.7 mL, 100 mmol) at 23 °C under an open atmosphere. Aqueous 0.6 M K_2CO_3 (50 mL), *t*-BuOH (50 mL), MeCN (8.0 mL, 150 mmol, 1.5 equiv), 30% aqueous H_2O_2 (60 mL, 500 mmol), and 2,2,2-trifluoroacetophenone (1.4 mL, 10 mmol, 10 mol %) were added sequentially in one portion, and the reaction mixture continued to stir at 23 °C under an open atmosphere for 28 h. After this period, H_2O (50 mL) was added, and the resulting reaction mixture was

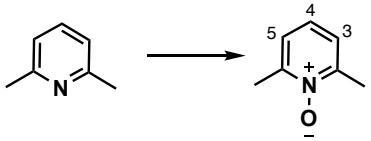

allowed to stir for 14 h at 23 °C under an open atmosphere. The reaction mixture was extracted with CH_2Cl_2 (4 × 50 mL) using a separatory funnel. The combined organic layers were dried over anhydrous Na_2SO_4, filtered, and concentrated *in vacuo*. The crude residue was purified by flash chromatography (60 to 100% EtOAc in hexanes) on silica gel (200 mL) to afford 2,6-dimethylpyridine 1-oxide as a white solid (6.66 g, 54% yield).

Data for 2,6-dimethylpyridine 1-oxide: ^{1}H NMR (300 MHz, 293 K, $CDCl_3$): δ 7.15 (d, J = 7.8 Hz, 2H, 3-H and 5-H), 7.10–7.06 (m, 1H, 4-H), 2.53 (s, 6 H, 2×-CH_3). The ^{1}H NMR spectrum for 2,6-dimethylpyridine 1-oxide was consistent with those in the literature.[1]

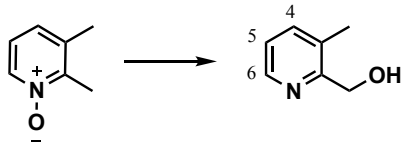

Preparation of (3-methylpyridin-2-yl)methanol: A 250-mL round-bottom flask with 2,3-dimethylpyridine 1-oxide (4.36 g, 35.4 mmol) was purged with nitrogen gas three times and charged with CH_2Cl_2 (60 mL) at 23 °C. TFAA (15.0 mL, 106 mmol, 3 equiv) in CH_2Cl_2 (35 mL) was added, and the resulting reaction mixture was stirred at 23 °C for 40 h. After this period, the reaction mixture was cooled to 0 °C. Then, *t*-BuOH (22 mL) and saturated aqueous K_2CO_3 (22 mL) were added to the reaction mixture. The resulting mixture was stirred for 3 h and gradually warmed to 23 °C. The mixture was extracted with CH_2Cl_2 (3 × 70 mL) using a separatory funnel. The combined organic layers were dried over anhydrous Na_2SO_4, filtered, and concentrated *in vacuo*. The resulting crude residue was purified by flash chromatography (50 to 80% EtOAc in hexanes) on silica gel (100 mL) to afford (3-methylpyridin-2-yl)methanol as a dark brown oil (4.18 g, 96% yield).

Data for (3-methylpyridin-2-yl)methanol: R_f = 0.36 (100% EtOAc); IR: ν_{max} = 3393 (br, O-H), 3065, 2983, 1737, 1589, 1452, 1408, 1374, 1243, 1177, 1126, 1055 cm^{-1}; ^{1}H NMR (300 MHz, 293 K, $CDCl_3$): δ 8.40 (d, J = 5.0 Hz, 1H, 6-H), 7.46 (d, J = 7.5 Hz, 1H, 4-H), 7.14 (dd, J = 7.5, 5.0 Hz, 1H, 5-H), 4.68 (s, 2H, -CH_2OH), 2.21 (s, 3H, -CH_3); ^{13}C NMR (100 MHz, 293 K, $CDCl_3$): δ 156.0, 145.1, 137.5, 129.5, 122.1, 61.5, 16.4; HRMS (ESI+) calcd for $C_7H_{10}NO$ $[M + H]^+$ = 124.0757, found 124.0755.

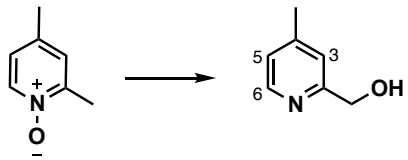

Preparation of (4-methylpyridin-2-yl)methanol: A 200-mL pear-shaped flask with 2,4-dimethylpyridine 1-oxide (1.98 g, 16.1 mmol) was purged with nitrogen gas three times and charged with CH_2Cl_2 (25 mL) at 23 °C. TFAA (6.8 mL, 48 mmol, 3 equiv) in CH_2Cl_2 (18 mL) was added, and the resulting reaction mixture was stirred at 23 °C for 48 h. After this period, the reaction mixture was cooled to 0 °C. Then, *t*-BuOH (10 mL) and saturated aqueous K_2CO_3 (10 mL) were added to the reaction mixture. The resulting mixture was stirred for 20 h and gradually warmed to 23 °C. The mixture was extracted with CH_2Cl_2 (3 × 20 mL) using a separatory funnel. The combined organic layers were dried over anhydrous Na_2SO_4, filtered, and concentrated *in vacuo*. The resulting crude residue was purified by flash chromatography (50 to 95% EtOAc in hexanes) on silica gel (60 mL) to afford (4-methylpyridin-2-yl)methanol as a dark brown oil (1.16 g, 51% yield).

Data for (4-methylpyridin-2-yl)methanol: R_f = 0.27 (100% EtOAc); IR: ν_{max} = 3210 (br, O-H), 2923, 1605, 1564, 1448, 1380, 1358, 1266, 1114, 1087, 1004 cm^{-1}; ^1H NMR (400 MHz, 293 K, $CDCl_3$): δ 8.35 (d, J = 4.8 Hz, 1H, 6-H), 7.11 (s, 1H, 3-H), 7.00 (d, J = 4.8, 1H, 5-H), 4.70 (s, 2H, -CH_2OH), 2.34 (s, 3H, -CH_3); ^{13}C NMR (100 MHz, 293 K, $CDCl_3$): δ 159.4, 159.4, 148.3, 123.5, 121.7, 64.3, 21.1. The ^1H and ^{13}C NMR spectra for (4-methylpyridin-2-yl)methanol were consistent with those in the literature.[3]

Preparation of (5-methylpyridin-2-yl)methanol: A 250-mL round-bottom flask with 2,5-dimethylpyridine 1-oxide (5.01 g, 40.6 mmol) was purged with nitrogen gas three times and charged with CH_2Cl_2 (75 mL) at 23 °C. TFAA (17.2 mL, 122 mmol, 3 equiv) in CH_2Cl_2 (35 mL) was added, and the resulting reaction mixture was stirred at 23 °C for 48 h. After this period, the reaction mixture was cooled to 0 °C. Then, *t*-BuOH (25 mL) and saturated aqueous K_2CO_3 (25 mL) were added to the reaction mixture. The resulting mixture was stirred for 6 h and gradually warmed to 23 °C. The mixture was extracted with CH_2Cl_2 (3 × 40 mL) using a separatory funnel. The combined organic layers were dried over anhydrous Na_2SO_4, filtered, and concentrated *in vacuo*. The resulting crude residue was purified by flash chromatography (50 to 80% EtOAc in hexanes) on silica gel (80 mL) to afford (5-methylpyridin-2-yl)methanol as a dark brown oil (2.60 g, 52% yield).

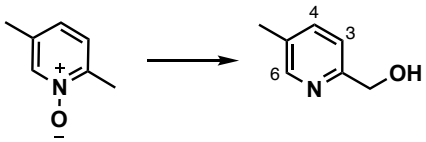

Data for (5-methylpyridin-2-yl)methanol: R_f = 0.27 (100% EtOAc); IR: ν_{max} = 3216 (br, O-H), 2923, 1681, 1605, 1574, 1491, 1451, 1383, 1200,1133, 1068 cm^{-1}; ^1H NMR (400 MHz, 293 K, $CDCl_3$): δ = 8.37 (s, 1H, 6-H), 7.49 (d, J = 8 Hz, 1H, 4-H), 7.17 (d, J = 8.0 Hz, 1H, 3-H), 4.72 (s, 2 H, -CH_2OH), 2.33 (s, 3H, -CH_3); ^{13}C (100 MHz, 293 K, $CDCl_3$): δ = 156.0, 145.1, 137.5, 129.5, 122.1, 61.5, 16.4; HRMS (ESI+) calcd for $C_7H_{10}ON$ $[M + H]^+$ = 124.0757, found 124.0755.

Preparation of (6-methylpyridin-2-yl)methanol: A 200-mL pear-shaped flask with 2,6-dimethylpyridine 1-oxide (2.37 g, 19.3 mmol) was purged with nitrogen gas three times and charged with CH_2Cl_2 (25 mL) at 23 °C. TFAA (8.14 mL, 57.8 mmol, 3 equiv) in CH_2Cl_2 (27 mL) was added, and the resulting reaction mixture was stirred at 23 °C for 42 h. After this period, the reaction mixture was cooled to 0 °C. Then, *t*-BuOH (10 mL) and saturated aqueous K_2CO_3 (10 mL) were added to the reaction mixture. The resulting mixture was stirred for 3 h and gradually warmed to 23 °C. The mixture was extracted with CH_2Cl_2 (3 × 50 mL) using a separatory funnel. The combined organic layers were dried over anhydrous Na_2SO_4, filtered, and concentrated *in vacuo*. The resulting crude residue was purified by flash chromatography (50 to 90% EtOAc in hexanes) on silica gel (80 mL) to afford (6-methylpyridin-2-yl)methanol as a dark brown oil (949 mg, 40% yield).

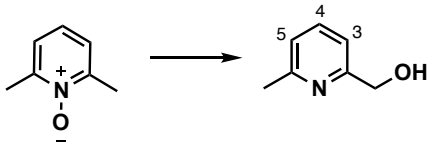

Data for (6-methylpyridin-2-yl)methanol: R_f = 0.32 (100% EtOAc); IR: ν_{max} = 3256 (br, O-H), 2920, 1680, 1598, 1579, 1458, 1206, 1137 cm^{-1}; ^1H NMR (400 MHz, 293 K, $CDCl_3$): δ 7.56 (app triplet, J = 7.4 Hz, 1H, 4-

H), 7.05 (app triplet, J = 7.4 Hz, 2H, 3-H and 5-H), 4.71 (s, 2 H, -CH_2OH), 2.54 (s, 3H, -CH_3); ^{13}C NMR (100 MHz, 293 K, $CDCl_3$): δ 158.5, 157.5, 137.1, 122.0, 117.6, 64.1, 24.3; HRMS (ESI+) calcd for $C_7H_{10}NO$ $[M + H]^+$ = 124.0757, found 124.0755.

Preparation of 3-methylpicolinaldehyde: A 200-mL pear-shaped flask with a reflux condenser was purged with nitrogen gas three times, and (3-methylpyridin-2-yl)methanol (3.25 g, 26.1 mmol), DCE (113 mL), and MnO_2 (11.38 g, 130.9 mmol, 5 equiv) were added consecutively. The mixture was heated to reflux. After 9 h, the reaction mixture was cooled to 23 °C, filtered through Celite®, washed with EtOAc, and concentrated *in vacuo*. The crude residue was purified by flash chromatography (40 to 70% EtOAc in hexanes) on silica gel (100 mL) to afford 3-methylpicolinaldehyde as a yellow oil (1.87 g, 59% yield).

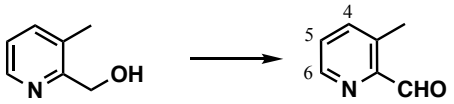

Data for 3-methylpicolinaldehyde: R_f = 0.67 (60% EtOAc in hexanes); IR: ν_{max} = 3385, 3058, 2931, 2826, 1705 (C=O), 1585, 1569, 1461, 1411, 1383, 1300, 1225, 1205, 1191, 1124, 1078 cm^{-1}; ^{1}H NMR (300 MHz, 293 K, $CDCl_3$): δ 10.18 (s, 1H, -C*H*O), 8.64 (d, J = 4.5 Hz, 1H, 6-H), 7.61 (d, J = 7.8 Hz, 1H, 4-H), 7.37 (dd, J = 7.6, 4.8 Hz, 1H, 5-H), 2.65 (s, 3H, -CH_3); ^{13}C NMR (100 MHz, 293 K, $CDCl_3$): δ 195.6, 150.2, 147.7, 140.1, 135.9, 126.7, 19.1. The ^{1}H and ^{13}C NMR spectra for 3-methylpicolinaldehyde were consistent with those in the literature.[4]

Preparation of 4-methylpicolinaldehyde: A 50-mL pear-shaped flask with a reflux condenser was purged with nitrogen gas three times, and (4-methylpyridin-2-yl)methanol (780 mg, 6.28 mmol), DCE (27 mL), and MnO_2 (2.73 g, 31.4 mmol, 5 equiv) were added consecutively. The mixture was heated to reflux. After 13 h, the reaction mixture was cooled to 23 °C, filtered through Celite®, washed with EtOAc, and concentrated *in vacuo*. The crude residue was purified by flash chromatography (40 to 70% EtOAc in hexanes) on silica gel (50 mL) to afford 4-methylpicolinaldehyde as a yellow oil (462 mg, 60% yield).

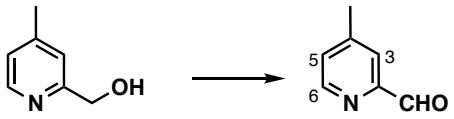

Data for 4-methylpicolinaldehyde: R_f = 0.67 (60% EtOAc in hexanes); R_f = 0.57 (60% EtOAc in hexanes); IR: ν_{max} = 3398, 3054, 2926, 2827, 1710 (C=O), 1603, 1476, 1448, 1381, 1366, 1265, 1246, 1138, 1103, 1088, 1041 cm^{-1}; ^{1}H NMR (300 MHz, 293 K, $CDCl_3$): δ = 10.06 (s, 1H, C*H*O), 8.63 (d, J = 5.0 Hz, 1H, 6-H), 7.78 (s, 1H, 3-H), 7.33 (dd, J = 5.0, 7.6 Hz, 1H, 5-H), 2.44 (s, 3H, -CH_3); ^{13}C (100 MHz, 293 K, $CDCl_3$): δ = 193.7, 152.7, 149.9, 148.5, 128.7, 122.5, 21.0. The ^{1}H and ^{13}C NMR spectra for 4-methylpicolinaldehyde were consistent with those in the literature.[3]

Preparation of 5-methylpicolinaldehyde: A 100-mL pear-shaped flask with a reflux condenser was purged with nitrogen gas three times, and (5-methylpyridin-2-yl)methanol (1.54 g, 12.4 mmol), DCE (54 mL), and MnO_2 (5.39 g, 62.1 mmol, 5 equiv) were added consecutively. The mixture was heated to reflux. After 8 h,

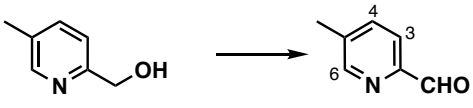

the reaction mixture was cooled to 23 °C, filtered through Celite®, washed with EtOAc, and concentrated *in vacuo*. The crude residue was purified by flash chromatography (40 to 70% EtOAc in hexanes) on silica gel (60 mL) to afford 5-methylpicolinaldehyde as a yellow oil (1.15 g, 77% yield).

Data for 5-methylpicolinaldehyde: R_f = 0.65 (60% EtOAc in hexanes); IR: ν_{max} = 3398, 3061, 2803, 2709, 2499, 1736 (C=O), 1587, 1371, 1241, 1045 cm^{-1}; ^1H NMR (300 MHz, 293 K, $CDCl_3$): δ 10.04 (s, 1H, -C*H*O), 8.61 (s, 1H, 6-H), 7.87 (d, J = 7.6 Hz, 1H, 4-H), 7.70 (d, J = 7.6 Hz, 1H, 3-H), 2.44 (s, 3H, -CH_3); ^{13}C NMR (100 MHz, 293 K, $CDCl_3$): δ 193.6, 151.2, 139.1, 137.7, 121.4, 19.2; HRMS (ESI+) calcd for C_7H_8NO $[M + H]^+$ = 122.0600, found 122.0597.

Preparation of 6-methylpicolinaldehyde: A 50-mL pear-shaped flask with a reflux condenser was purged with nitrogen gas three times, and (6-methylpyridin-2-yl)methanol (5.16 mg, 4.16 mmol), DCE (18 mL), and MnO_2 (1.91 g, 22.0 mmol, 5 equiv) were added consecutively. The mixture was heated to reflux. After 22 h, the reaction mixture was cooled to 23 °C, filtered through Celite®, washed with EtOAc, and concentrated *in vacuo*. The crude residue was purified by flash chromatography (40 to 70% EtOAc in hexanes) on silica gel (10 mL) to afford 6-methylpicolinaldehyde as a yellow oil (213 mg, 42% yield).

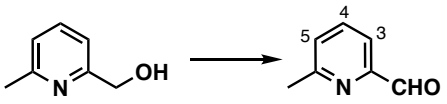

Data for 6-methylpicolinaldehyde: R_f = 0.68 (60% EtOAc in hexanes); IR: ν_{max} = 3407, 3064, 2927, 2826, 1712 (C=O), 1677, 1593, 1461, 1376, 1350,1287, 1254, 1215, 1156, 1087, 1040 cm^{-1}; ^1H NMR (400 MHz, 293 K, $CDCl_3$): δ 9.94 (s, 1H, -C*H*O), 7.93 (app t, J = 7.4 Hz, 1H, 4-H), 7.74 (d, J = 7.4 Hz, 1H, 3-H), 7.57 (d, J = 7.4 Hz, 1H, 5-H), 2.65 (s, 3H, -CH_3); ^{13}C NMR (100 MHz, 293 K, DMSO-d_6): δ 151.1, 150.1, 147.3, 139.4, 132.7, 123.5, 20.6; HRMS (ESI+) calcd for C_7H_8NO $[M + H]^+$ = 122.0600, found 122.0598.

Preparation of (E)-3-methylpicolinaldehyde oxime: A 200-mL pear-shaped flask open to air was charged with 3-methylpicolinaldehyde (1.15 g, 9.53 mmol), MeOH (96 mL), H_2O (15 mL), K_2CO_3 (1.58 g, 11.4 mmol, 1.2 equiv), and NH_2OH•HCl (662 mg, 9.53 mmol, 1 equiv). A reflux condenser was attached, and after the reaction mixture was heated to reflux for 4 h, the reaction mixture was cooled to 23 °C. The organic solvent was removed *in vacuo*, and the resulting aqueous layer was extracted with EtOAc (3 × 25 mL) using a separatory funnel. The combined organic layers were dried over anhydrous Na_2SO_4, filtered, and concentrated *in vacuo* to afford (*E*)-3-methylpicolinaldehyde oxime as a light pink solid (677 mg, 53% yield). This material was used directly without further purification.

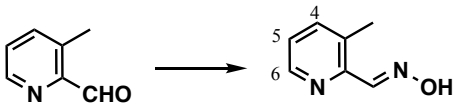

Data for (E)-3-methylpicolinaldehyde oxime: m.p. = 155–157 °C; R_f = 0.42 (60% EtOAc in hexanes); IR (film): ν_{max} = 3423 (br), 1642 cm^{-1}; ^1H NMR (400 MHz, 293 K, DMSO-d_6): δ 11.61 (s, 1H, -CH=NO*H*), 8.46 (d, J = 4.8 Hz, 1H, 6-H), 8.44 (s, 1H, -C*H*=NOH), 7.70 (d, J = 7.6 Hz, 1H, 4-H), 7.30 (dd, J = 7.6, 4.8 Hz, 1H, 5-H),

2.49 (s, 3H, -C*H*$_3$); ^{13}C NMR (100 MHz, 293 K, DMSO-d_6): δ 151.1, 150.1, 147.3, 139.4, 132.7, 123.5, 20.6; HRMS (ESI+) calcd for $C_7H_9N_2O$ $[M + H]^+$ = 137.0709, found 137.0709.

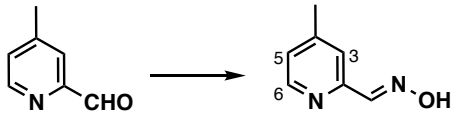

Preparation of (E)-4-methylpicolinaldehyde oxime: A 50-mL pear-shaped flask open to air was charged with 4-methylpicolinaldehyde (312 mg, 2.57 mmol), MeOH (26 mL), H_2O (4 mL), K_2CO_3 (427 mg, 3.08 mmol, 1.2 equiv), and NH_2OH•HCl (179 mg, 2.57 mmol, 1 equiv). A reflux condenser was attached, and after the reaction mixture was heated to reflux for 4 h, the reaction mixture was cooled to 23 °C. The organic solvent was removed *in vacuo*, and the resulting aqueous layer was extracted with EtOAc (3 × 30 mL) using a separatory funnel. The combined organic layers were dried over anhydrous Na_2SO_4, filtered, and concentrated *in vacuo* to afford (*E*)-4-methylpicolinaldehyde oxime as a light brown solid (303 mg, 86% yield). This material was used directly without further purification.

Data for (E)-4-methylpicolinaldehyde oxime: m.p. = 155–158 °C; R_f = 0.42 (60% EtOAc in hexanes); IR (film): ν_{max} = 3426 (br), 2101, 1631 cm^{-1}; ^{1}H NMR (400 MHz, 293 K, DMSO-d_6): δ 11.62 (s, 1H, -CH=NO*H*), 8.44 (d, J = 4.6 Hz, 1H, 6-H), 8.05 (s, 1H, -C*H*=NOH), 7.63 (s, 1H, 3-H), 7.22 (d, J = 4.6 Hz, 1H, 5-H), 2.36 (s, 3H, -C*H*$_3$); ^{13}C NMR (100 MHz, 293 K, DMSO-d_6): δ 152.2, 149.4, 149.2, 147.7, 125.1, 120.6, 20.8; HRMS (ESI+) calcd for $C_7H_9N_2O$ $[M + H]^+$ = 137.0709, found 137.0709.

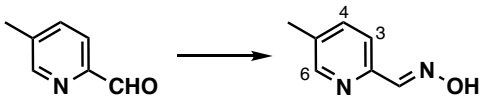

Preparation of (E)-5-methylpicolinaldehyde oxime: A 200-mL pear-shaped flask open to air was charged with 5-methylpicolinaldehyde (756 mg, 6.24 mmol), MeOH (63 mL), H_2O (10 mL), K_2CO_3 (1.03 g, 7.49 mmol, 1.2 equiv), and NH_2OH•HCl (433 mg, 6.24 mmol, 1 equiv). A reflux condenser was attached, and after the reaction mixture was heated to reflux for 4 h, the reaction mixture was cooled to 23 °C. The organic solvent was removed *in vacuo*, and the resulting aqueous layer was extracted with EtOAc (3 × 25 mL) using a separatory funnel. The combined organic layers were dried over anhydrous Na_2SO_4, filtered, and concentrated *in vacuo* to afford (*E*)-5-methylpicolinaldehyde oxime as a white solid (474 mg, 56% yield). This material was used directly without further purification.

*Data for (E)-5-methylpicolinaldehyde oxim**e***: m.p. = 157–158 °C; R_f = 0.45 (60% EtOAc in hexanes); IR (film): ν_{max} = 3436 (br), 2077, 1635 cm^{-1}; ^{1}H NMR (400 MHz, 293 K, DMSO-d_6): δ 11.55 (s, 1H, -CH=NO*H*), 8.43 (s, 1H, 6-H), 8.05 (s, 1H, -C*H*=NOH), 7.71 (d, J = 8.2 Hz, 1H, 4-H), 7.65 (d, J = 8.2 Hz, 1H, 3-H), 2.33 (s, 3H, -C*H*$_3$); ^{13}C NMR (100 MHz, 293 K, DMSO-d_6): δ 150.0, 149.3, 137.6, 133.9, 119.7, 18.3; HRMS (ESI+) calcd for $C_7H_9N_2O$ $[M + H]^+$ = 137.0709, found 137.0709.

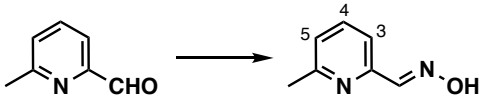

Preparation of (E)-6-methylpicolinaldehyde oxime: A 50-mL pear-shaped flask open to air was charged with 6-methylpicolinaldehyde

(309 mg, 2.55 mmol), MeOH (26 mL), H_2O (4 mL), K_2CO_3 (423 mg, 3.05 mmol, 1.2 equiv), and NH_2OH•HCl (177 mg, 2.55 mmol, 1 equiv). A reflux condenser was attached, and after the reaction mixture was heated to reflux for 3 h, the reaction mixture was cooled to 23 °C. The organic solvent was removed *in vacuo*, and the resulting aqueous layer was extracted with EtOAc (3 × 20 mL) using a separatory funnel. The combined organic layers were dried over anhydrous Na_2SO_4, filtered, and concentrated *in vacuo* to afford (*E*)-6-methylpicolinaldehyde oxime as an ivory solid (177 mg, 52% yield). This material was used directly without further purification.

Data for (E)-6-methylpicolinaldehyde oxime: m.p. = 159–161 °C; R_f = 0.53 (60% EtOAc in hexanes); IR (film): ν_{max} = 3423 (br), 2708, 1635, 1591, 1459 cm^{-1}; ^1H NMR (400 MHz, 293 K, DMSO-d_6): δ 11.61 (s, 1H, -CH=NO*H*), 8.04 (s, 1H, -C*H*=NOH), 7.72 (app t, J = 8 Hz 1H, 4-H), 7.60 (d, J = 8.0 Hz, 1H, 3-H), 7.25 (d, J = 8.0 Hz, 1H, 5-H), 2.49 (s, 3H, -CH_3); ^{13}C NMR (100 MHz, 293 K, DMSO-d_6): δ 158.1, 151.2, 149.3, 137.3, 123.5, 117.1 24.1; HRMS (ESI+) calcd for $C_7H_9N_2O$ $[M + H]^+$ = 137.0709, found 137.0709.

Preparation of (E)-2-((hydroxyimino)methyl)-1,3-dimethylpyridin-1-ium iodide: A 10-mL sealed tube with (*E*)-3-methylpicolinaldehyde oxime (401 mg, 2.94 mmol) was charged with acetone (6 mL) and MeI (1.82 mL, 29.4 mmol, 10 equiv). The vessel was sealed and heated to 45 °C (external temperature). After 15 h at the same temperature, the reaction mixture was cooled to 23 °C. A small amount of charcoal was added and the mixture was stirred for 2 h at 23 °C. The mixture was filtered by gravity through filter paper, and the remaining residue was rinsed with MeOH. The filtrate was concentrated *in vacuo* to yield (*E*)-2-[(hydroxyimino)methyl]-1,3-dimethylpyridin-1-ium iodide as a light brown solid (332 mg, 42% yield).

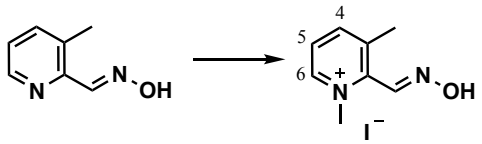

Data for (E)-2-((hydroxyimino)methyl)-1,3-dimethylpyridin-1-ium iodide: m.p. = 192–193 °C; R_f = 0.18 (4:1:1 *n*-BuOH:H_2O:AcOH); IR (film): ν_{max} = 3444 (br), 1636 cm^{-1}; ^1H NMR (400 MHz, 293 K, DMSO-d_6): δ 12.90 (s, 1H, -CH=NO*H*), 8.97 (d, J = 6.2 Hz, 1H, 6-H), 8.58 (s, 1H, -C*H*=NOH), 7.55 (d, J = 8 Hz, 1H, 4-H), 7.04 (dd, J = 8.0, 6.2 Hz, 1H, 5-H), 4.33 (s, 3H, -N^+CH_3), 2.57 (s, 3H, -CH_3); ^{13}C NMR (100 MHz, 293 K, DMSO-d_6): δ 147.6, 145.8, 145.7, 142.4, 138.9, 126.8, 47.8, 20.2; HRMS (ESI+) calcd for $C_8H_{11}N_2O$ $[M]^+$ = 151.0866, found 151.0864.

Preparation of (E)-2-((hydroxyimino)methyl)-1,4-dimethylpyridin-1-ium iodide: A 10-mL sealed tube with (*E*)-4-methylpicolinaldehyde oxime (202 mg, 1.48 mmol) was charged with acetone (3 mL) and MeI (978 μL, 14.8 mmol, 10 equiv). The vessel was sealed and heated to 45 °C (external temperature). After 20 h at the same temperature, the reaction mixture was cooled to 23 °C. A small amount of charcoal was added and the mixture was stirred for 4 h at 23 °C. The mixture was filtered by gravity through filter paper, and the remaining residue was rinsed with MeOH. The filtrate was concentrated *in vacuo* to yield (*E*)-2-[(hydroxyimino)methyl]-

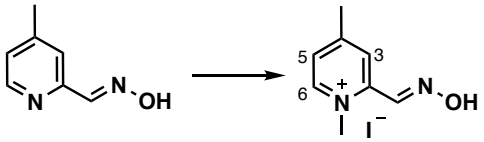

1,4-dimethylpyridin-1-ium iodide as a light brown solid (295 mg, 72% yield).

Data for (E)-2-((hydroxyimino)methyl)-1,4-dimethylpyridin-1-ium iodide: m.p. = 201–203 °C; R_f = 0.18 (4:1:1 *n*-BuOH:H_2O:AcOH); IR (film): ν_{max} = 3444 (br), 2101, 1640 cm^{-1}; ^1H NMR (400 MHz, 293 K, DMSO-d_6): δ 13.04 (s, 1H, -CH=NO*H*), 8.82 (d, J = 6.4 Hz, 1H, 6-H), 8.64 (s, 1H, -C*H*=NOH), 8.21 (s, 1H, 3-H), 7.91 (d, J = 6.4 Hz, 1H, 5-H), 4.30 (s, 3H, -N^+CH_3), 2.62 (s, 3H, -CH_3); ^{13}C NMR (100 MHz, 293 K, DMSO-d_6): δ 154.2, 143.3, 143.2, 138.4, 118.5, 116.5, 59.3, 16.2; HRMS (ESI+) calcd for $C_8H_{11}N_2O$ $[M]^+$ = 151.0866, found 151.0861.

Preparation of (E)-2-((hydroxyimino)methyl)-1,5-dimethylpyridin-1-ium iodide: A 10-mL sealed tube with (*E*)-5-methylpicolinaldehyde oxime (197 mg, 1.45 mmol) was charged with acetone (3 mL) and MeI (897 μL, 14.5 mmol, 10 equiv). The vessel was sealed and heated to 45 °C (external temperature). After 15 h at the same temperature, the reaction mixture was cooled to 23 °C. A small amount of charcoal was added and the mixture was stirred for 5 h at 23 °C. The mixture was filtered by gravity through filter paper, and the remaining residue was rinsed with MeOH. The filtrate was concentrated *in vacuo* to yield (*E*)-2-[(hydroxyimino)methyl]-1,5-dimethylpyridin-1-ium iodide as a light brown solid (310 mg, 77% yield).

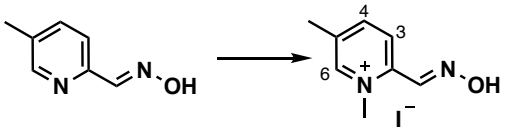

Data for (E)-2-((hydroxyimino)methyl)-1,5-dimethylpyridin-1-ium iodide: m.p. = 140–142 °C; R_f = 0.18 (4:1:1 *n*-BuOH:H_2O:AcOH); IR (film): ν_{max} = 3432 (br), 1634 cm^{-1}; ^1H NMR (400 MHz, 293 K, DMSO-d_6): δ 13.01 (s, 1H, -CH=NO*H*), 8.93 (s, 1H, 6-H), 8.67 (s, 1H, -C*H*=NOH), 8.39 (d, J = 8.4 Hz, 1H, 4-H), 8.29 (d, J = 8.4 Hz, 1H, 3-H), 4.34 (s, 3H, -N^+CH_3), 2.49 (s, 3H, -CH_3); ^{13}C NMR (100 MHz, 293 K, DMSO-d_6): δ 146.4, 145.8, 145.3, 142.1, 138.4, 124.8, 46.5, 18.2; HRMS (ESI+) calcd for $C_8H_{11}N_2O$ $[M]^+$ = 151.0866, found 151.0863.

Preparation of (E)-2-((hydroxyimino)methyl)-1,6-dimethylpyridin-1-ium iodide: A 75-mL sealed tube with (*E*)-6-methylpicolinaldehyde oxime (408 mg, 3.0 mmol) was charged with acetone (20 mL), and MeI (1.87 mL, 30.0 mmol). The reaction mixture was stirred at 55 °C for 2 d. After this period, the reaction mixture was transferred to a 50-mL round-bottomed flask, concentrated *in vacuo*, and recrystallized from acetone/EtOAc (1:1) to yield (*E*)-2-[(hydroxyimino)methyl]-1,6-dimethylpyridin-1-ium iodide as a light brown solid (171.2 mg, 21% yield).

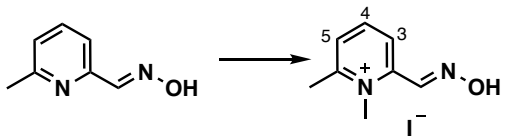

(E)-2-((hydroxyimino)methyl)-1,6-dimethylpyridin-1-ium iodide: m.p. = 140–142 °C; R_f = 0.18 (4:1:1 *n*-BuOH:H_2O:AcOH); IR (film): ν_{max} = 3405 (br), 1653 cm^{-1}; ^1H NMR (400 MHz, 293 K, DMSO-d_6): δ 12.98 (s, 1H, -CH=NO*H*), 8.80 (s, 1H, -C*H*=NOH), 8.41 (app t, J = 7.6 Hz, 1H, 4-H), 8.19 (d, J = 7.6 Hz, 1H, 3-H), 8.02 (d, J = 7.6 Hz, 1H, 5-H), 4.17 (s, 3H, -N^+CH_3), 2.83 (s, 3H, -CH_3); ^{13}C NMR (100 MHz, 293 K, DMSO-d_6): δ

156.9, 148.4, 144.5, 143.0, 129.4, 124.0, 41.6, 21.9; HRMS (ESI+) calcd for $C_8H_{11}N_2O$ $[M]^+$ = 151.0866, found 151.0864.

Supplementary Biological Data

Table S 1 Background subtracted absorbance values at 60 min with hAChE

[oxime] (μM)	3-Me-2-PAM			4-Me-2-PAM			5-Me-2-PAM			6-Me-2-PAM			2-PAM		
9.375	0.007	0.003	0.006	0.054	0.057	0.061	0.016	0.010	0.039	0.033	0.026	0.022	0.097	0.077	0.086
18.75	0.026	0.011	0.015	0.083	0.104	0.090	0.051	0.031	0.057	0.066	0.057	0.053	0.152	0.116	0.144
37.5	0.028	0.025	0.034	0.140	0.150	0.148	0.059	0.049	0.086	0.127	0.110	0.112	0.215	0.215	0.213
75	0.051	0.044	0.059	0.225	0.214	0.231	0.090	0.089	0.110	0.159	0.161	0.173	0.306	0.224	0.258
150	0.092	0.074	0.084	0.259	0.274	0.288	0.188	0.186	0.199	0.279	0.287	0.287	0.388	0.368	0.373
300	0.160	0.173	0.207	0.331	0.341	0.341	0.267	0.280	0.286	0.359	0.396	0.389	0.410	0.463	0.509
600	0.286	0.246	0.347	0.413	0.419	0.410	0.404	0.410	0.411	0.541	0.487	0.515	0.532	0.578	0.600

Table S 2 Background subtracted absorbance values for 18.8 μM oxime with hAChE

time (min)	3-Me-2-PAM			4-Me-2-PAM			5-Me-2-PAM			6-Me-2-PAM			2-PAM		
0	0.009	0.003	0.001	0.003	0.002	0.005	0.005	0.003	0.006	0.002	0.001	0.002	0.001	0.001	0.001
3	0.010	0.003	0.001	0.007	0.007	0.010	0.006	0.000	0.008	0.008	0.004	0.003	0.008	0.008	0.008
6	0.013	0.007	0.001	0.012	0.014	0.018	0.013	0.002	0.014	0.010	0.007	0.006	0.021	0.016	0.022
9	0.015	0.004	0.001	0.018	0.024	0.023	0.023	0.005	0.020	0.015	0.009	0.010	0.031	0.024	0.029
12	0.014	0.002	0.001	0.022	0.029	0.026	0.022	0.004	0.021	0.018	0.014	0.012	0.038	0.032	0.034
15	0.013	0.003	0.001	0.028	0.032	0.031	0.023	0.006	0.024	0.019	0.016	0.014	0.054	0.042	0.048
18	0.015	0.006	0.004	0.034	0.041	0.039	0.029	0.010	0.030	0.027	0.022	0.021	0.056	0.044	0.051
21	0.018	0.007	0.006	0.038	0.048	0.043	0.032	0.015	0.034	0.032	0.027	0.024	0.070	0.051	0.062
24	0.017	0.007	0.007	0.042	0.050	0.048	0.032	0.016	0.035	0.036	0.029	0.026	0.084	0.066	0.076
27	0.019	0.007	0.006	0.046	0.056	0.051	0.036	0.017	0.037	0.036	0.033	0.029	0.089	0.069	0.081
30	0.019	0.007	0.009	0.048	0.060	0.056	0.036	0.018	0.036	0.041	0.034	0.032	0.088	0.066	0.082
33	0.022	0.009	0.008	0.054	0.064	0.058	0.038	0.023	0.039	0.045	0.038	0.033	0.098	0.075	0.093
36	0.023	0.007	0.009	0.057	0.068	0.064	0.040	0.022	0.039	0.047	0.039	0.036	0.110	0.087	0.106
39	0.023	0.009	0.009	0.060	0.074	0.067	0.041	0.025	0.044	0.049	0.042	0.039	0.104	0.078	0.098
42	0.023	0.008	0.011	0.063	0.076	0.069	0.041	0.025	0.045	0.052	0.046	0.040	0.116	0.089	0.111
45	0.024	0.011	0.011	0.068	0.081	0.074	0.043	0.026	0.046	0.054	0.046	0.042	0.123	0.096	0.117
48	0.025	0.010	0.012	0.072	0.085	0.077	0.046	0.025	0.050	0.056	0.050	0.045	0.128	0.099	0.122
51	0.024	0.012	0.013	0.076	0.089	0.079	0.049	0.027	0.051	0.061	0.052	0.046	0.129	0.101	0.123
54	0.026	0.010	0.014	0.077	0.095	0.083	0.049	0.029	0.055	0.062	0.053	0.048	0.140	0.109	0.133
57	0.026	0.011	0.012	0.081	0.099	0.087	0.049	0.030	0.057	0.065	0.054	0.051	0.144	0.113	0.137
60	0.026	0.011	0.015	0.083	0.104	0.090	0.051	0.031	0.057	0.066	0.057	0.053	0.152	0.116	0.144
63	0.027	0.013	0.013	0.085	0.105	0.092	0.052	0.031	0.059	0.067	0.061	0.054	0.149	0.113	0.140
66	0.027	0.013	0.015	0.088	0.110	0.096	0.054	0.033	0.061	0.070	0.062	0.056	0.157	0.120	0.148
69	0.029	0.013	0.015	0.091	0.112	0.099	0.056	0.033	0.063	0.072	0.063	0.058	0.159	0.120	0.150
72	0.028	0.013	0.017	0.096	0.116	0.101	0.056	0.036	0.066	0.074	0.064	0.062	0.158	0.119	0.149

Table S 3 Background subtracted absorbance values at 20 min with eel AChE

[oxime] (μM)	3-Me-2-PAM			4-Me-2-PAM			5-Me-2-PAM			6-Me-2-PAM			2-PAM		
9.375	0.035	0.033	0.013	0.433	0.430	0.413	0.206	0.165	0.165	0.367	0.358	0.361	0.524	0.516	0.550
18.75	0.082	0.077	0.076	0.594	0.589	0.497	0.254	0.273	0.298	0.540	0.559	0.526	0.583	0.642	0.634
37.5	0.129	0.123	0.110	0.675	0.748	0.762	0.318	0.433	0.442	0.701	0.681	0.731	0.858	0.835	0.798
75	0.168	0.159	0.158	0.729	0.742	0.726	0.518	0.511	0.525	0.755	0.762	0.807	0.904	0.887	0.906
150	0.253	0.233	0.219	0.629	0.723	0.689	0.541	0.533	0.568	0.795	0.813	0.836	0.893	0.893	0.910
300	0.261	0.256	0.240	0.648	0.629	0.662	0.503	0.504	0.552	0.734	0.763	0.726	0.919	0.883	0.903
600	0.289	0.292	0.299	0.528	0.456	0.513	0.463	0.439	0.464	0.626	0.663	0.665	0.849	0.815	0.835

Table S 4 Background subtracted absorbance values for 18.8 μM oxime with eel AChE

time (min)	3-Me-2-PAM			4-Me-2-PAM			5-Me-2-PAM			6-Me-2-PAM			2-PAM		
0	0.004	0.006	0.004	0.117	0.113	0.083	0.048	0.040	0.041	0.076	0.074	0.078	0.080	0.086	0.095
3	0.015	0.018	0.013	0.203	0.202	0.164	0.083	0.074	0.081	0.167	0.159	0.160	0.221	0.236	0.251
6	0.024	0.027	0.024	0.284	0.281	0.234	0.112	0.106	0.115	0.245	0.238	0.231	0.334	0.353	0.371
9	0.034	0.036	0.033	0.363	0.356	0.295	0.139	0.136	0.152	0.314	0.311	0.297	0.423	0.448	0.469
12	0.043	0.049	0.043	0.433	0.424	0.349	0.170	0.167	0.185	0.377	0.377	0.359	0.497	0.530	0.552
15	0.052	0.055	0.052	0.493	0.480	0.400	0.199	0.197	0.217	0.430	0.434	0.413	0.560	0.603	0.616
18	0.068	0.067	0.063	0.545	0.532	0.450	0.228	0.228	0.253	0.483	0.490	0.464	0.616	0.654	0.667
21	0.082	0.077	0.076	0.594	0.589	0.497	0.254	0.272	0.298	0.540	0.559	0.526	0.660	0.693	0.703
24	0.091	0.092	0.090	0.661	0.654	0.542	0.306	0.309	0.331	0.608	0.616	0.582	0.697	0.729	0.738
27	0.099	0.101	0.102	0.700	0.688	0.609	0.338	0.333	0.359	0.646	0.653	0.619	0.743	0.775	0.777

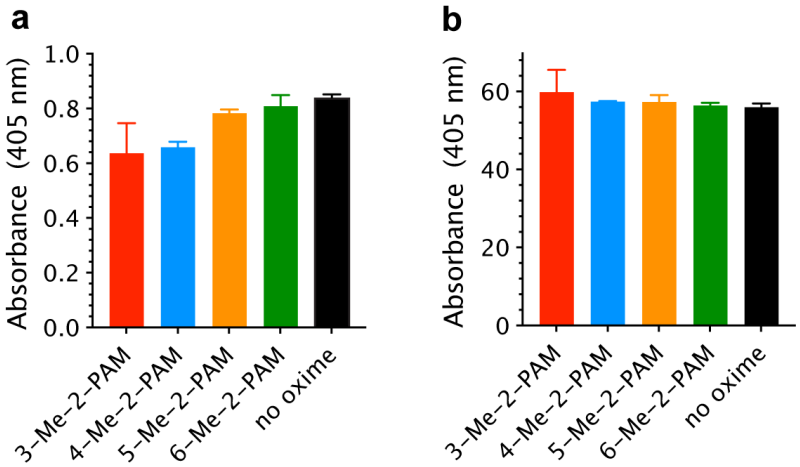

Figure S1. Inhibition data for C-methylated 2-PAM analogs at 12 min (a) hAChE (b) eel AChE.

UV-Vis Spectroscopic analysis of 4-Me-2-PAM

The absorbance of 4-Me-2-PAM was measured to ask whether aggregation was the cause of reduced activity at higher concentrations. A 38 μM solution of 4-Me-2-PAM in 100 mM phosphate pH 7.4 buffer (2 mL) was prepared. The solution (1 mL) was transferred to a quartz cuvette and the absorbance was measured. This solution was diluted with 100 mM phosphate pH 7.4 buffer to 25, 19, and 9.5 μM. The absorbance of each solution was measured and plotted. Because the increase in absorbance was linearly proportional to the concentration, aggregation was not deemed the source of reduced activity.

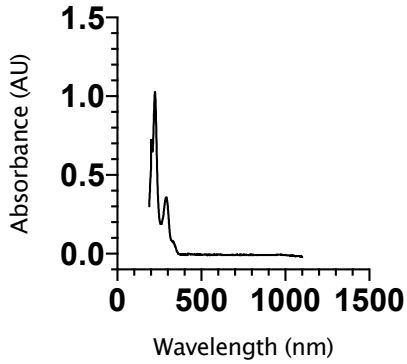

Figure S2. Absorbance spectrum of 38 μM **4-Me-2-PAM** in 100 mM phosphate pH 7.4 buffer.

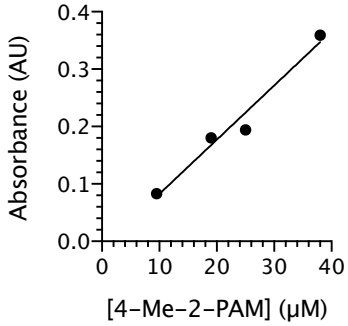

Figure S3. Absorbance of varying concentrations of **4-Me-2-PAM** at 290 nm.

Computational calculations of the ALogP, Solubility, and BBB permeability of 2-PAM and the methyl scan derivatives.*

Compound	ALogP [1]	LogS [2]	LogBBB [3]
2-PAM	1.86	-1.14	-0.42
3-Me-2-PAM	2.35	-1.68	-0.27
4-Me-2-PAM	2.35	-1.68	-0.27
5-Me-2-PAM	2.35	-1.68	-0.27
6-Me-2-PAM	2.14	-1.50	-0.33

Table S2. Calculated ALogP, Solubility, and BBB penetration.
[1] ALogP: incorporates the octanol-water partition coefficient (LogP) and molar refractivity (MR) of a compound. MR adds information about molecular volume and polarizability to the calculation.
[2] LogS (solubility): solvent = water, 25°C, pH = 7.0). an increase in negative value indicates a decrease in solubility.
[3] LogBBB (blood brain barrier permeability): an increase in negative value indicates an increase in BBB permeability.
* All calculations were performed using Discovery Studio v18 **(**Dassault Systèmes BIOVIA, San Diego, CA**)**. ALogP, LogS, and Log BBB were calculated using the Calculate Molecular Properties module.

Electrostatic potential surface maps: The Poisson-Boltzmann electrostatic surface map calculator in Maestro (Schrödinger, LLC, New York, NY) was used to generate maps for 2-PAM, 3-Me-2-PAM, 4-Me-2-PAM, 5-Me-2-PAM, and 6-Me-2-PAM (Figure S4). The maps were calculated with the following parameters: all atoms in

each molecule included; forcefield: OPLS3; solute dielectric constant: 1.0, solvent dielectric constant: 80.0; solvent radius: 0.3 Å, temperature: 298.0K; and surface resolution: 0.1.

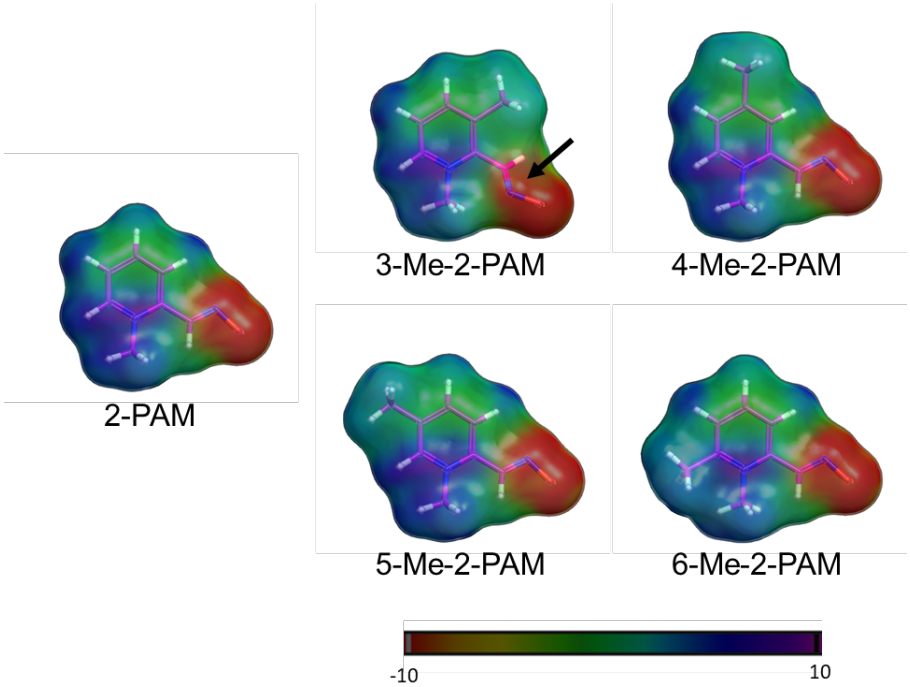

Figure S4. *Electrostatic surface potential maps for 2-PAM, 3-Me-2-PAM, 4-Me-2-PAM, 5-Me-2-PAM, and 6-Me-2-PAM. Surface potent color ranges from red, which corresponds to highest electron potential to purple, which corresponds to lowest electron potential. The oxime moiety possesses the highest electron surface potential; the pyridinium nitrogen possesses the lowest electron surface potential. Notably, unlike the other derivatives, the 3-Me-2-PAM oxime group adopts a twist-plane conformation (black arrow).*

Protein refinement: The AChE structure co-crystallized with 2-PAM (PDB entry 5HFA, resolution = 2.2 Å)[5] was used for molecular modeling studies to provide biochemically feasible rationales for the assay results. As noted in the manuscript, the 2-PAM in the active site of PDB 5HFA is positioned such that, although engaging in a cation-π interaction with the Trp 86 side chain indole: 1) the oxime moiety points away from the covalently bound paraoxon-ethyl, with the ligand's oxygen atom located 8.42 Å distance from the phosphorous atom of paraoxon (Figure S5a), and 2) methyl substitutions on the pyridinium ring of 2-PAM, as it is located in the X-ray structure, did not rationalize the reactivation potencies (Figure 3 of the manuscript) of the methyl scan derivatives (Figure S5b). Consequently, 2-PAM was removed from the X-ray structure prior to energy refinement. Using Insight II (2005), a conservative energy minimization strategy was performed on both PDB structures as follows: 1) hydrogens were added, all incorrect bond assignments were corrected, N and C termini were capped, and the distance-dependent dielectric was set to 1.0, 2) hydrogen atoms only were minimized (100 steps steepest descents followed by conjugate gradients until the norm of the gradient was < 0.001 kcal/mol/Å^2), and 3) protein side chains were relaxed using the same protocol (*i.e.*, 100 steps steepest descents followed by conjugate gradients until the norm of the gradient was < 0.001 kcal/mol/Å^2).

Small molecule docking: 2-PAM and all C-methylated derivatives described in the text were built using Discovery Studio 2016, and energy refined in Insight II (2005) (cff91 forcefield, with the pyridinium nitrogen

atom charge set to +1 and the oxime oxygen charge set to -1, distance dialectic = 1.0, and conjugate gradients minimization until the norm of the gradient < 001 kcal/mol/Å^2).

As a starting point for subsequent comparisons with derivatives, 2-PAM was first docked in the AChE binding site of 5HFA using the Insight II (2005) **(**Dassault Systèmes BIOVIA, San Diego, CA**)** graphical user interface with 3-D visualization enabled, thereby allowing for detailed small molecule positional manipulation via dial box control. The covalently bound KTA (*i.e*., an acetylcholine mimetic) in PDB entry 2HA0[6] was initially used to guide the binding location and orientation of 2-PAM in the AChE binding site (Figure 4a). Specifically, the energy refined structure of 5HFA and the structure of 2HA0 were superimposed in Maestro, and indicated a nearly identical alignment, with an RMSD = 0.482 Å (Figure S7). The protein structures were then imported back into Insight II (2005), and 2-PAM was superimposed on the bound substrate mimetic by aligning its oxygen oxime and pyridinium nitrogen with the KTA carbon atom that is covalently bound to the Ser-203 side chain oxygen and the ammonium nitrogen, respectively. With 2-PAM thus positioned in the binding site, the van der Waals bump was set to 0.25 Å, and translational and rotational adjustments, as well as torsional adjustments to protein residue side chains (within acceptable limits defined by rotamer libraries and empirical data) were used to eliminate unacceptable atom-atom overlaps and optimize non-bonded interactions. Subsequently, HINT program (eduSoft, La Jolla, CA) analysis, iterative rounds of additional manual adjustments (translational, rotational, and torsional), conjugate gradients minimizations (2-PAM and surrounding protein residue side chains within a 10 Å radius of the binding site), and additional HINT analysis were used to direct micro-environmental adjustments between enzyme side chain atoms and 2-PAM until an optimized, biochemically feasible binding mode, which also positioned the oxime oxygen 2.3 Å from the paraoxon phosphorous, was achieved. Following, methyl scan analogs were docked in the AChE active site using the same protocol as indicated for 2-PAM (see above).

To further elaborate on the HINT (for "Hydropathic INTeractions") program (eduSoft, La Jolla, CA), the software scores a summation of the hydropathic interactions between two interacting species during a binding event.[7-9] In this study, HINT was used to score all intermolecular atom-atom interactions between AChE and either 2-PAM or its methyl scan derivatives. The hydropathic interactions that are scored by the program fall into 6 categories. Favorable atom-atom contact categories include hydrogen bonds, acid-base, and hydrophobic interactions; unfavorable atom-atom contact categories include acid-acid, base-base, and hydrophobic-polar interactions. In the HINT program, each atom potential type possesses a corresponding hydrophobic atom constant a_i that is derived from the LogP partition coefficient constants calculated by Hansch and Leo[8,10]. Hence, the derived atom constants implicitly incorporate an estimate of entropy, which is ignored in molecular mechanics models. The hydropathic interaction value for an atom pair b_{ij} is calculated as a function of the hydrophobic constants for each atom, the distance between the atoms, and the solvent accessible surface areas (SASA) of the two atoms.

$b_{ij} = s_i a_i s_j a_j R_{ij}$

The distance function, $R_{ij} = e^{-r}$, has been reported to give a good fit to published Leo polar proximity factors.[8,9] The SASA for atoms, s_i, is taken from literature values[11] for proteins. The interaction values, b_{ij}, for each

interacting atom pair are summed to provide a 'total 'HINT interaction score' for two molecular species during a binding event. The higher and more positive a total HINT interaction score, the more favorable the binding between two species is predicted to be.

Compound	Total Hint Score*	Hydrogen Bond*	Acid/Base*	Hydrophobic*	Acid/Acid**	Base/Base**	Hydrophobic /Polar**
2-PAM	152.0	21.6	422.2	207.6	79.2	74.7	345.5
4-Me-2-PAM	143.1	21.9	414.2	268.5	55.7	86.4	419.4
6-Me-2-PAM	197.2	22.0	479.4	291.3	54.2	76.1	365.2

Table S3. Final quantitative HINT scores for active compounds 4-Me-2-PAM, 6-Me-2-PAM and 2-PAM (for comparison)

*: Favorable interaction
**: Unfavorable interaction

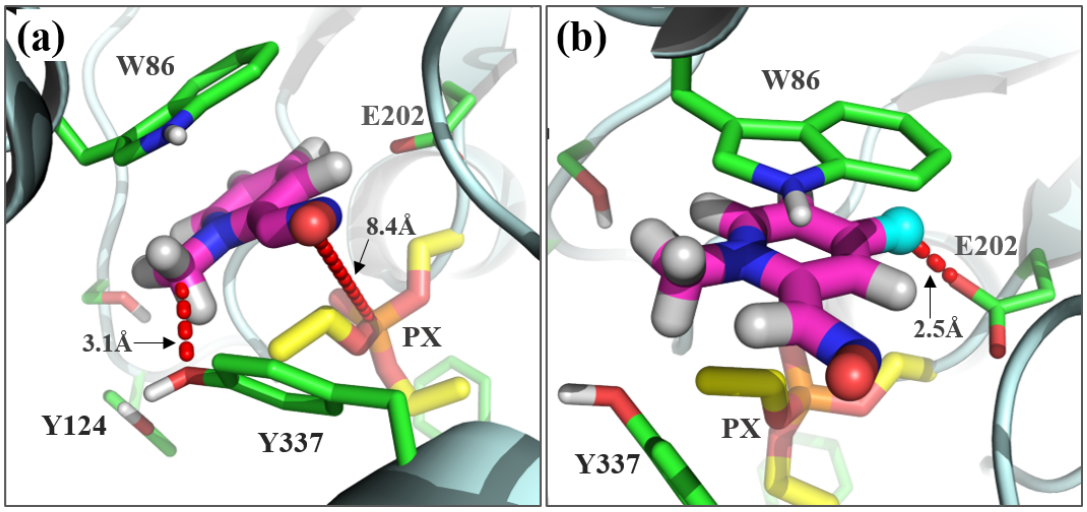

Figure S5. The binding mode of 2-PAM taken directly from PDB entry code 5HFA is not biochemically feasible with respect to rationalizing the reactivation of paraoxon deactivated AChE, nor does the position of 2-PAM from the X-ray structure rationalize the observed reactivation of AChE by methyl-scan derivatives. 5HFA is shown in pale cyan cartoon with select residues shown with green carbons. **(a)** In the X-ray structure of the 2-PAM (magenta carbons) binding mode, the oxime oxygen of the small molecule is oriented away from covalently bound paraoxon (yellow carbons, orange phosphorous), and is 8.4 Å (red dash) away from the paraoxon phosphorous atom. This distance, and the location of the 2-PAM oxime moiety precludes a rational, structure-based foundation for understanding the reactivation of the enzyme by the small molecule. Moreover, the methyl substituted on the nitrogen atom of the pyridinium ring is located too close to the oxygen atom of the phenol side chain of Tyr 337 (red dash), which would result in a biochemically unacceptable hydrophobic-polar clash. **(b)** When the 2-PAM (magenta carbons) in the X-ray structure binding mode is substituted with a 4-methyl moiety (cyan carbon, hydrogens not shown for clarity of presentation), a highly unfavorable hydrophobic clash (red dash) is observed with the side chain carboxylate of residue Glu 202. This unfavorable binding is contrary to the biochemical data (Figure 3 of the manuscript) obtained for the reactivation potency of this derivative.

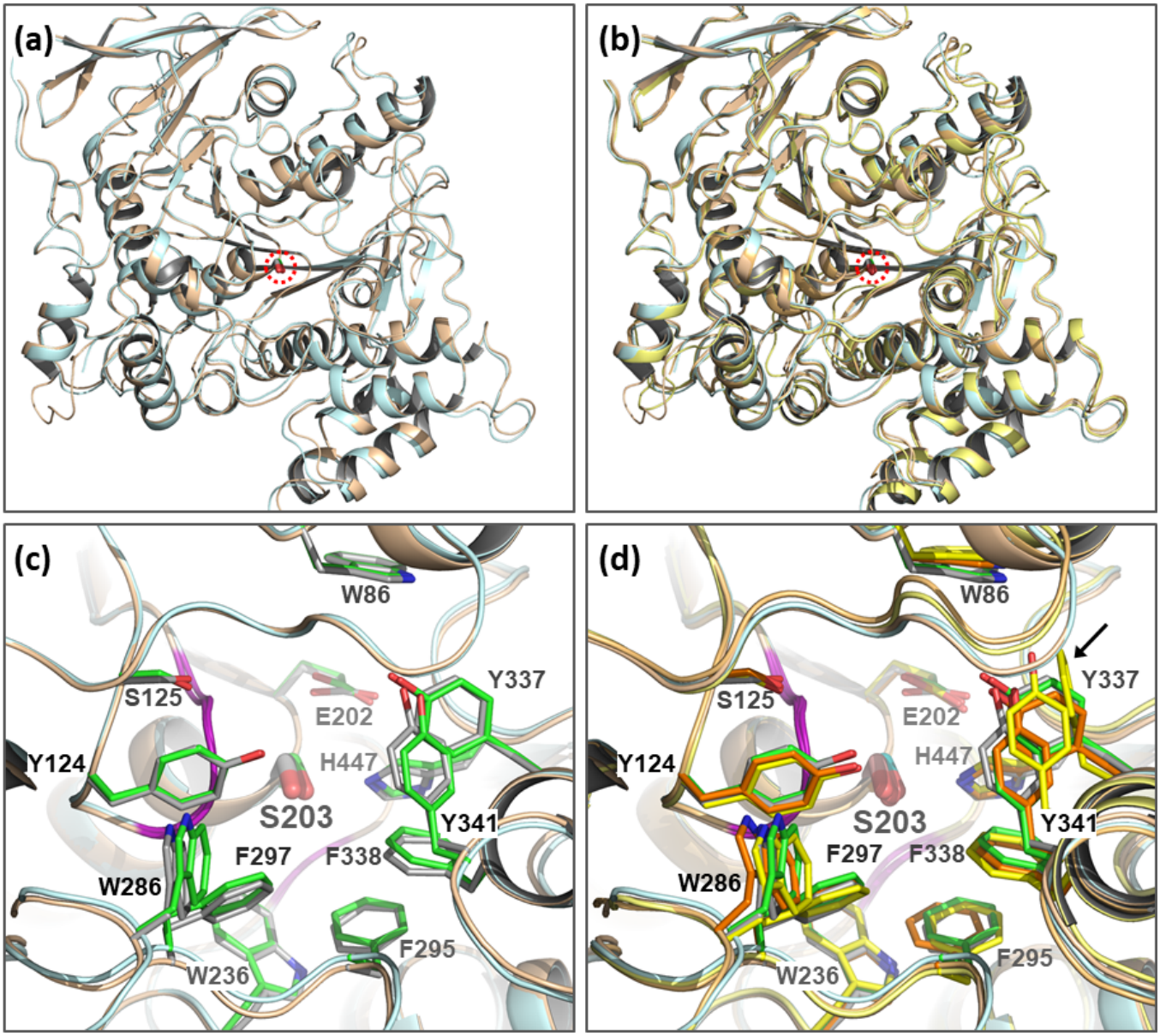

Figure S6. Superimpositions of the highest available resolution apo-state X-ray structures of AChE from phylum *Chordata* species indicate negligible differences in secondary structures, and residue conservation in the active site and gore - across species. a) the superimposition RMSD of human AChE (PDB entry 4EY4[12]; resolution: 2.156 Å; light cyan cartoon) and eel AChE (PDB entry: 1C2O[13]; resolution: 4.2 Å; wheat cartoon) is 0.642 Å. The red dashed circle indicates the location of catalytic Ser 203 in both species (human sequence number). b) superimpose of all X structures of available species from phylum *Chordata*. Human and eel structure descriptions are the same as indicated in 6a. Mouse AChE is PDB entry 5DTI[14] (resolution: 2.0 Å; light orange cartoon) and *Torpedo californica* AChE (*Tc*AChE) is PDB entry 1EA5[15] (resolution: 1.8 Å; light yellow cartoon). RMSD values for each non-human species X-ray structure versus the human X-ray structure: 1) human – eel: 0.642 Å, 2) human – *Torpedo*: 1.002 Å, and 3) human – mouse: 0.743 Å. The red dashed circle indicates the location of catalytic Ser 203 in all species (human residue sequence number). c) close-up view of the AChE active sites and gores from the superimposition of human PDB entry 4EY4 and eel PDB entry 1C2O shown in 6a. Residue side chain carbons are colored green and gray for the human and eel X-ray structures, respectively. The purple cartoon segments in both structures indicate conserved interspecies Gly residues. The image clearly shows both complete residue conservation and identical side chain orientations. d) close up view of the AChE active sites and gores from the superimposition of human PDB entry 4EY4, eel PDB entry 1C2O, mouse PDB entry 5DTI, and *Torpedo* PDB entry 1EA5 shown in 6b. Residue side chain carbons are colored green, gray, orange, and yellow for human, eel, mouse, and *Torpedo* X-ray structures, respectively. The purple cartoon segments in all structures indicate conserved interspecies Gly residues. As in 6c, the image clearly shows both complete residue and side chain orientation conservation for the human, eel, and mouse X-ray structures. Comparison with the *Torpedo* X-ray structure also indicates near complete residue and side chain orientation conservation, with two exceptions: 1) Tyr 341 (human sequence number) is slightly skewed versus the other three species, and 2) Y337 (human sequence number) is replaced with a Phe residue in *Tc*AChE.

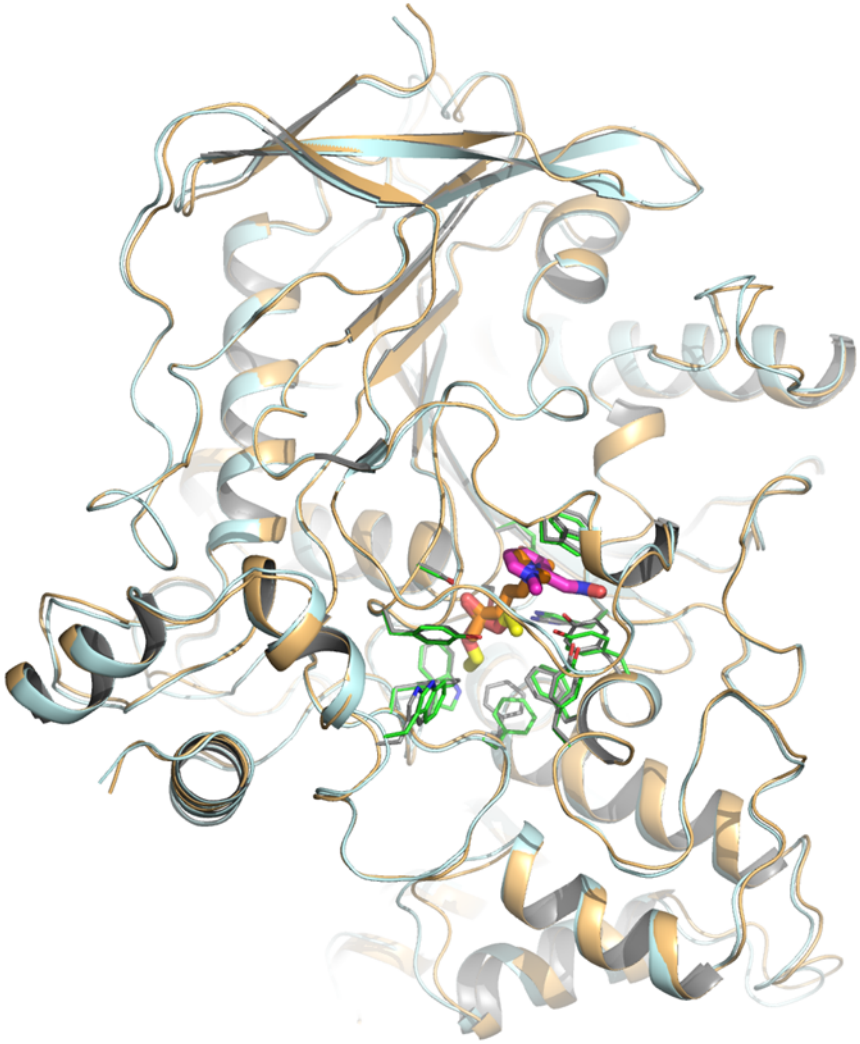

Figure S7. Alignment of the X-ray co-crystal structures PDB entry 2HA0 (mouse AChE (light orange cartoon) with KTA covalently bound to Ser 203) and 5HFA (human AChE (pale cyan cartoon) with bound 2-PAM (magenta carbons), and covalently bound paraoxon (yellow carbons)). The alignment RMSD for the two X-ray structures, including α-helices, sheets, and loops, is 0.572 Å. This image, as with the Figure S6 superimpositions of AChE from different species, shows how analogous AChE structures are across different species. As shown in greater detail in Figure S6, residues surrounding the active sites and gores are equivalent for 2HA0 and 5HFA and are shown with grey and green carbons in 2HA0 and 5HFA, respectively.

Cited References

(1) Tanga, M. J.; Bupp, J. E.; Tochimoto, T. K. Syntheses of five potential heterocyclic amine food mutagens. *J. Heterocycl. Chem.* **1997,** *34*, 717–727.

(2) Limnios, D.; Kokotos, C. G. 2,2,2-Trifluoroacetophenone as an organocatalyst for the oxidation of tertiary amines and azines to *N*-oxides. *Chem.- Eur. J.* **2014,** *20*, 559–563.

(3) Comba, P.; Morgen, M.; Wadepohl, H. Tuning of the properties of transition-metal bispidine complexes by variation of the basicity of the aromatic donor groups. *Inorg. Chem.* **2013,** *52*, 6481–6501.

(4) Krinochkin, A. P.; Kopchuk, D. S.; Chepchugov, N. V.; Kovalev, I. S.; Zyryanov, G. V.; Rusinov, V. L.; Chupakhin, O. N. Effect of substituent in pyridine-2-carbaldehydes on their heterocyclization to 1,2,4-triazines and 1,2,4-triazine 4-oxides. *Russ. J. Org. Chem.* **2017,** *53*, 963–970.

(5) Franklin Matthew, C.; Rudolph Michael, J.; Ginter, C.; Cassidy Michael, S.; Cheung, J. Structures of paraoxon-inhibited human acetylcholinesterase reveal perturbations of the acyl loop and the dimer interface. *Proteins: Structure, Function, and Bioinformatics* **2016,** *84*, 1246–1256.

(6) Bourne, Y.; Radić, Z.; Sulzenbacher, G.; Kim, E.; Taylor, P.; Marchot, P. Substrate and product trafficking through the active center gorge of acetylcholinesterase analyzed by crystallography and equilibrium binding. *J. Biol. Chem.* **2006,** *281*, 29256–29267.

(7) Kellogg, G. E.; Abraham, D. J. KEY, LOCK, and LOCKSMITH: Complementary hydropathic map predictions of drug structure from a known receptor-receptor structure from known drugs. *J. Mol. Graphics* **1992,** *10*, 212–217.

(8) Kellogg, G. E.; Semus, S. F.; Abraham, D. J. HINT: A new method of empirical hydrophobic field calculation for CoMFA. *J. Comput. Aided Mol. Des.* **1991,** *5*, 545–552.

(9) Kellogg, G. E., HINT, 2.01; eduSoft: Ashland, VA, 1993.

(10) Leo, A.; Hansch, C. *Substituent constants for correlation analysis in chemistry and biology*; John Wiley & Sons, 1979.

(11) Shrake, A.; Rupley, J. A. Environment and exposure to solvent of protein atoms. Lysozyme and insulin. *J. Mol. Biol.* **1973,** *79*, 351–371.

(12) Cheung, J.; Rudolph, M. J.; Burshteyn, F.; Cassidy, M. S.; Gary, E. N.; Love, J.; Franklin, M. C.; Height, J. J. Structures of human acetylcholinesterase in complex with pharmacologically important ligands. *J. Med. Chem.* **2012,** *55*, 10282–10286.

(13) Bourne, Y.; Grassi, J.; Bougis, P. E.; Marchot, P. Conformational flexibility of the acetylcholinesterase tetramer suggested by X-ray crystallography. *J. Biol. Chem.* **1999,** *274*, 30370–30376.

(14) Katz, F. S.; Pecic, S.; Tran, T. H.; Trakht, I.; Schneider, L.; Zhu, Z.; Ton-That, L.; Luzac, M.; Zlatanic, V.; Damera, S.; Macdonald, J.; Landry, D. W.; Tong, L.; Stojanovic, M. N. Discovery of new classes of compounds that reactivate acetylcholinesterase inhibited by organophosphates. *ChemBioChem* **2015,** *16*, 2205–2215.

(15) Dvir, H.; Jiang, H. L.; Wong, D. M.; Harel, M.; Chetrit, M.; He, X. C.; Jin, G. Y.; Yu, G. L.; Tang, X. C.; Silman, I.; Bai, D. L.; Sussman, J. L. X-ray structures of *Torpedo californica* acetylcholinesterase complexed with (+)-huperzine A and (-)-huperzine B: Structural evidence for an active site rearrangement. *Biochemistry* **2002,** *41*, 10810–10818.

NMR spectra

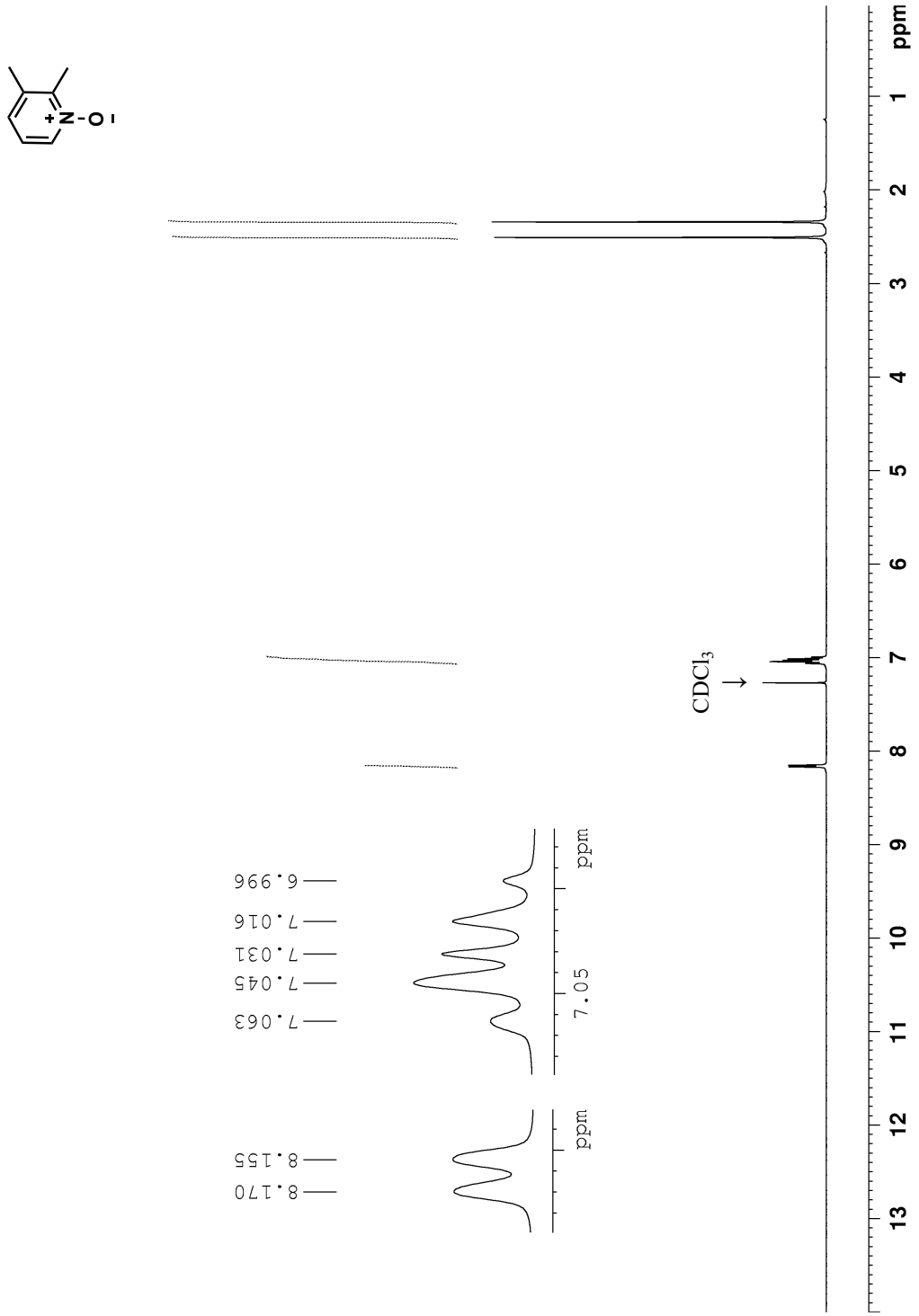

Spectrum 1. ^{1}H NMR spectrum of 2,3-dimethylpyridine 1-oxide (400 MHz, $CDCl_3$, 293K).

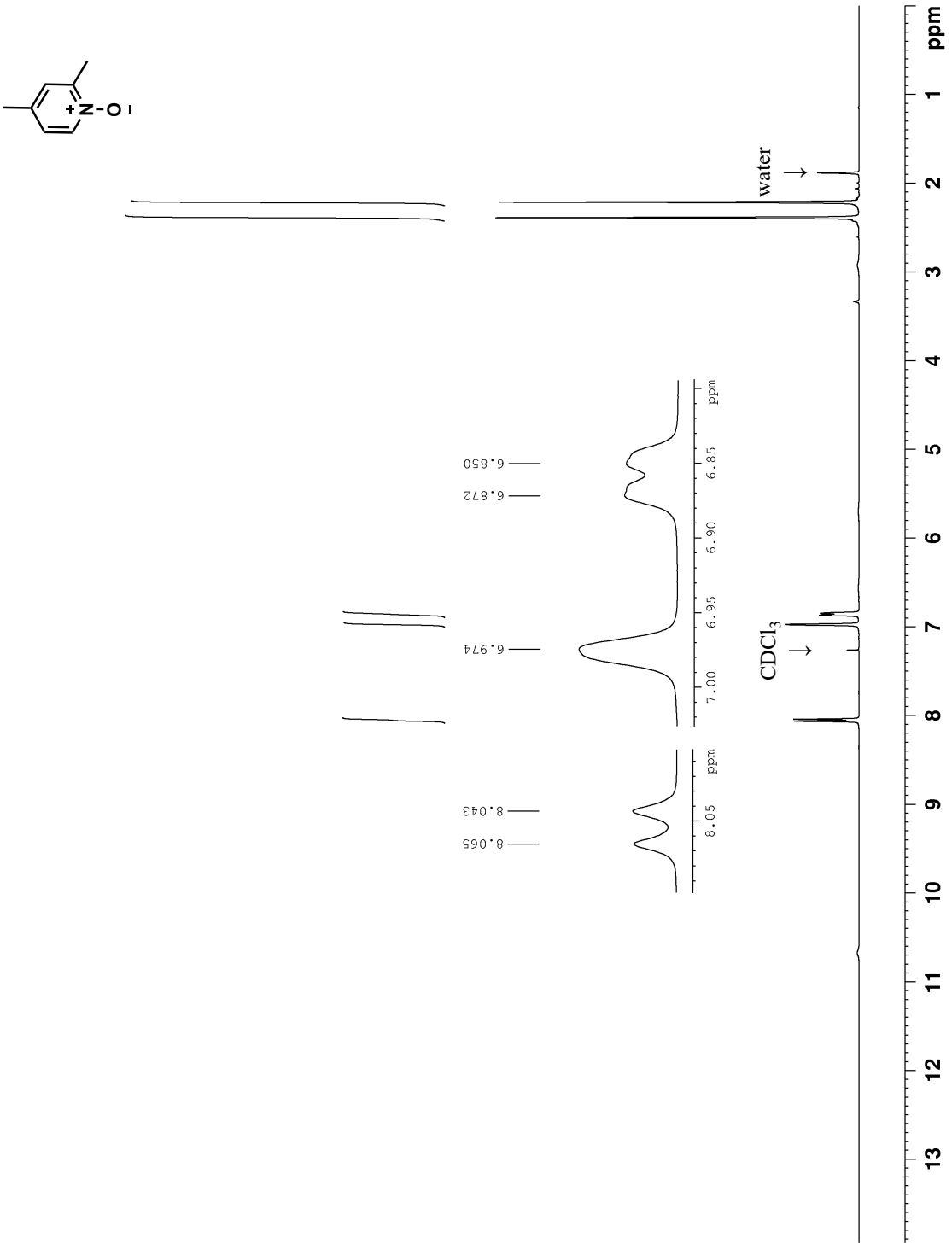

Spectrum 2. ^{1}H NMR spectrum of 2,4-dimethylpyridine 1-oxide (300 MHz, $CDCl_3$, 293K).

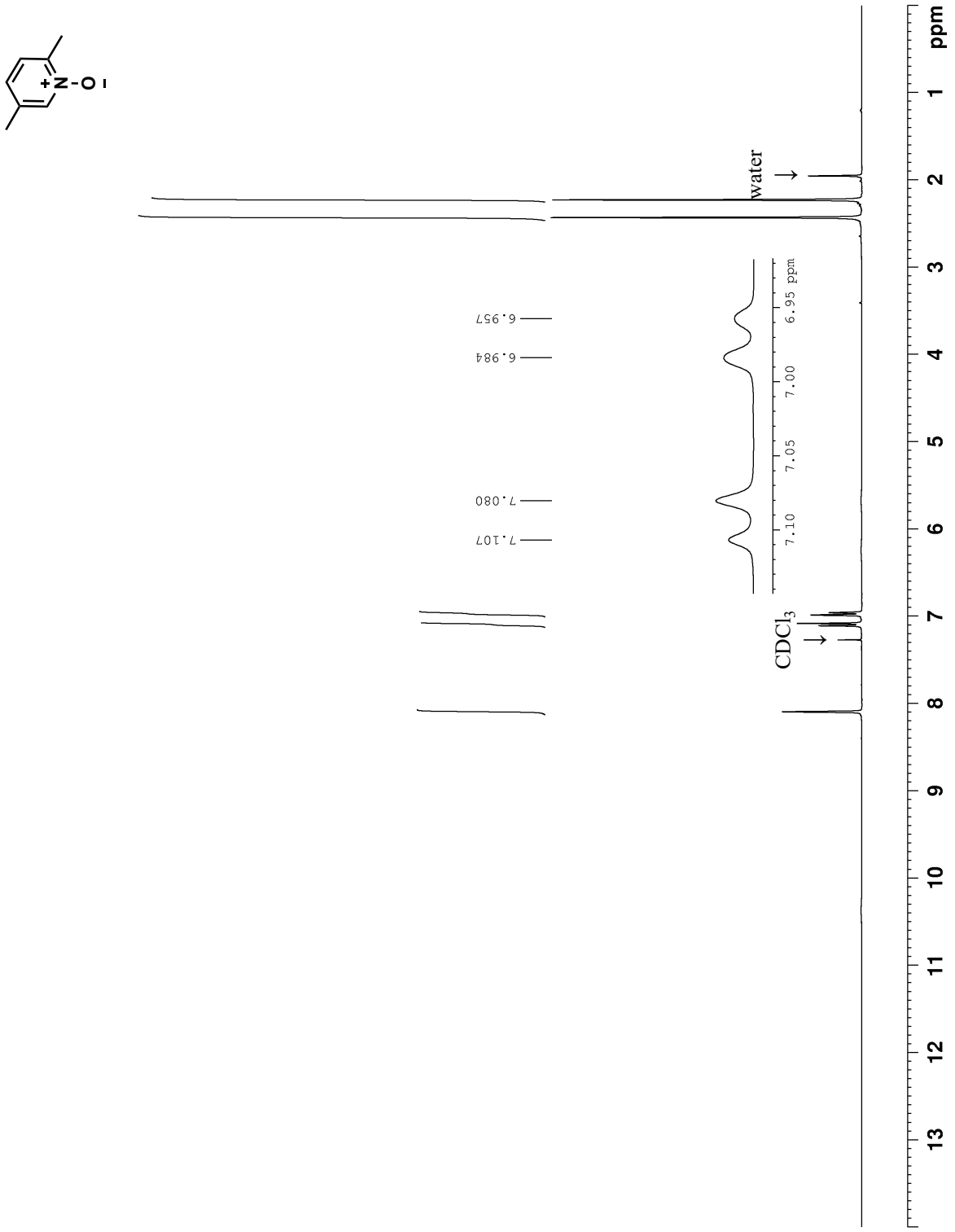

Spectrum 3. ^{1}H NMR spectrum of 2,5-dimethylpyridine 1-oxide (300 MHz, $CDCl_3$, 293K).

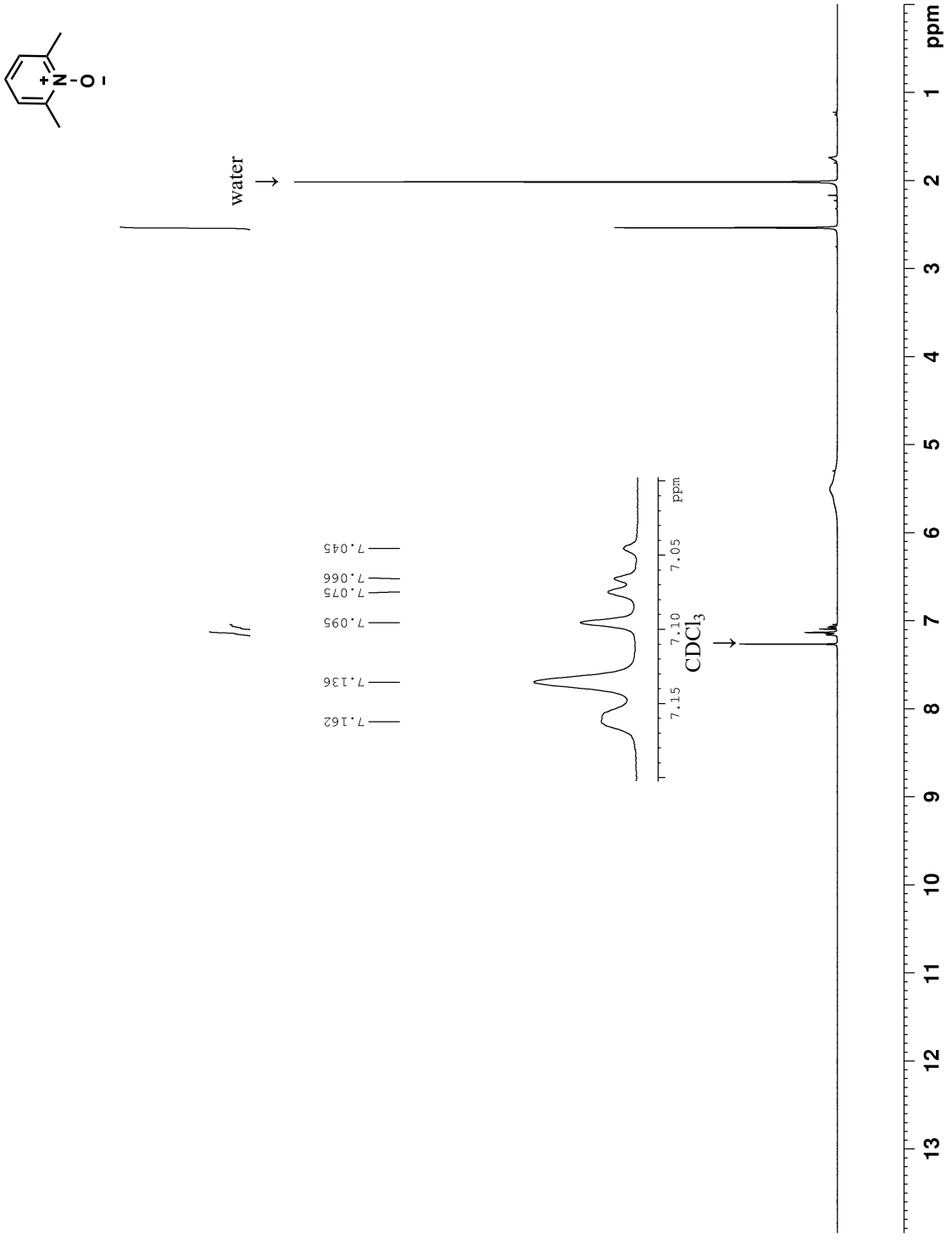

Spectrum 4. ^{1}H NMR spectrum of 2,6-dimethylpyridine 1-oxide (300 MHz, $CDCl_3$, 293K).

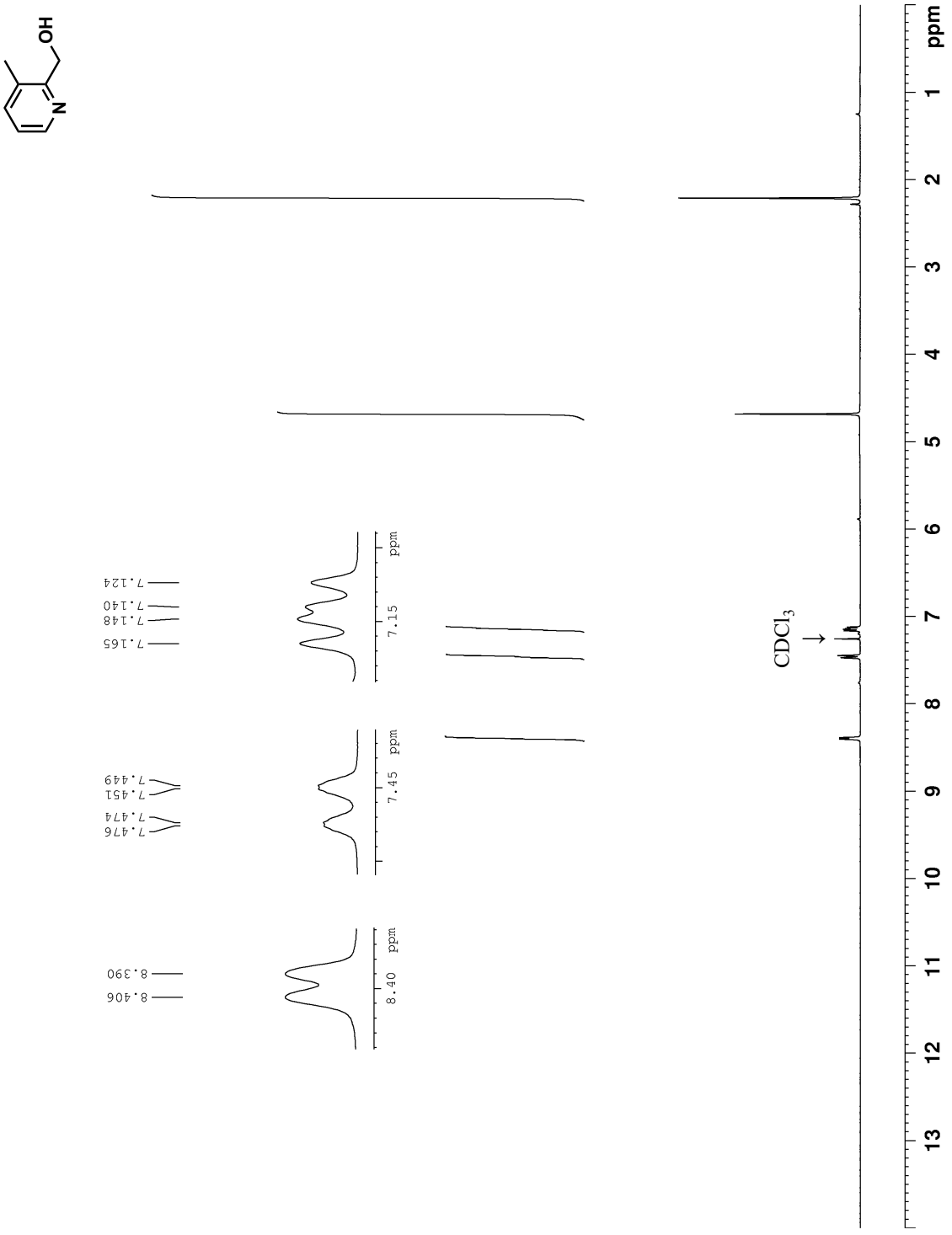

Spectrum 5. ^{1}H NMR spectrum of (3-methylpyridin-2-yl)methanol (300 MHz, $CDCl_3$, 293K).

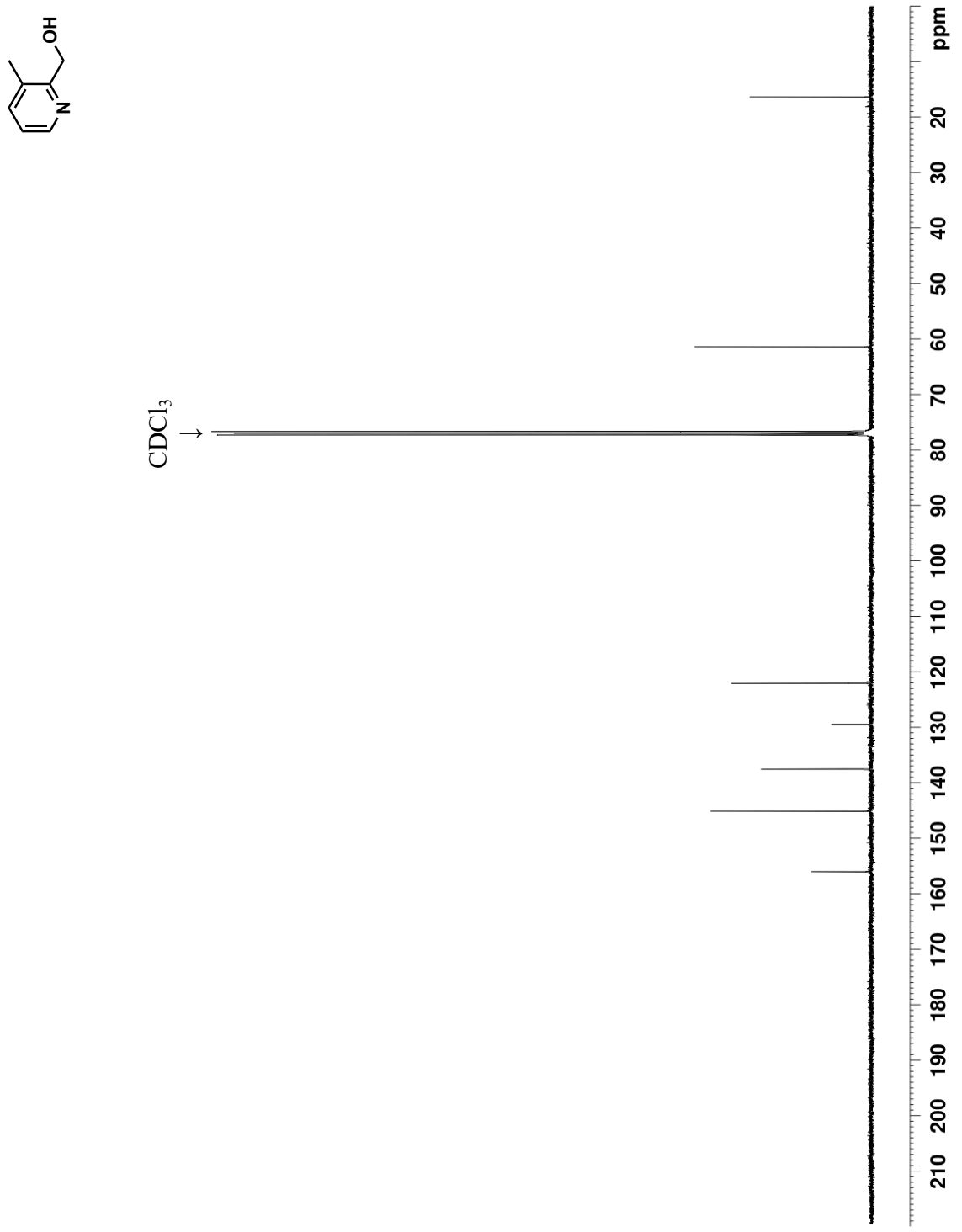

Spectrum 6. ^{13}C NMR spectrum of (3-methylpyridin-2-yl)methanol (100 MHz, $CDCl_3$, 293K).

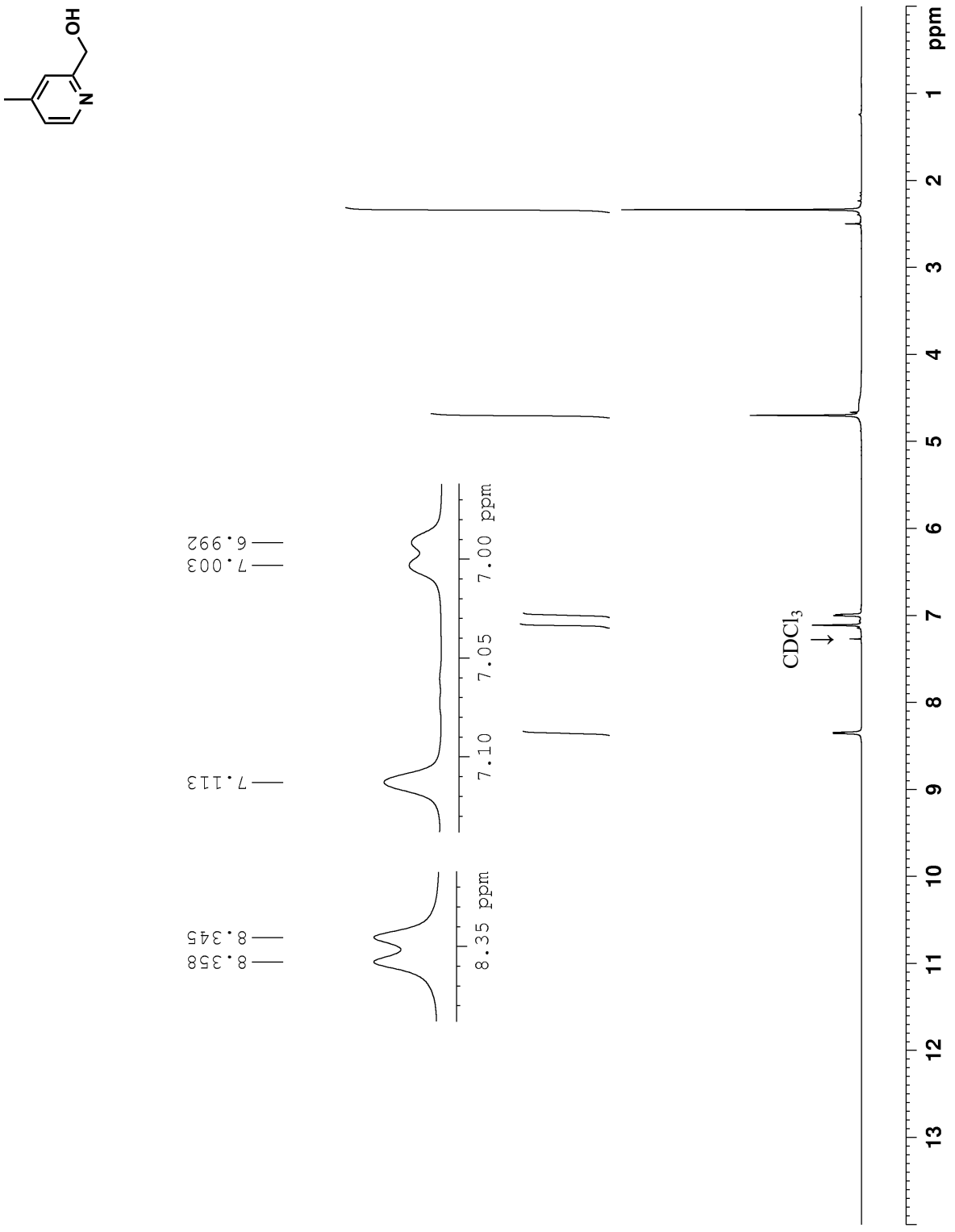

Spectrum 7. ^{1}H NMR spectrum of (4-methylpyridin-2-yl)methanol (400 MHz, $CDCl_3$, 293K).

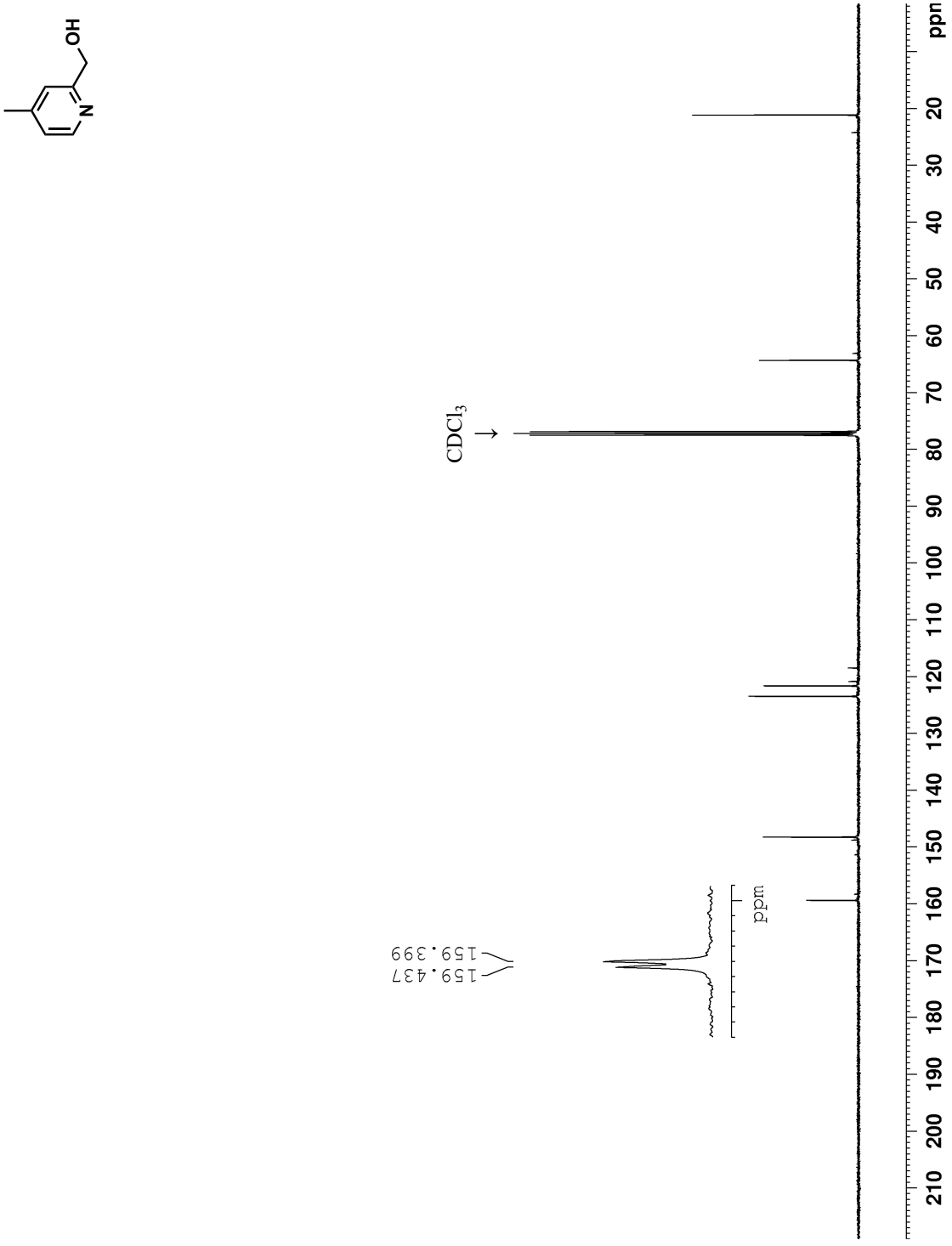

Spectrum 8. ^{13}C NMR spectrum of (4-methylpyridin-2-yl)methanol (100 MHz, $CDCl_3$, 293K).

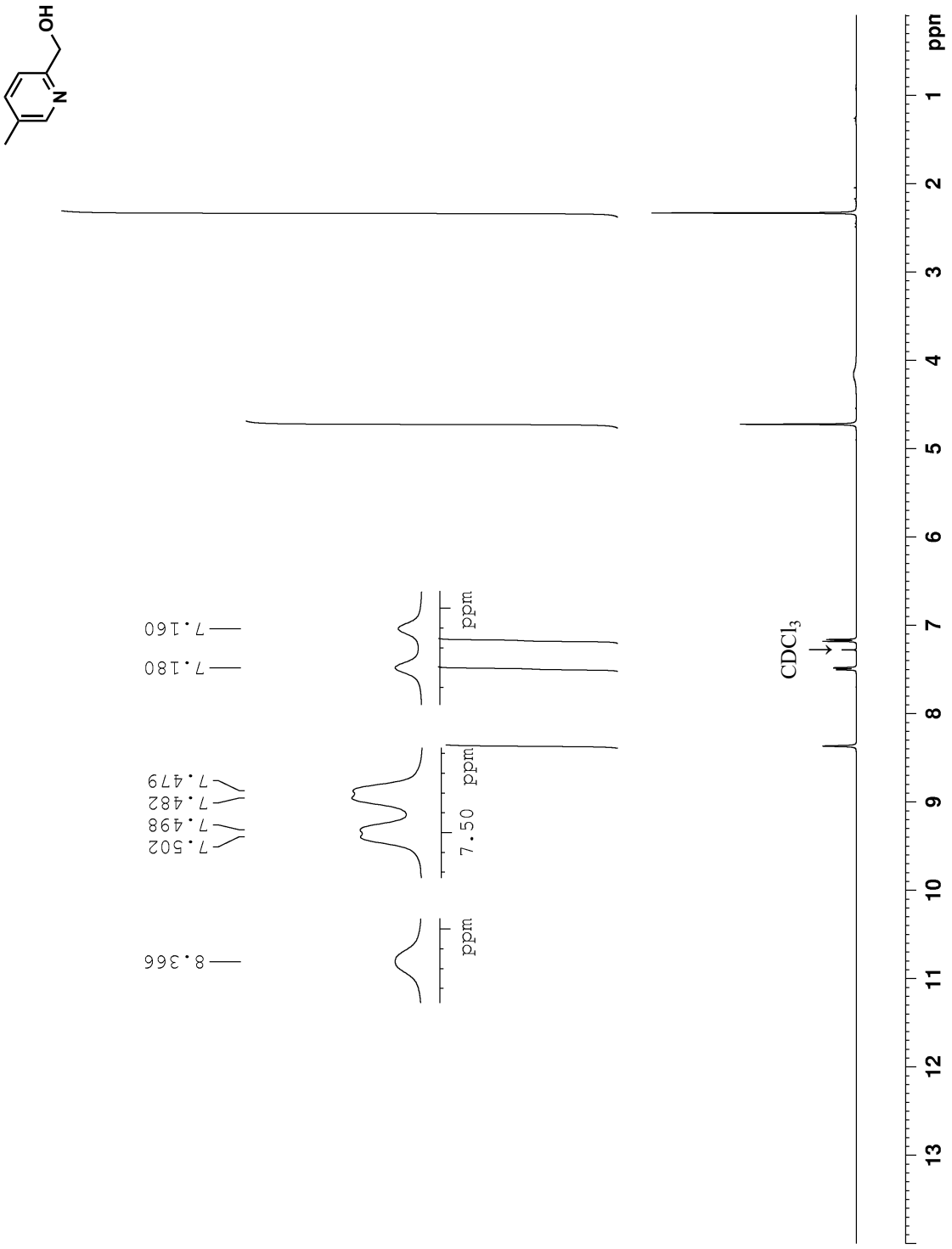

Spectrum 9. ^{1}H NMR spectrum of (5-methylpyridin-2-yl)methanol (400 MHz, $CDCl_3$, 293K).

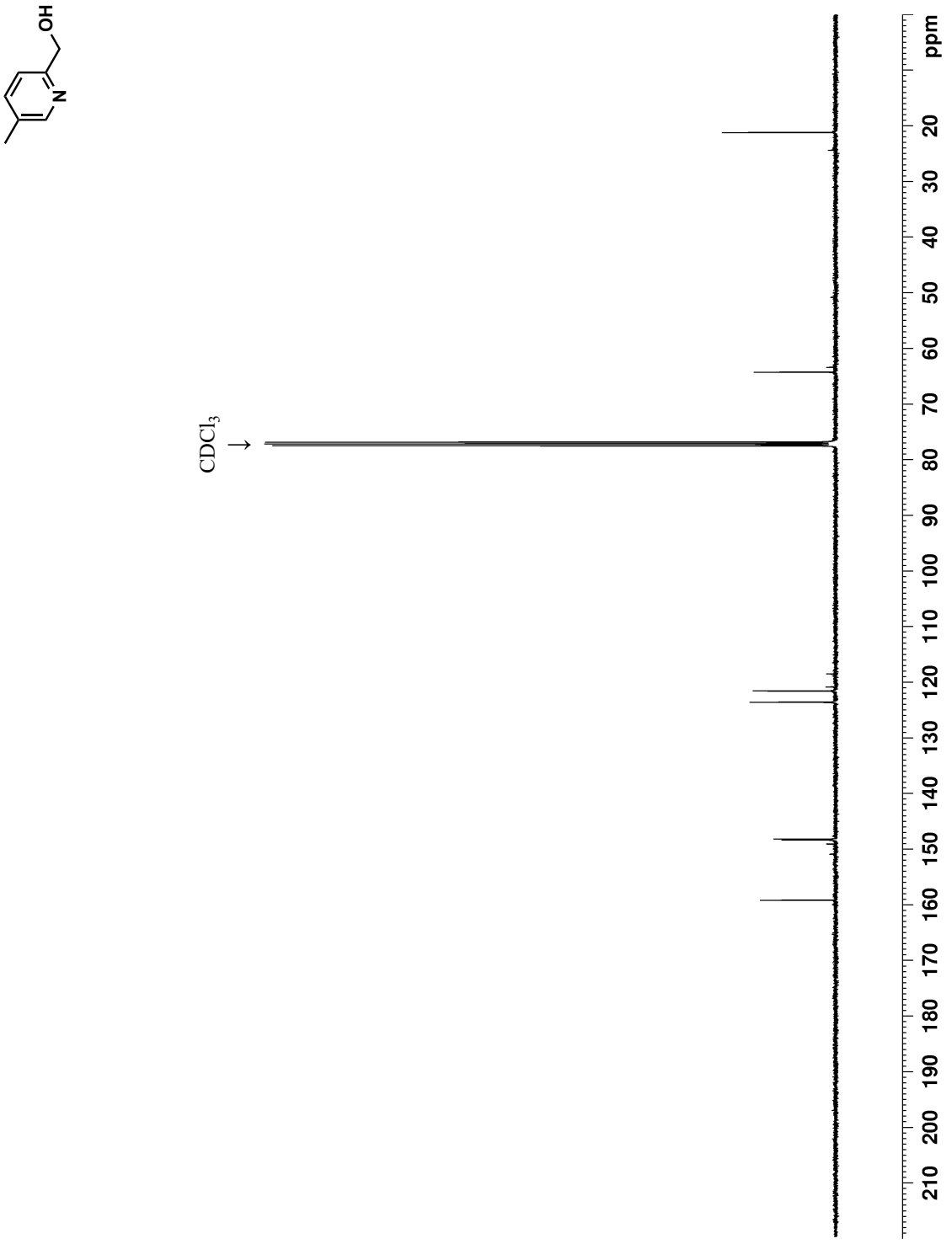

Spectrum 10. ^{13}C NMR spectrum of (5-methylpyridin-2-yl)methanol (100 MHz, $CDCl_3$, 293K).

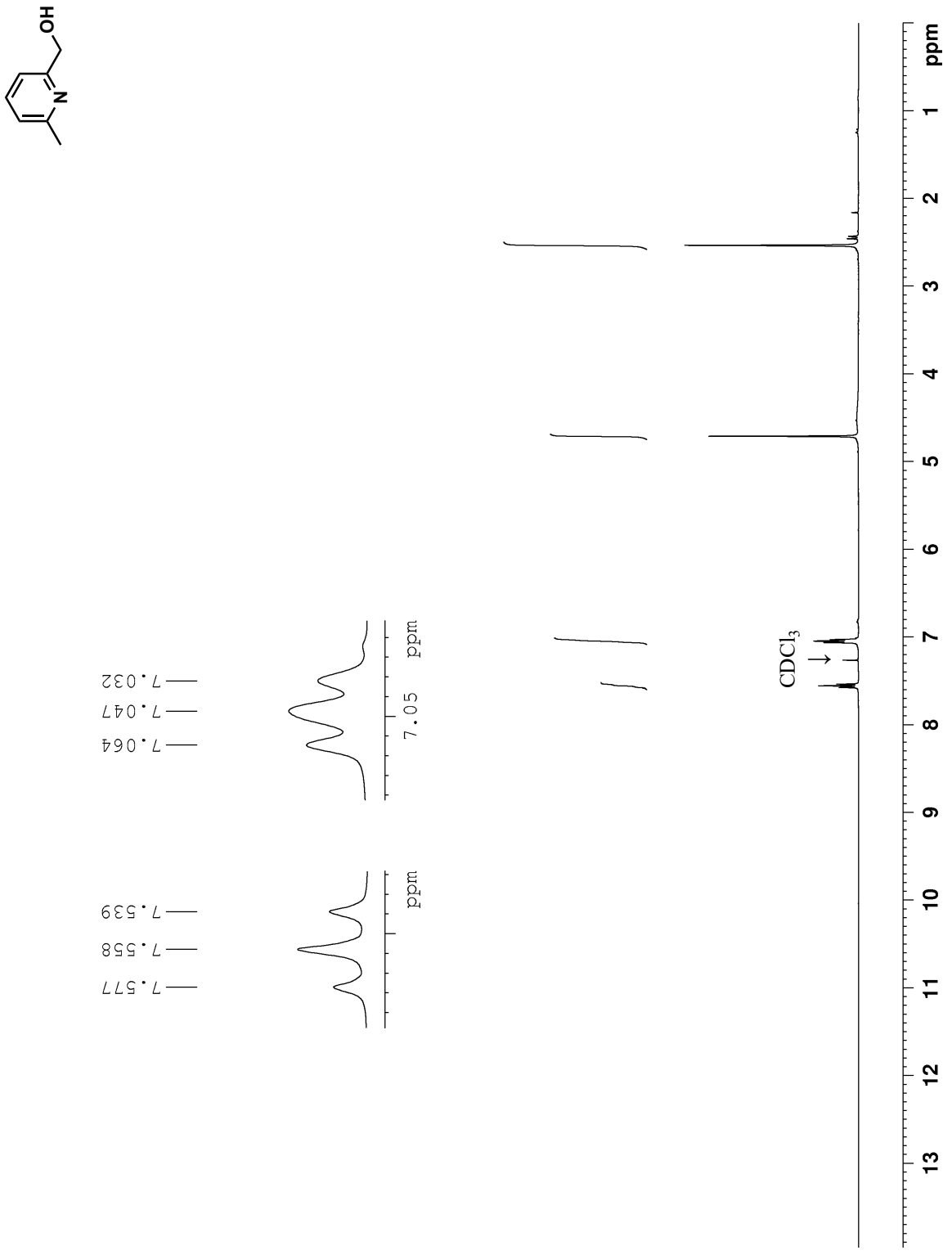

Spectrum 11. ^{1}H NMR spectrum of (6-methylpyridin-2-yl)methanol (400 MHz, $CDCl_3$, 293K).

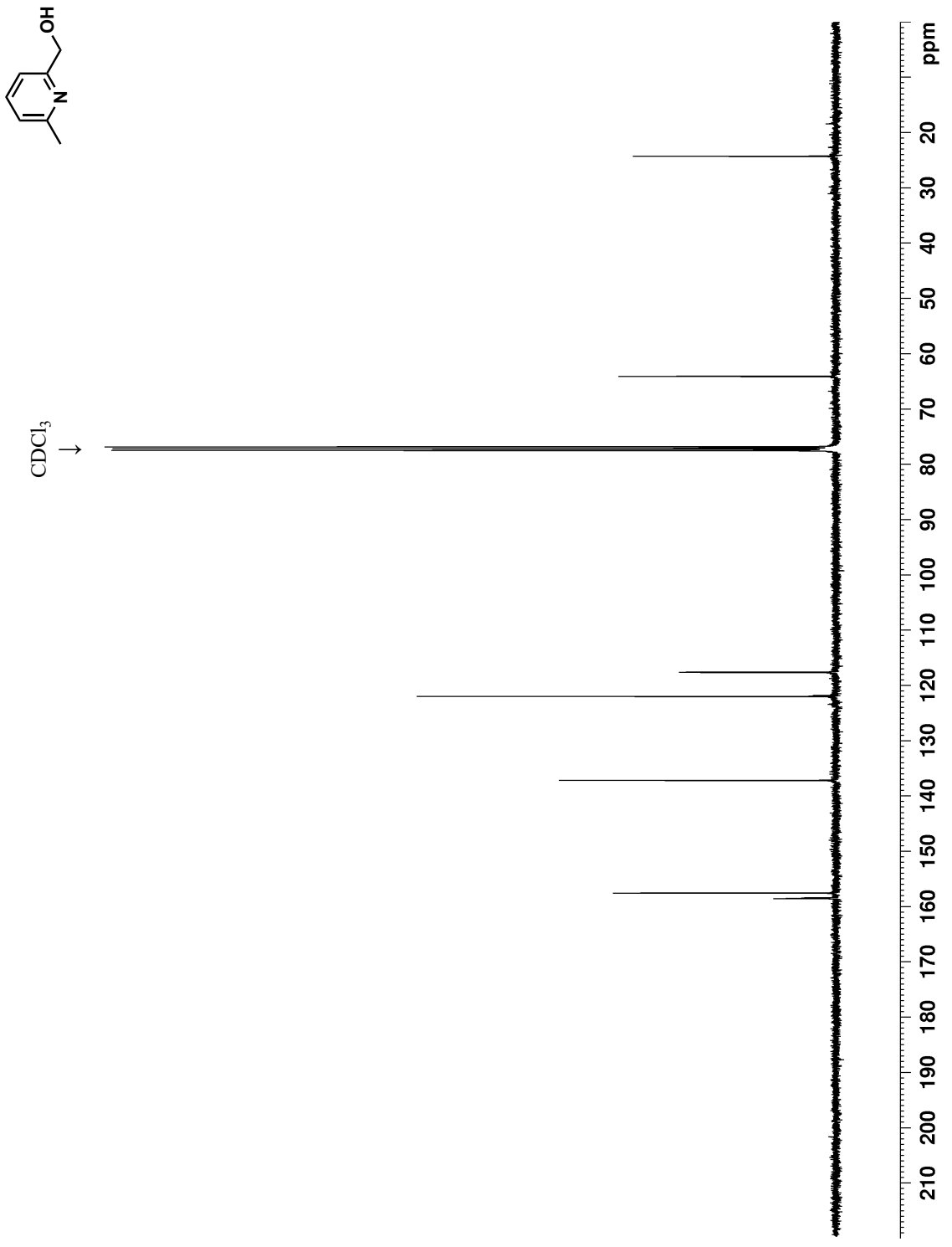

Spectrum 12. ^{13}C NMR spectrum of (6-methylpyridin-2-yl)methanol (100 MHz, $CDCl_3$, 293K).

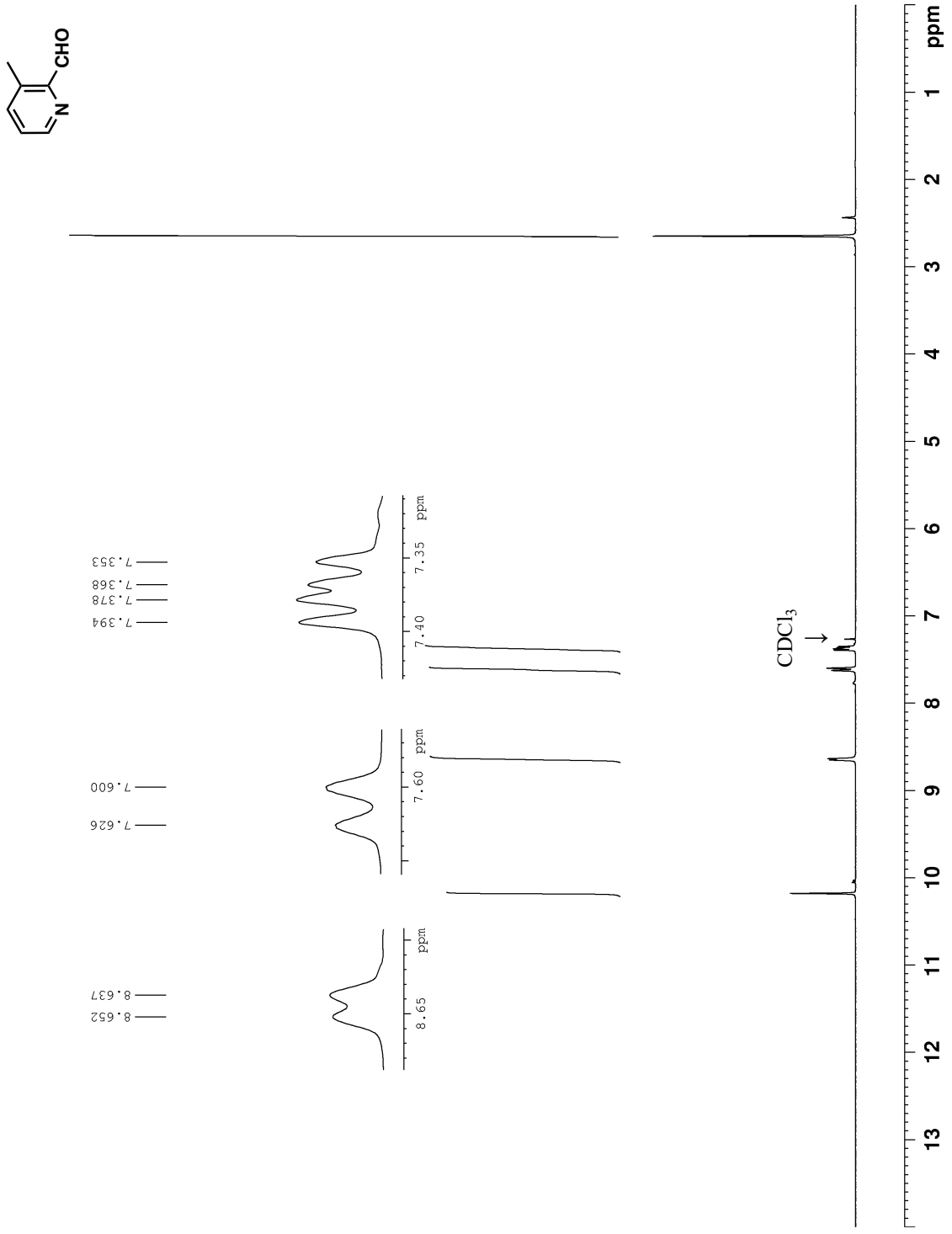

Spectrum 13. ^{1}H NMR spectrum of 3-methylpicolinaldehyde (300 MHz, $CDCl_3$, 293K).

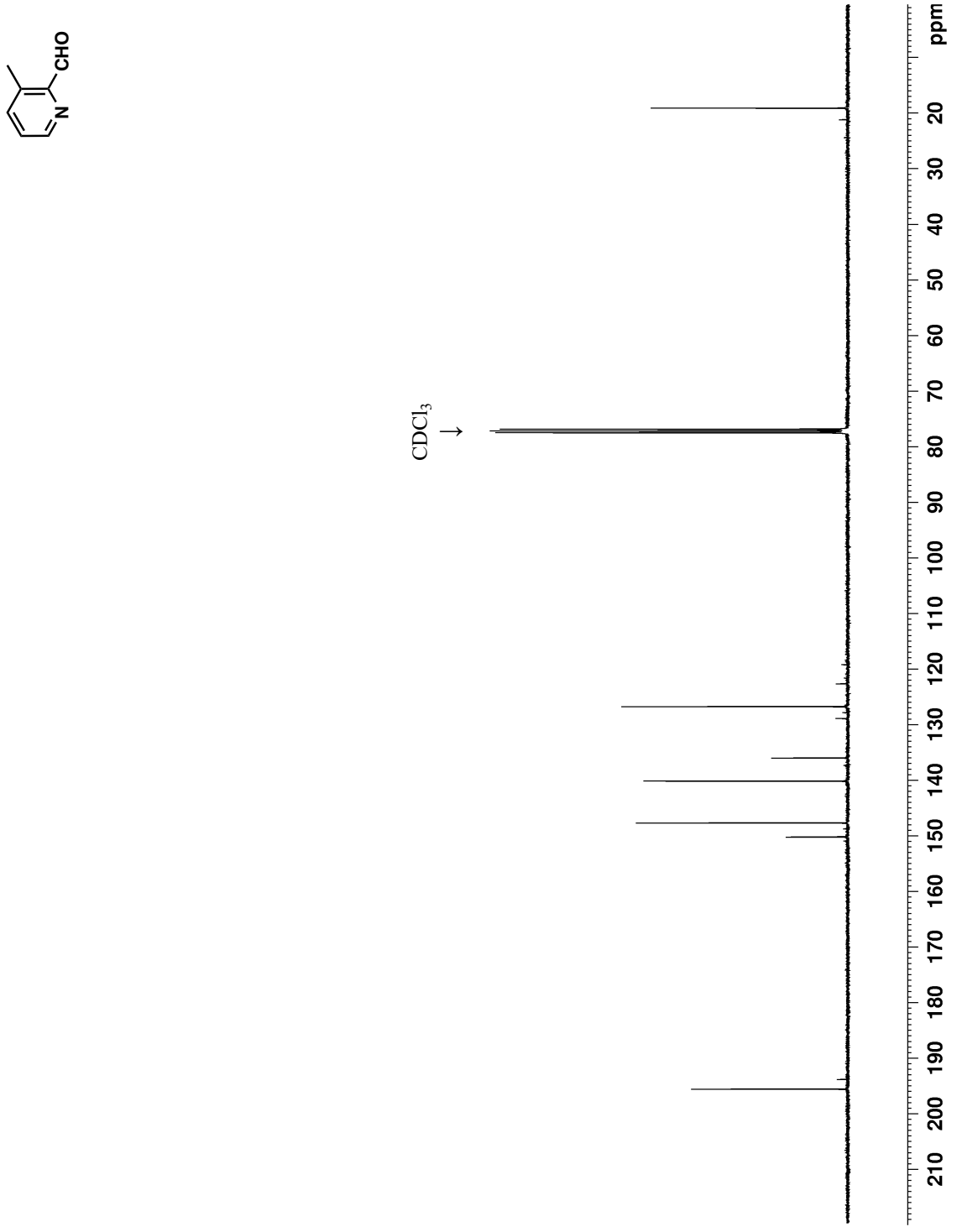

Spectrum 14. ^{13}C NMR spectrum of 3-methylpicolinaldehyde (100 MHz, $CDCl_3$, 293K).

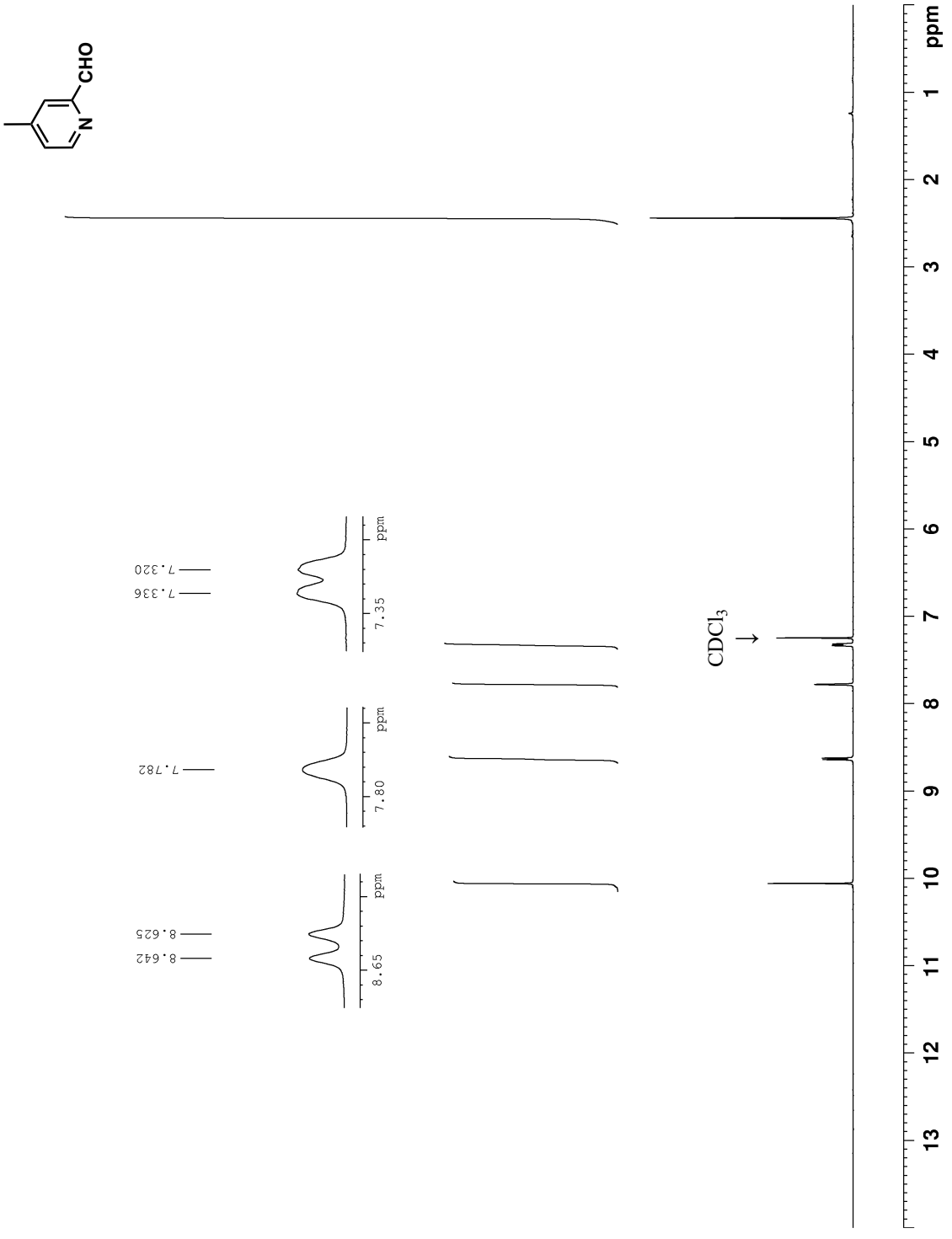

Spectrum 15. ^{1}H NMR spectrum of 4-methylpicolinaldehyde (300 MHz, $CDCl_3$, 293K).

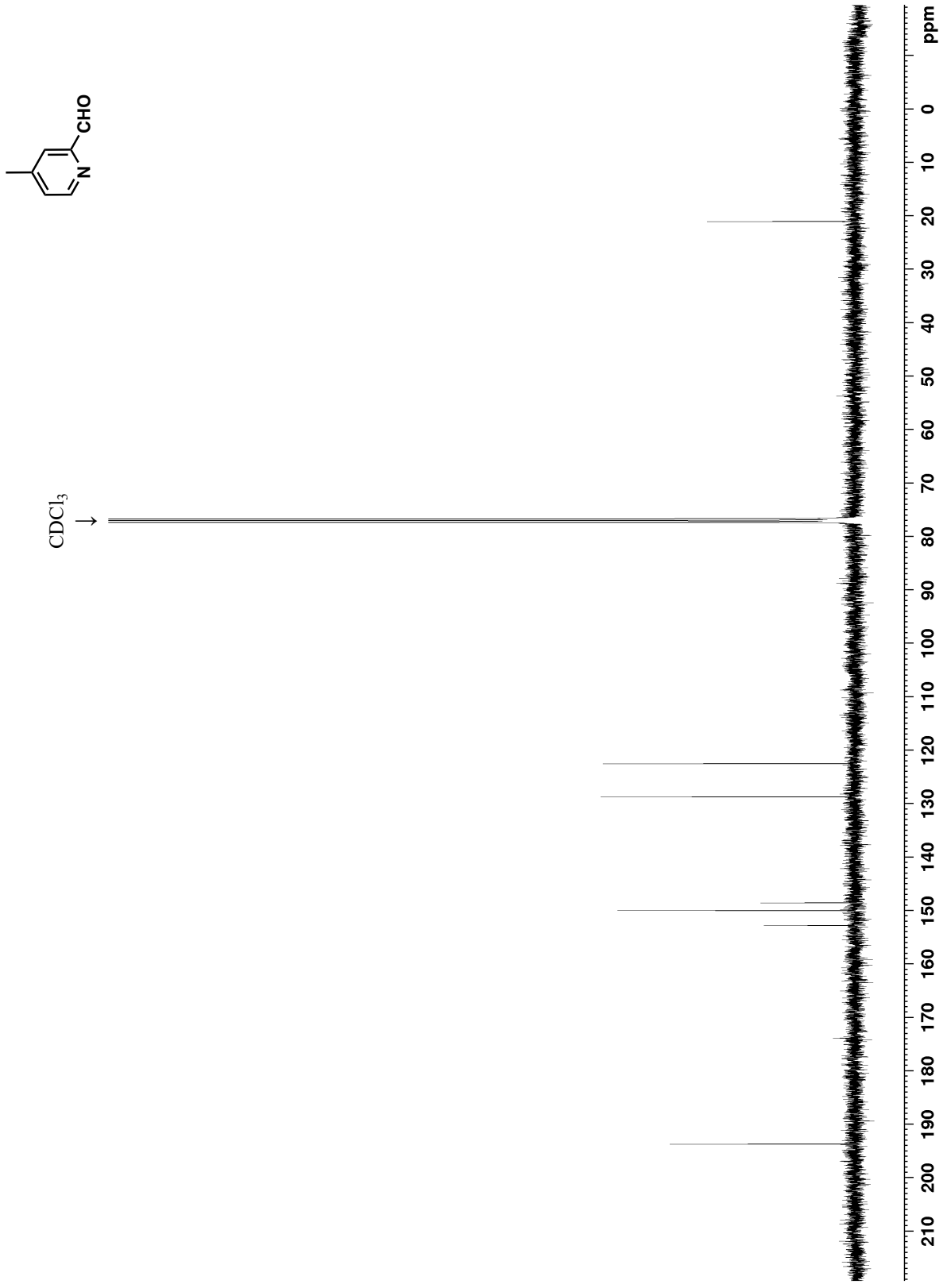

Spectrum 16. ^{13}C NMR spectrum of 4-methylpicolinaldehyde (100 MHz, $CDCl_3$, 293K).

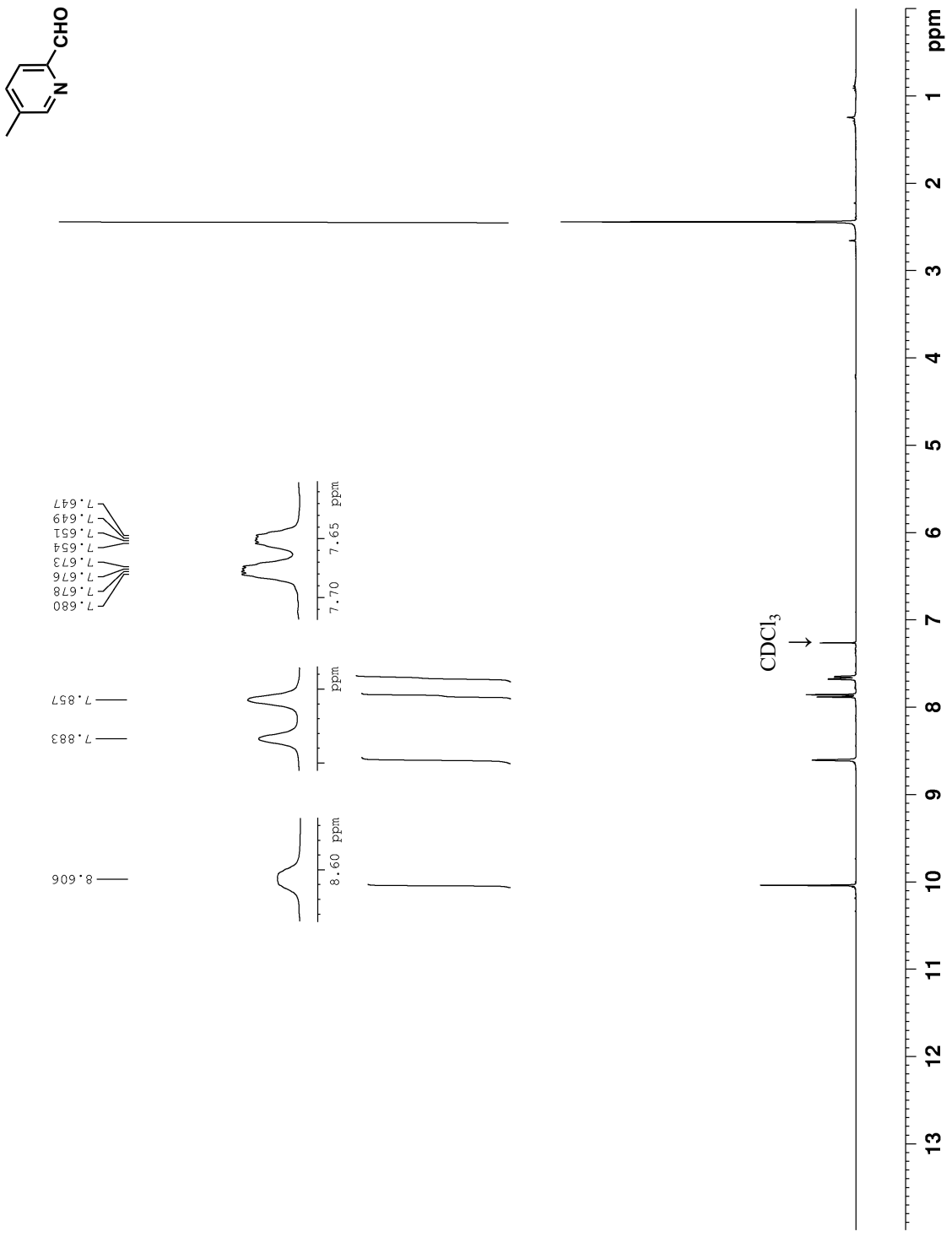

Spectrum 17. ^{1}H NMR spectrum of 5-methylpicolinaldehyde (300 MHz, $CDCl_3$, 293K).

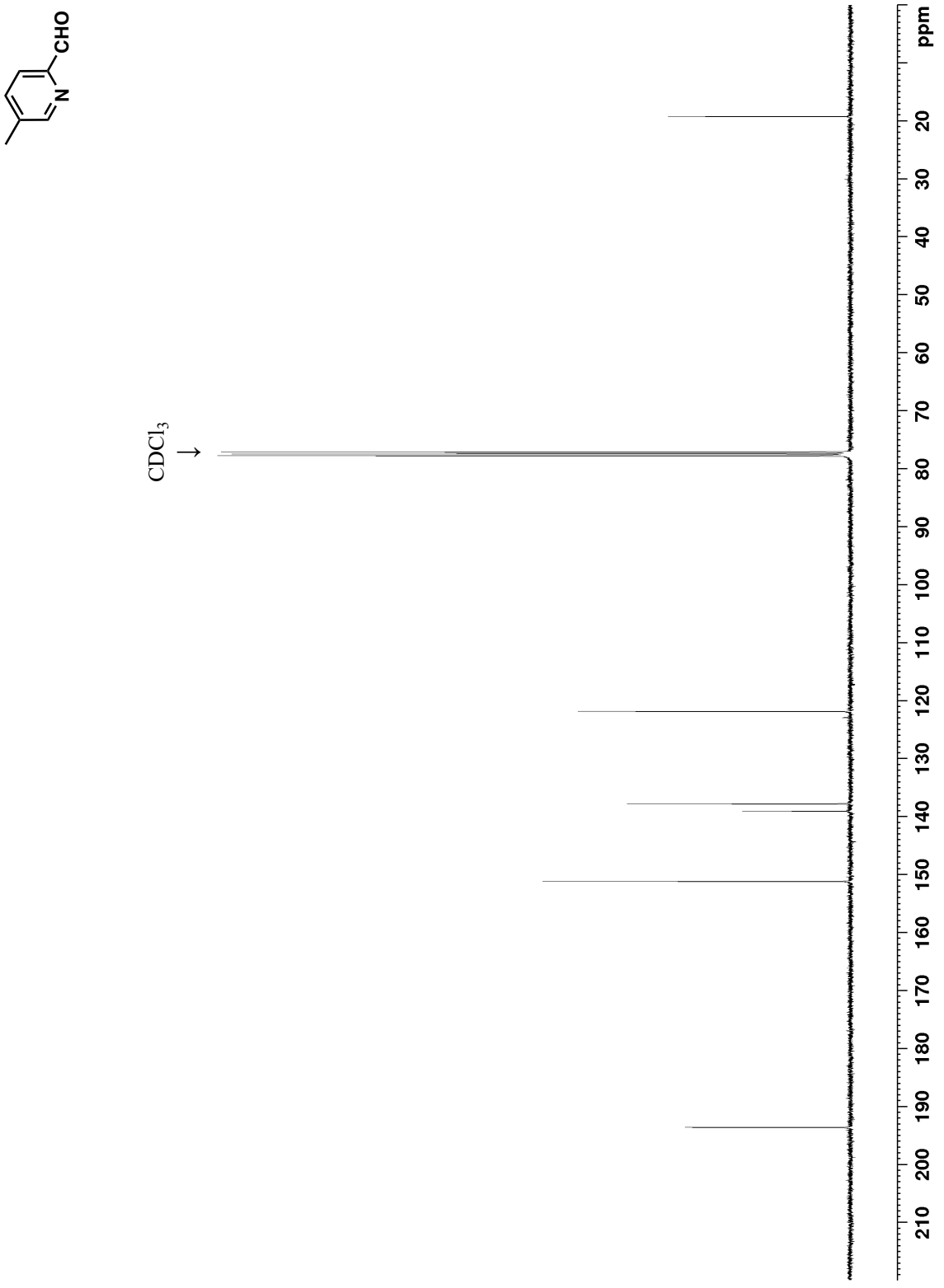

Spectrum 18. ^{13}C NMR spectrum of 5-methylpicolinaldehyde (100 MHz, $CDCl_3$, 293K).

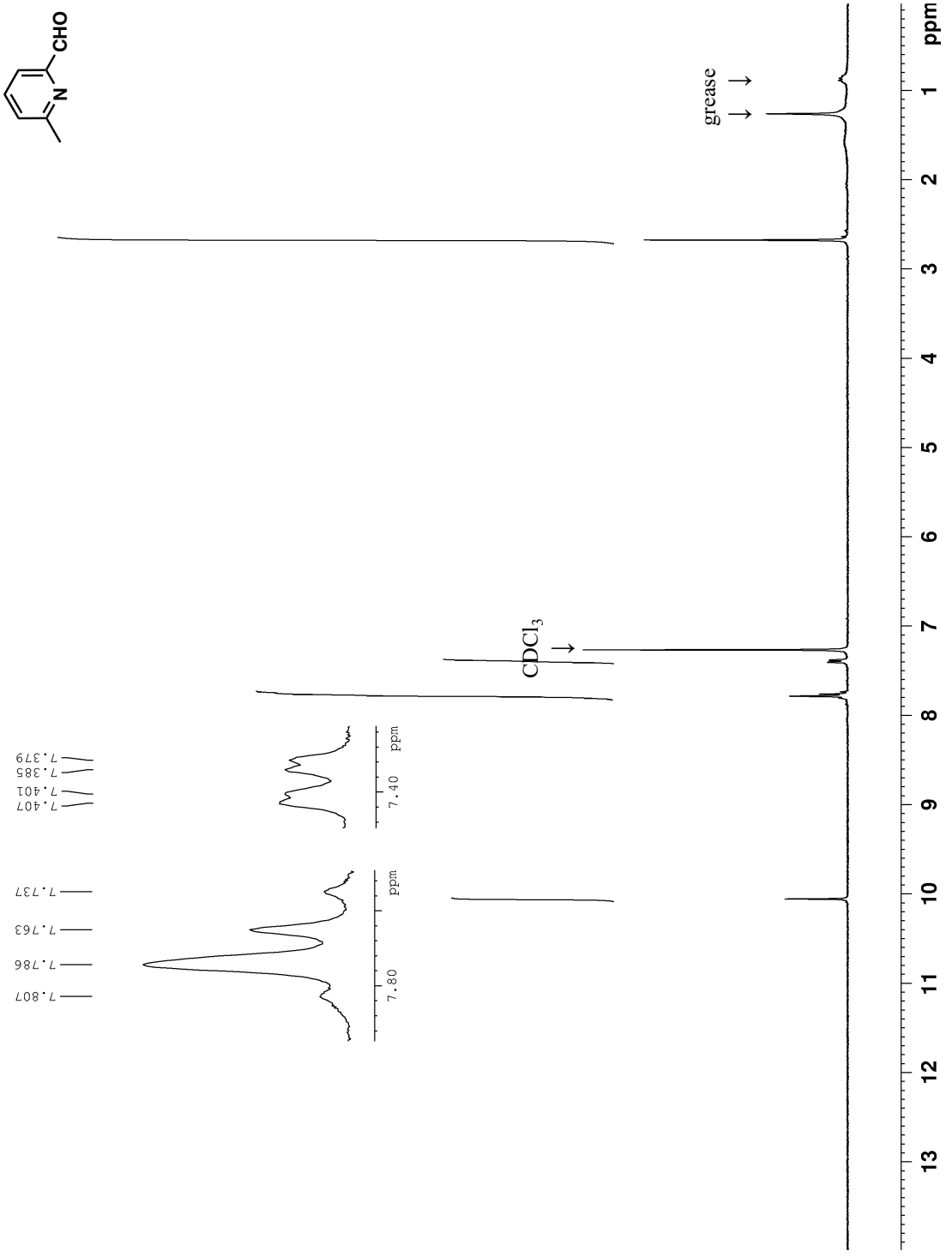

Spectrum 19. ^{1}H NMR spectrum of 6-methylpicolinaldehyde (400 MHz, $CDCl_3$, 293K).

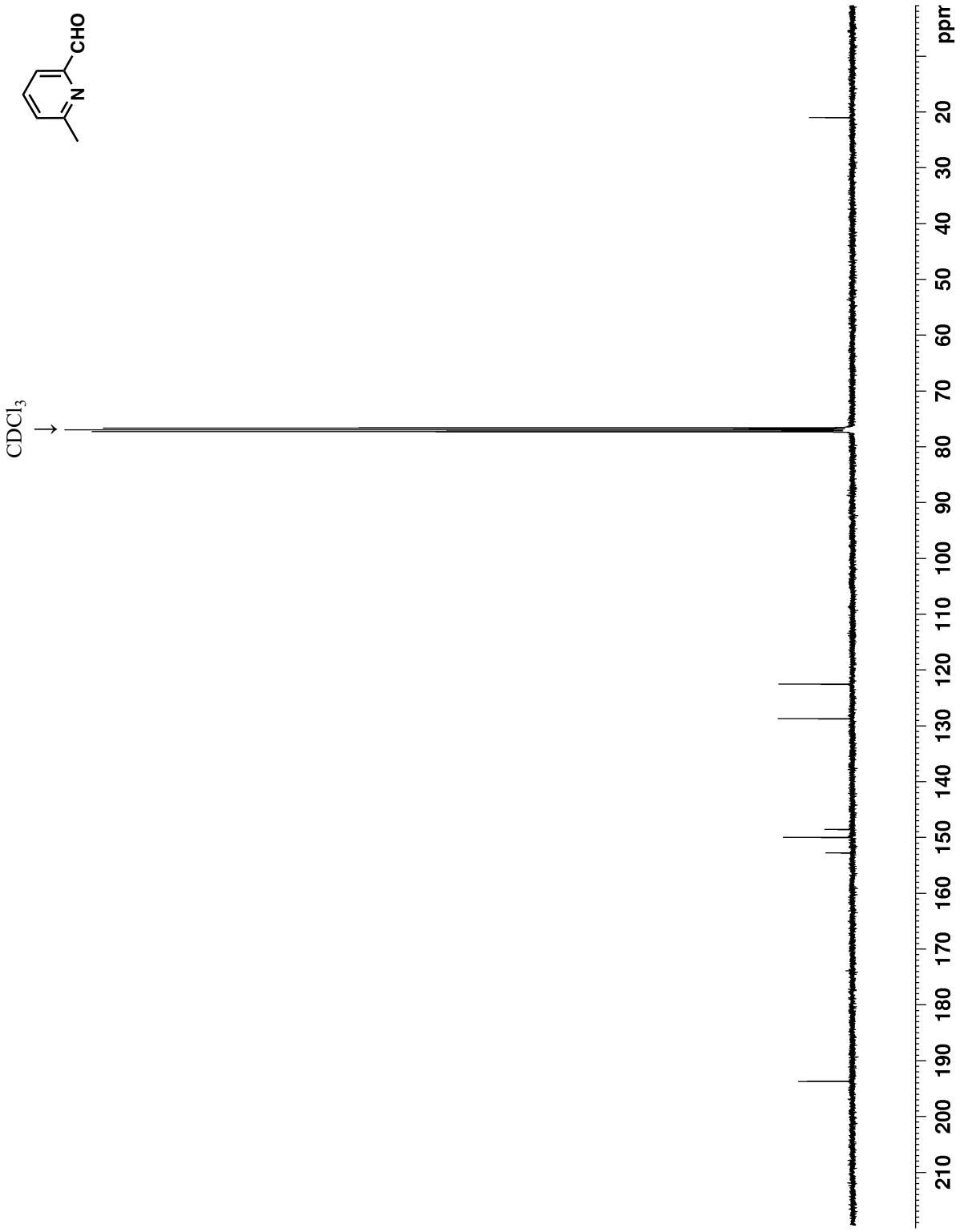

Spectrum 20. ^{13}C NMR spectrum of 6-methylpicolinaldehyde (100 MHz, $CDCl_3$, 293K).

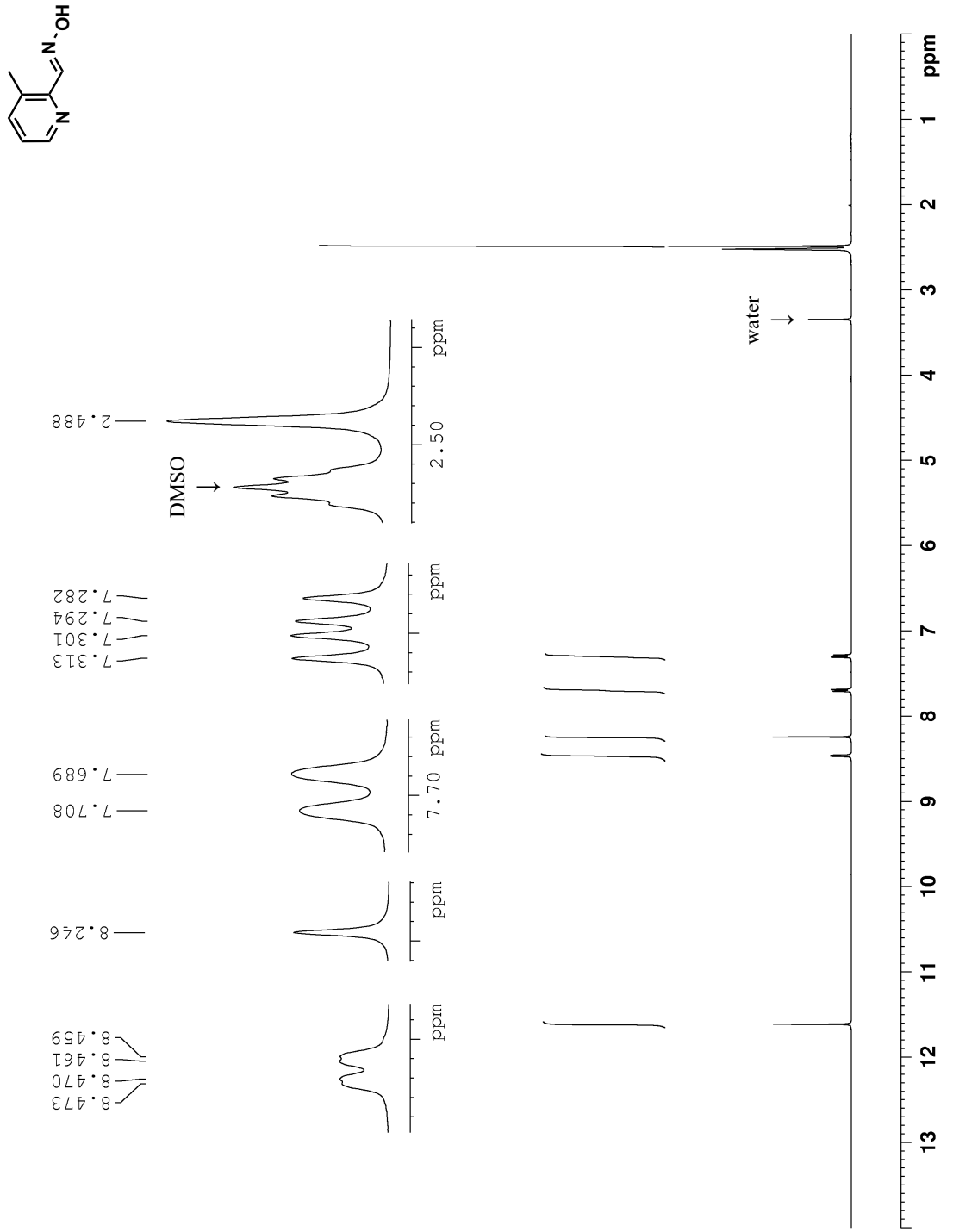

Spectrum 21. ^{1}H NMR spectrum of (E)-3-methylpicolinaldehyde oxime (400 MHz, DMSO-d_6, 293K).

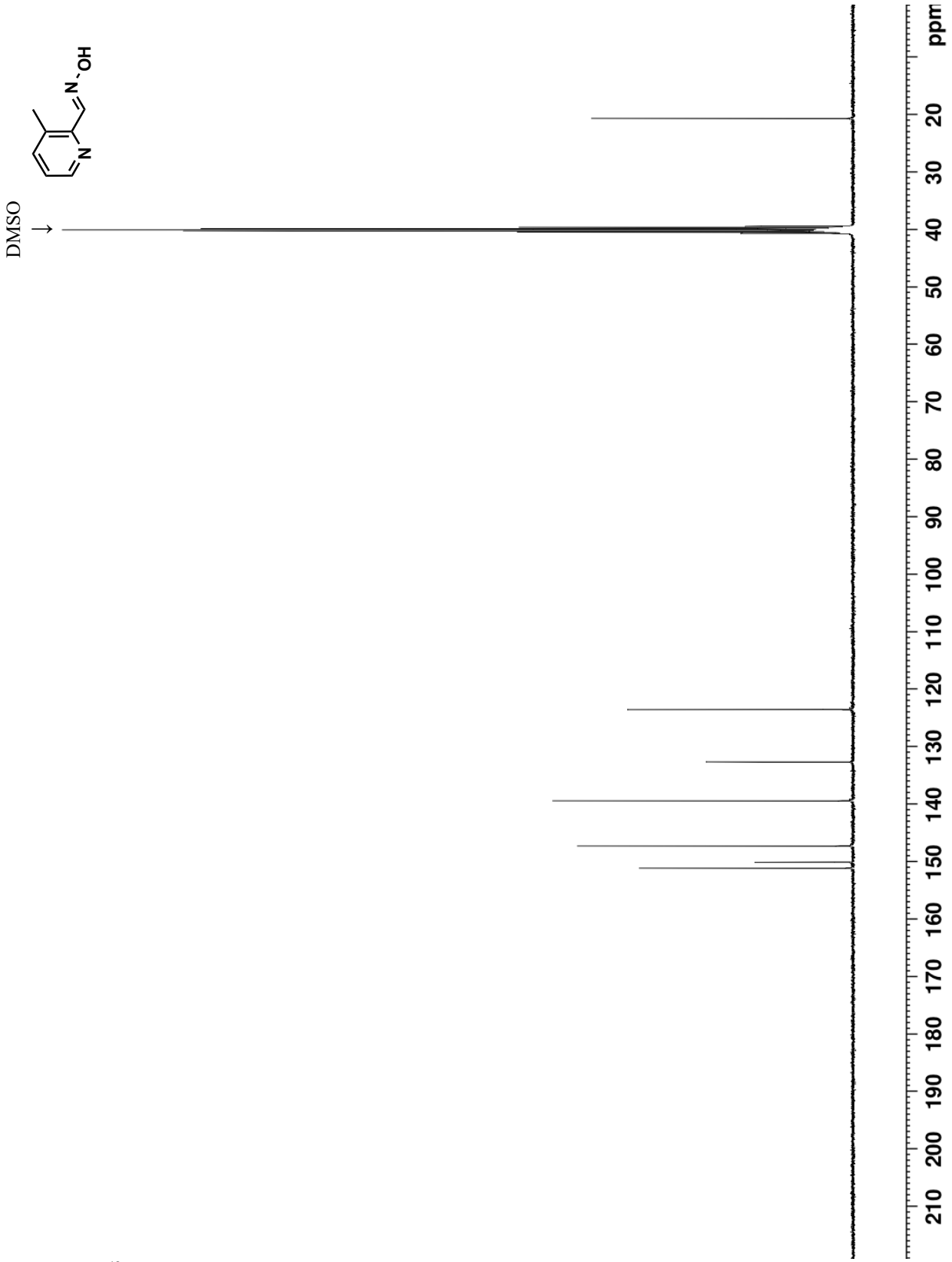

Spectrum 22. ^{13}C NMR spectrum of (E)-3-methylpicolinaldehyde oxime (100 MHz, DMSO-d_6, 293K).

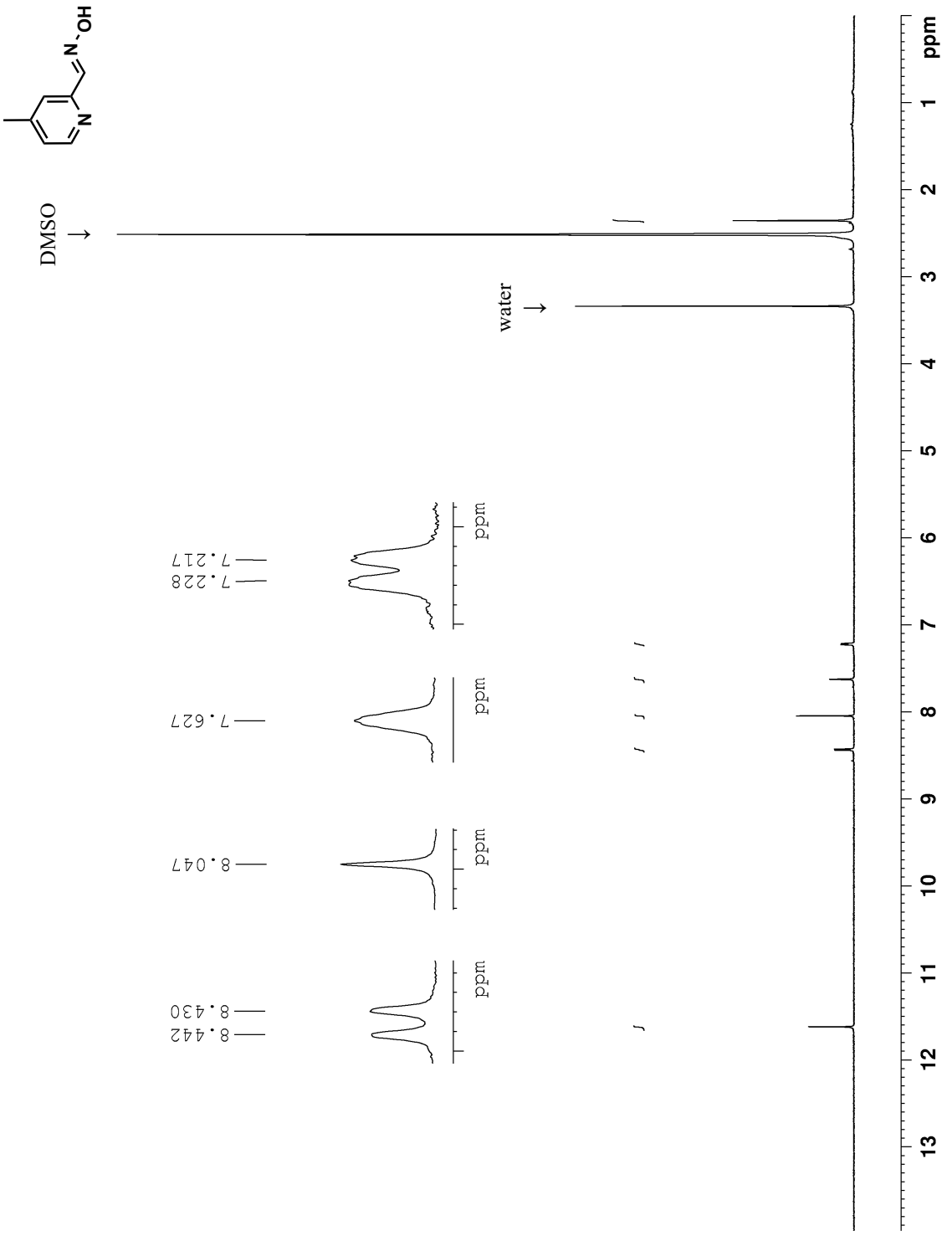

Spectrum 23. ^{1}H NMR spectrum of (E)-4-methylpicolinaldehyde oxime (400 MHz, DMSO-d_6, 293K)

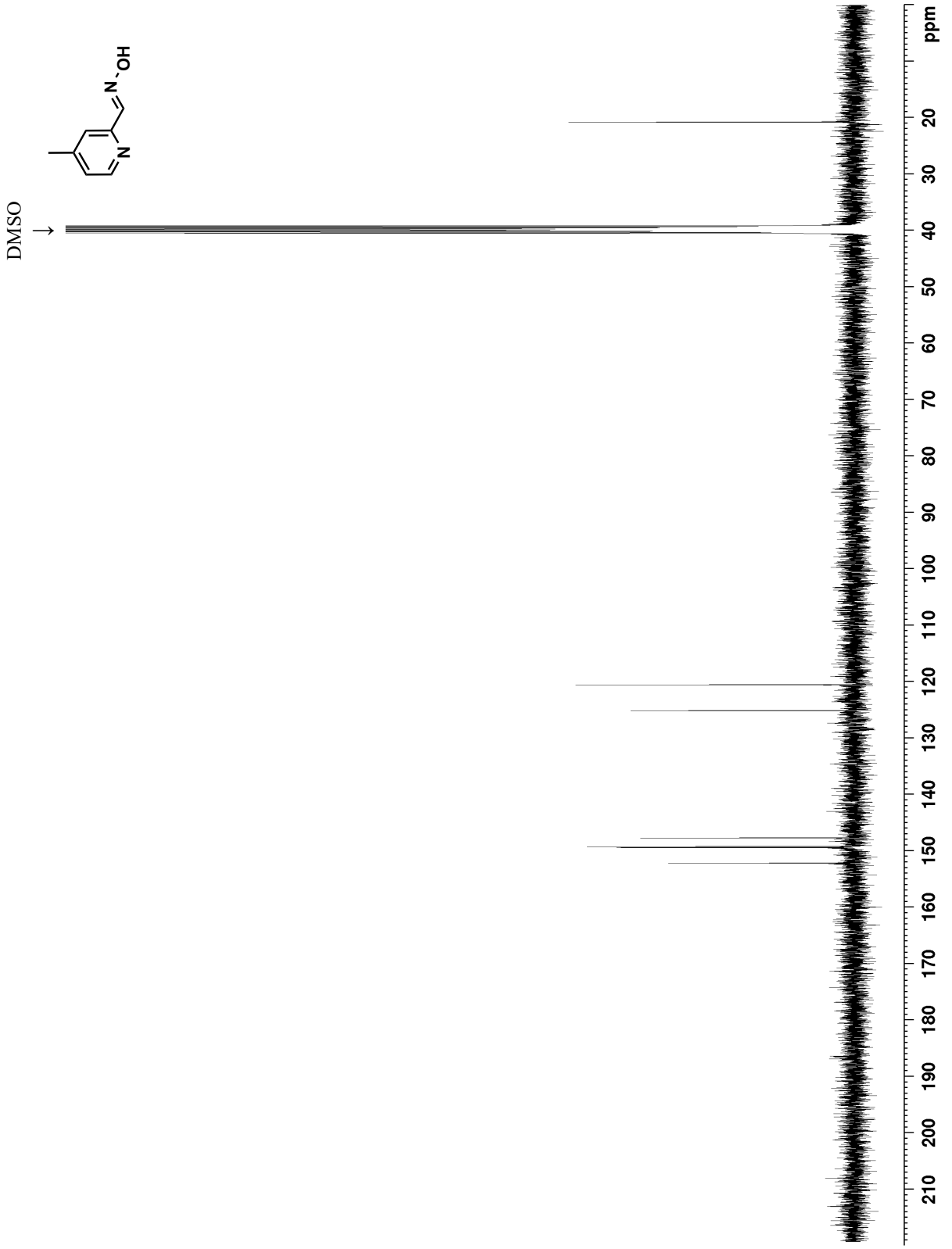

Spectrum 24. ^{13}C NMR spectrum of (E)-4-methylpicolinaldehyde oxime (100 MHz, DMSO-d_6, 293K).

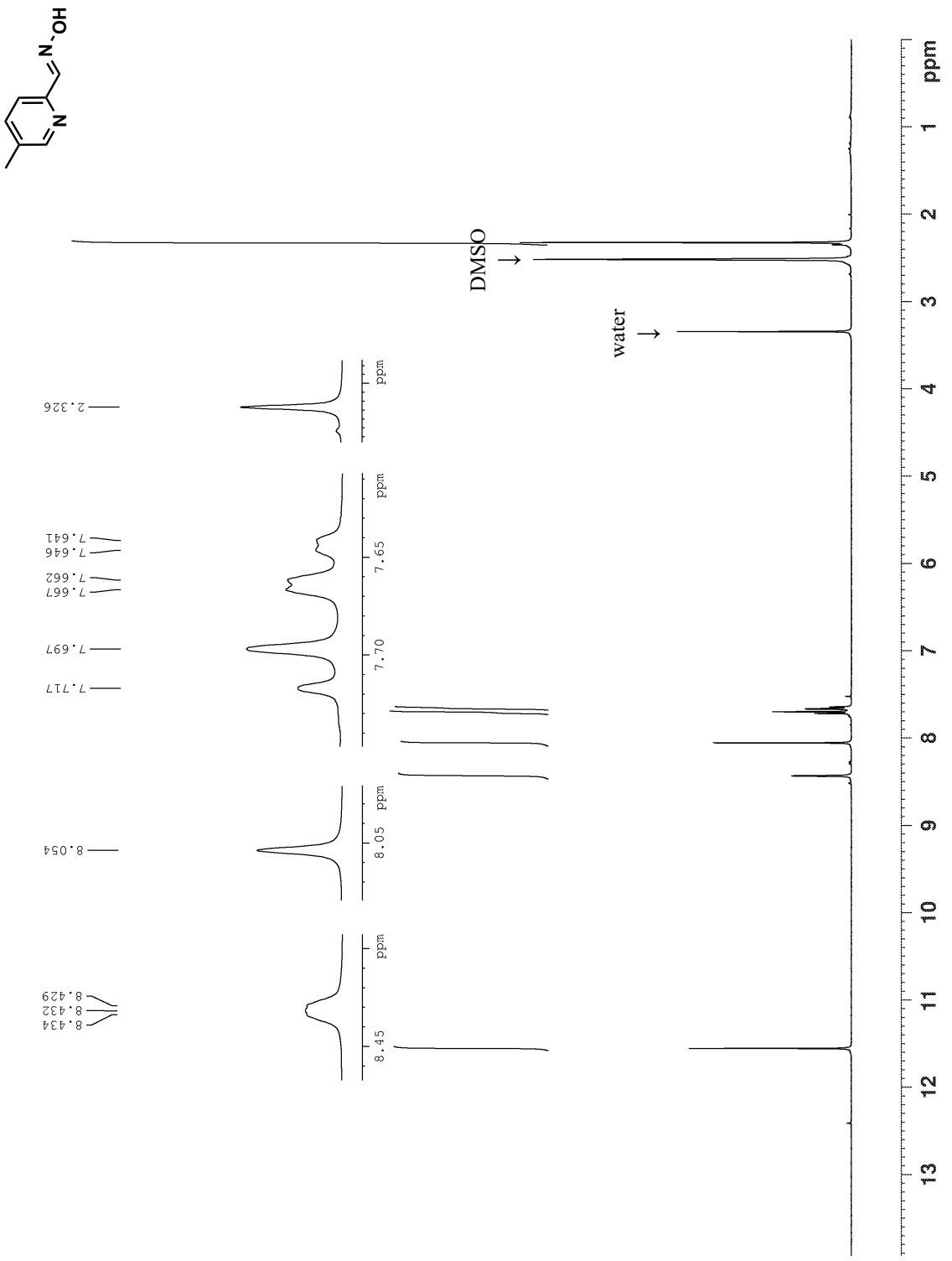

Spectrum 25. ^{1}H NMR spectrum of (E)-5-methylpicolinaldehyde oxime (400 MHz, DMSO-d_6, 293K).

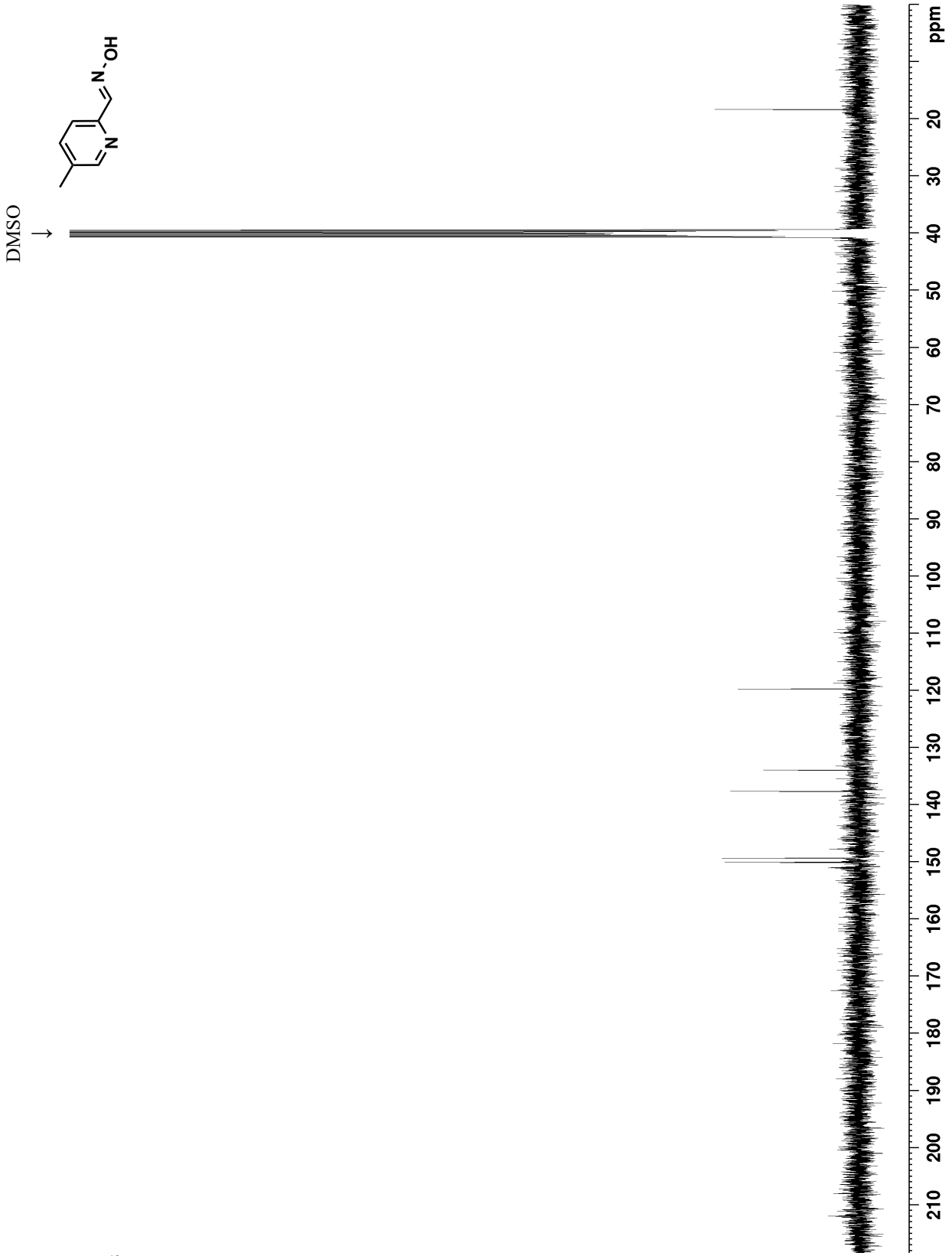

Spectrum 26. ^{13}C NMR spectrum of (E)-5-methylpicolinaldehyde oxime (100 MHz, DMSO-d_6, 293K).

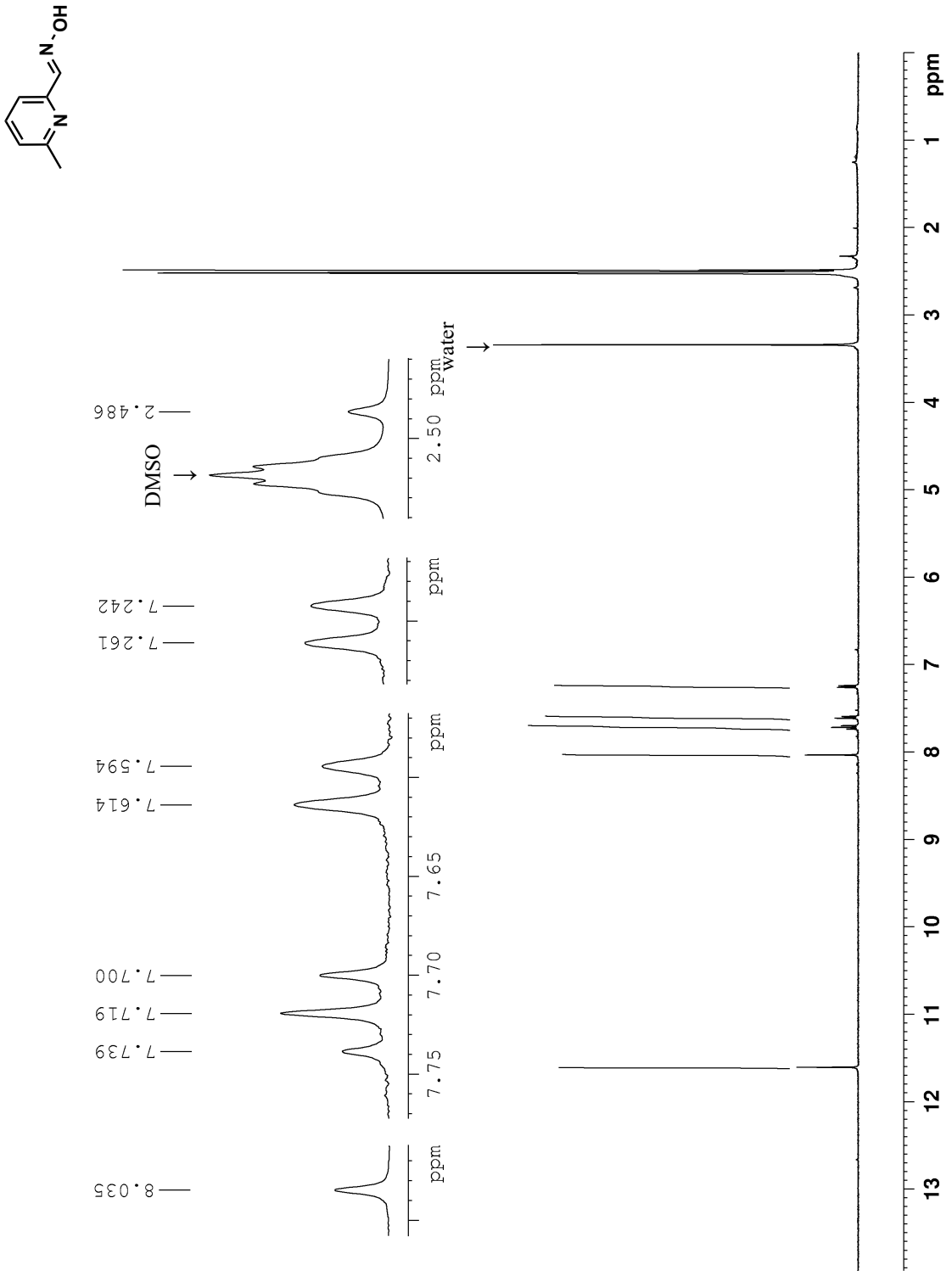

Spectrum 27. [1]H NMR spectrum of (E)-6-methylpicolinaldehyde oxime (400 MHz, DMSO-d_6, 293K).

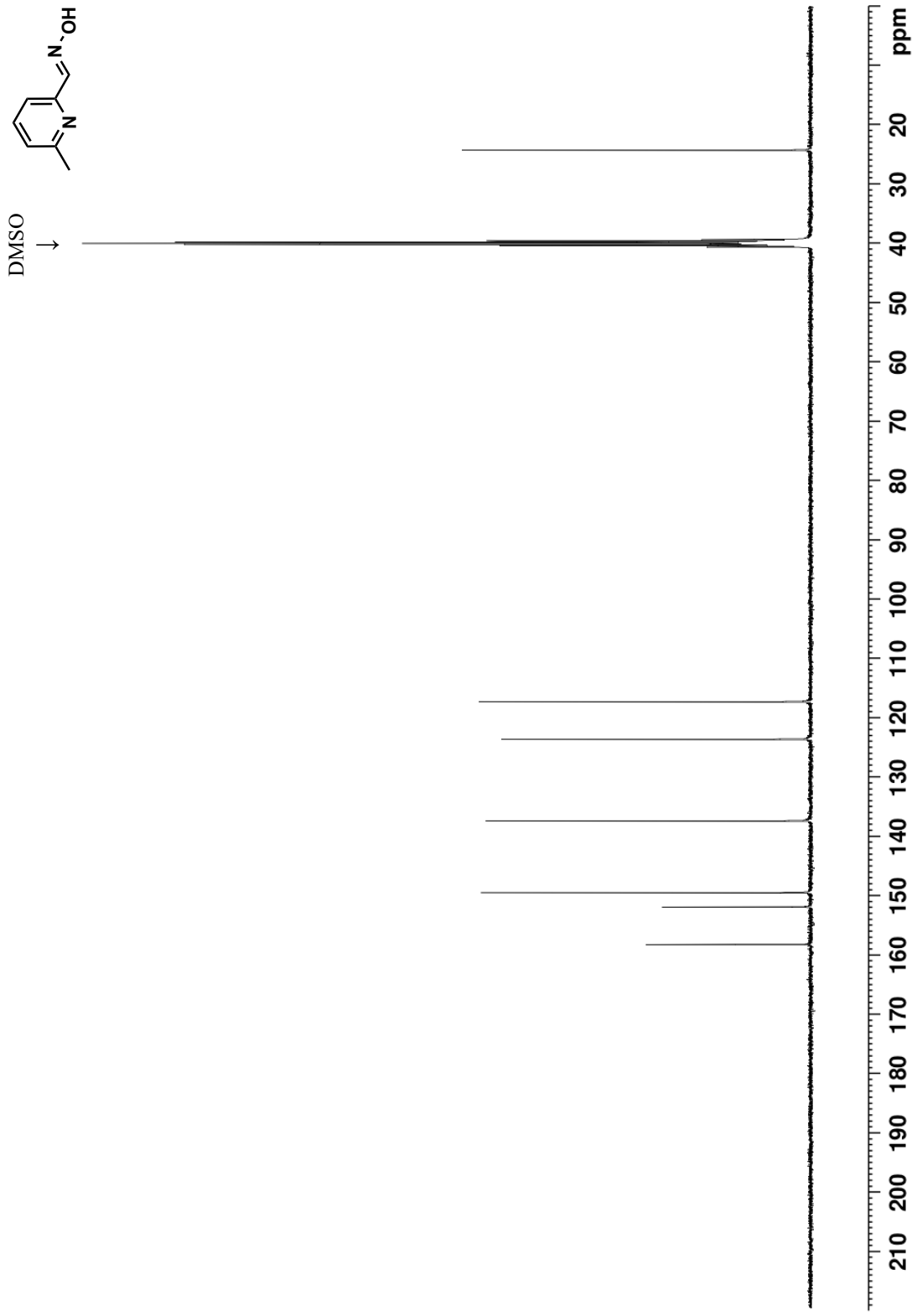

Spectrum 28. ^{13}C NMR spectrum of (E)-6-methylpicolinaldehyde oxime (100 MHz, DMSO-d_6, 293K).

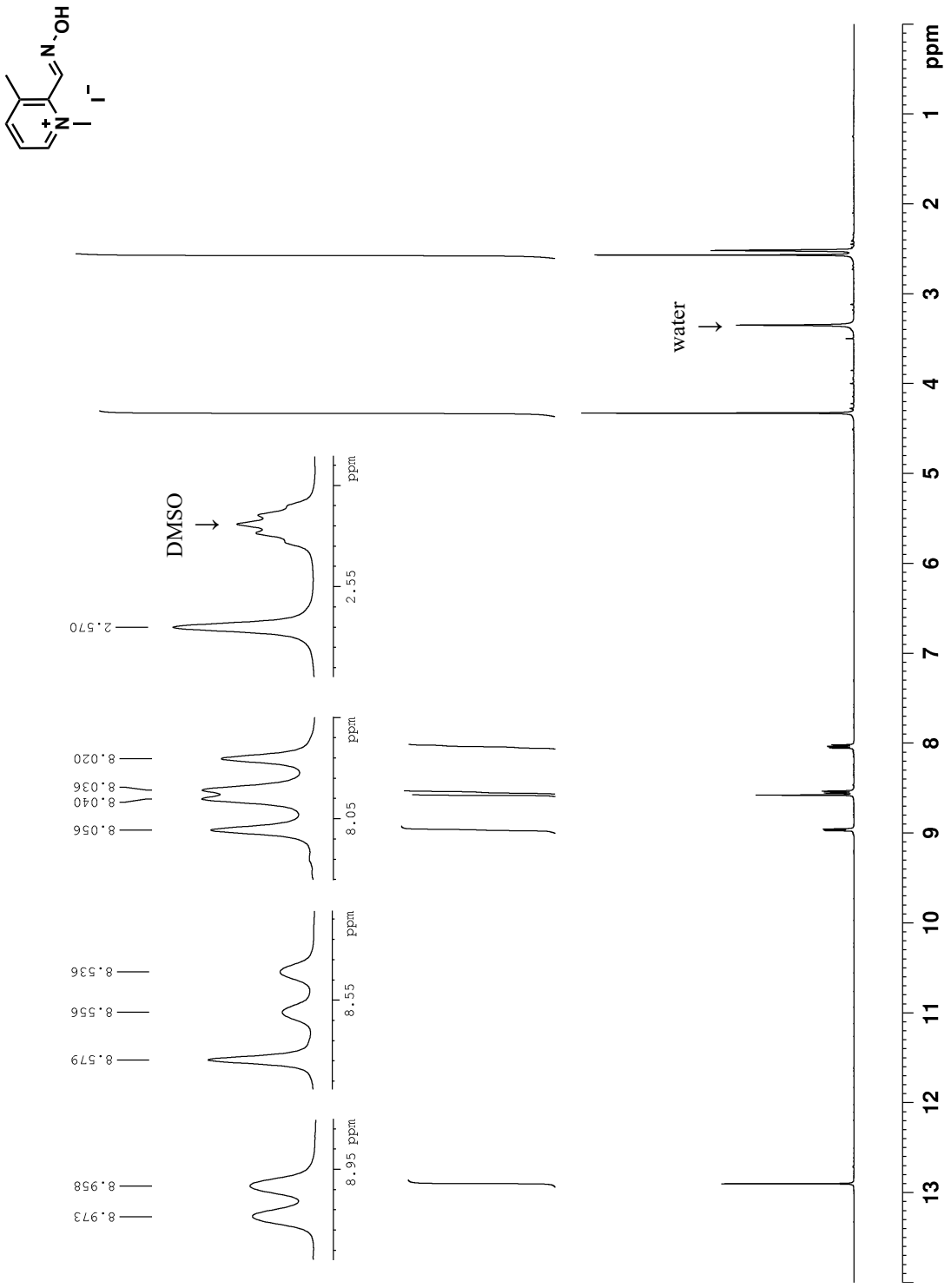

Spectrum 29. [1]H NMR spectrum of (E)-2-((hydroxyimino)methyl)-1,3-dimethylpyridin-1-ium iodide (400 MHz, DMSO-d_6, 293K).

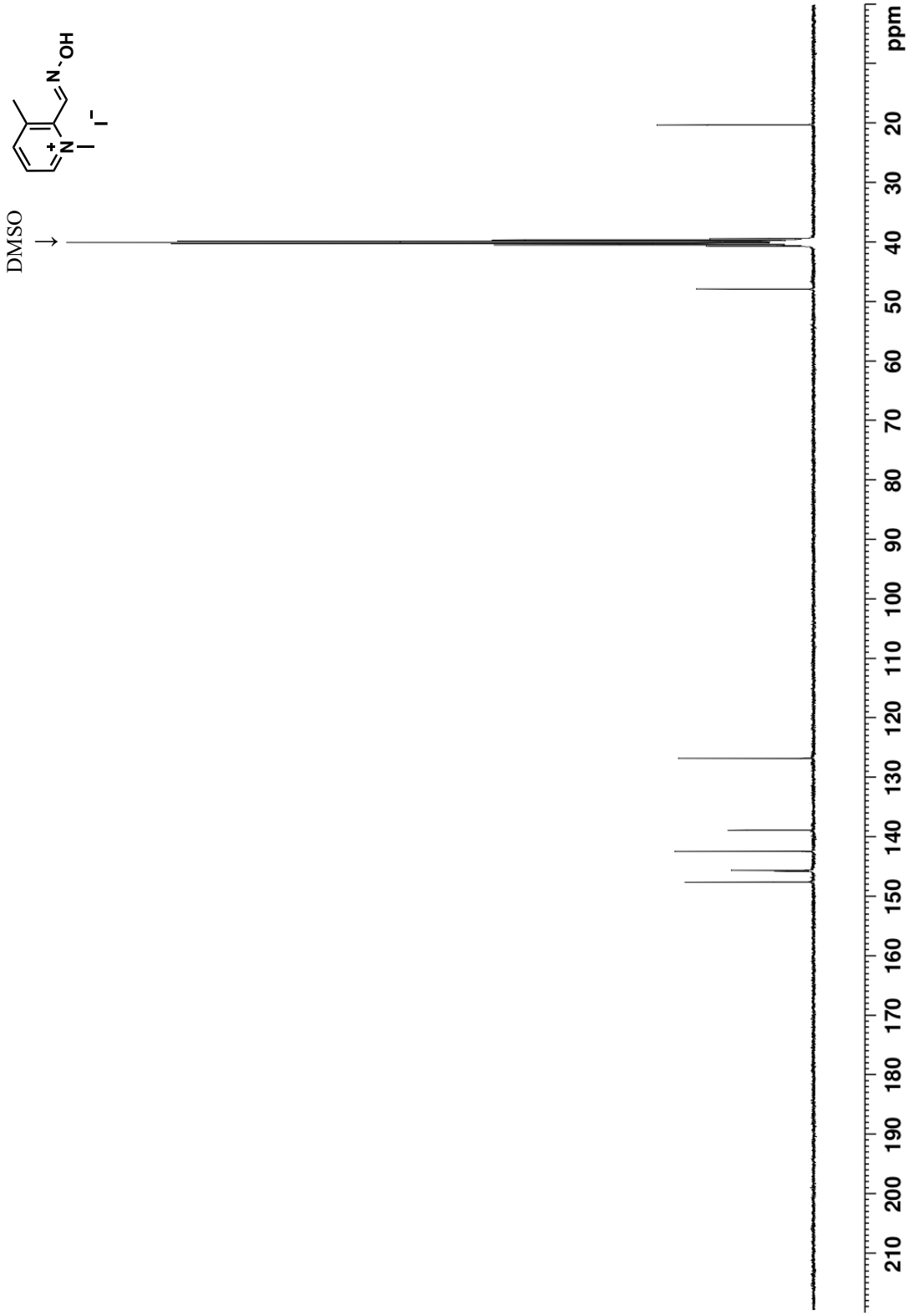

Spectrum 30. ^{13}C NMR spectrum of (E)-2-((hydroxyimino)methyl)-1,3-dimethylpyridin-1-ium iodide (100 MHz, DMSO-d_6, 293K).

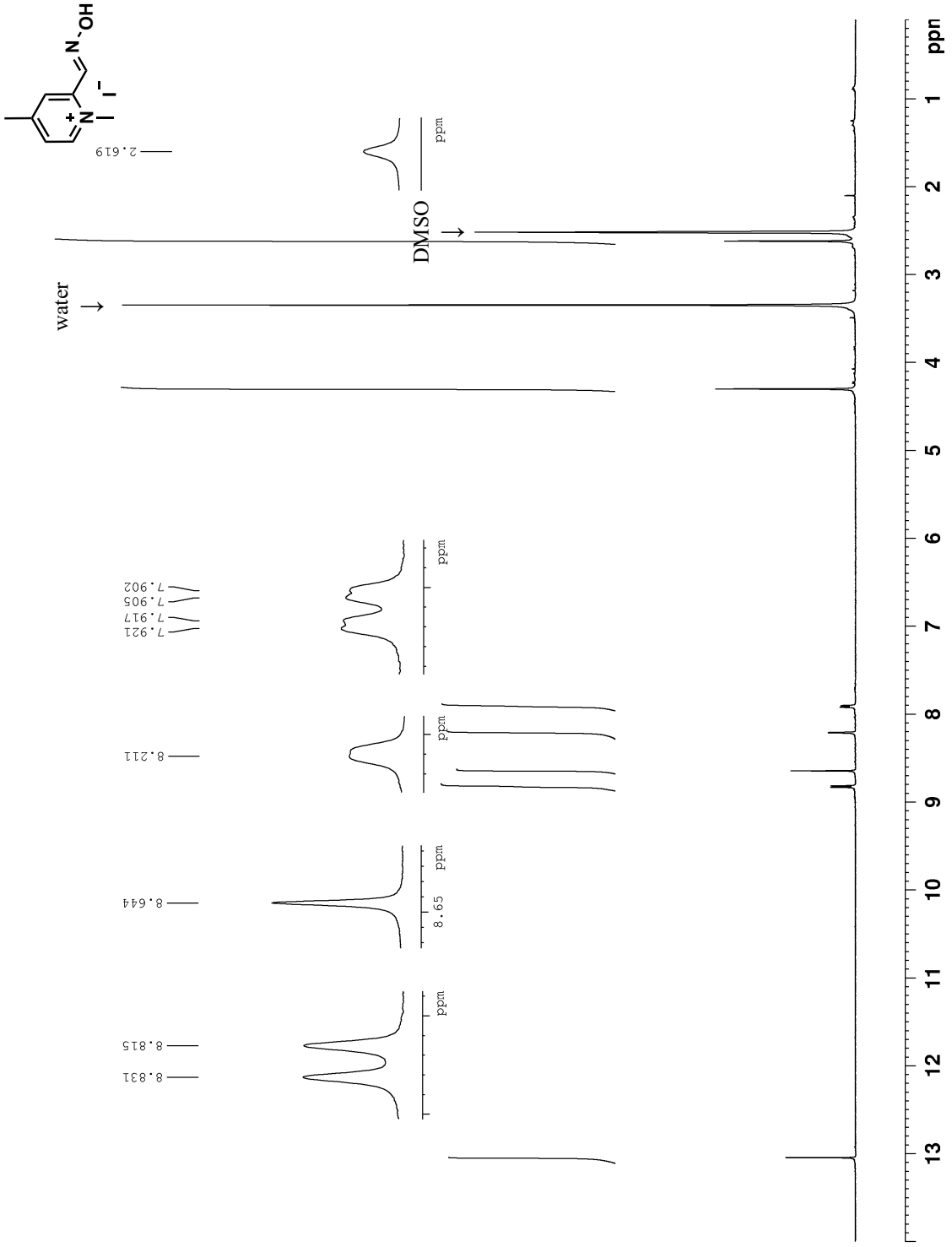

Spectrum 31. ^{1}H NMR spectrum of (E)-2-((hydroxyimino)methyl)-1,4-dimethylpyridin-1-ium iodide (400 MHz, DMSO-d_6, 293K).

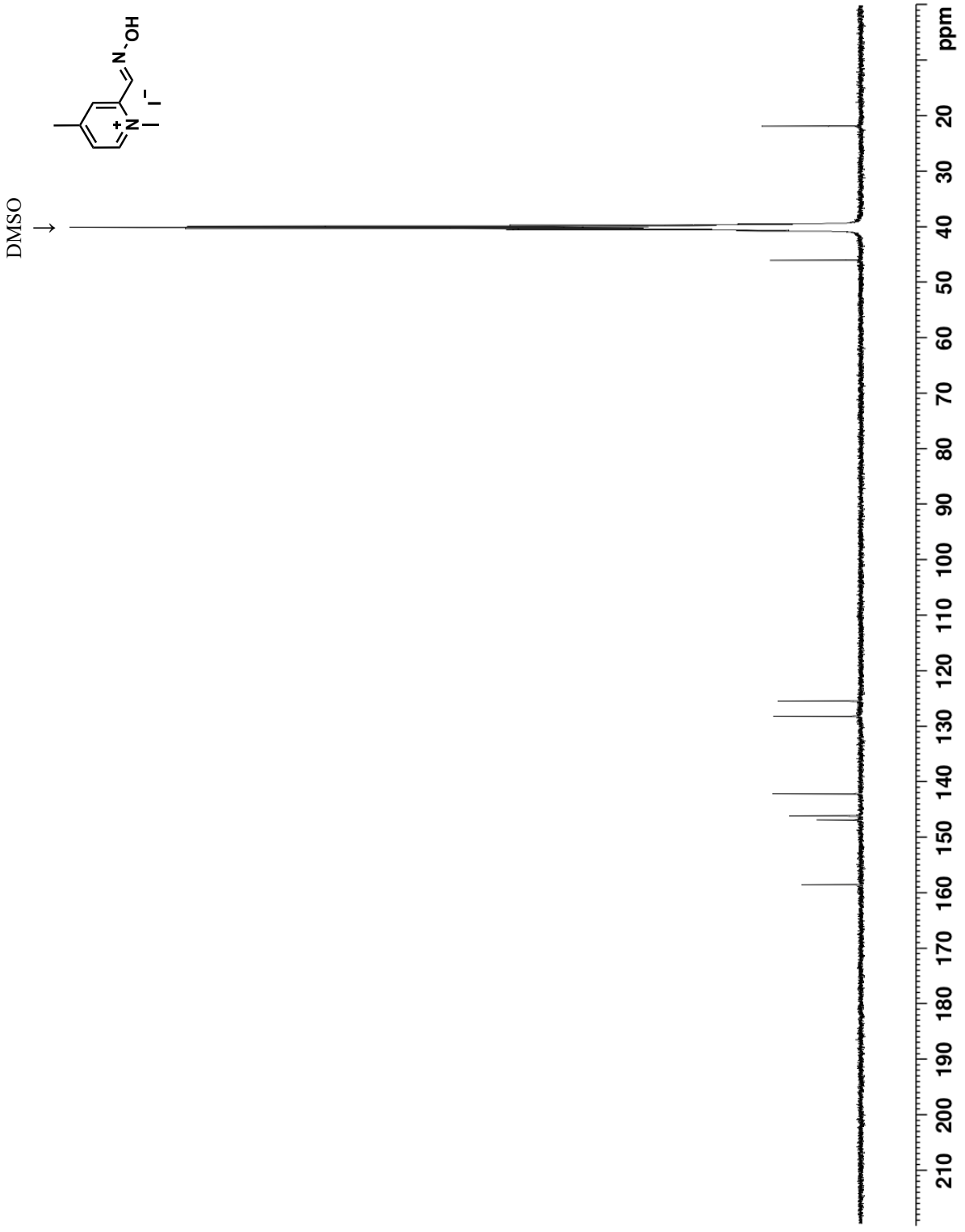

Spectrum 32. ^{13}C NMR spectrum of (E)-2-((hydroxyimino)methyl)-1,4-dimethylpyridin-1-ium iodide (100 MHz, DMSO-d_6, 293K).

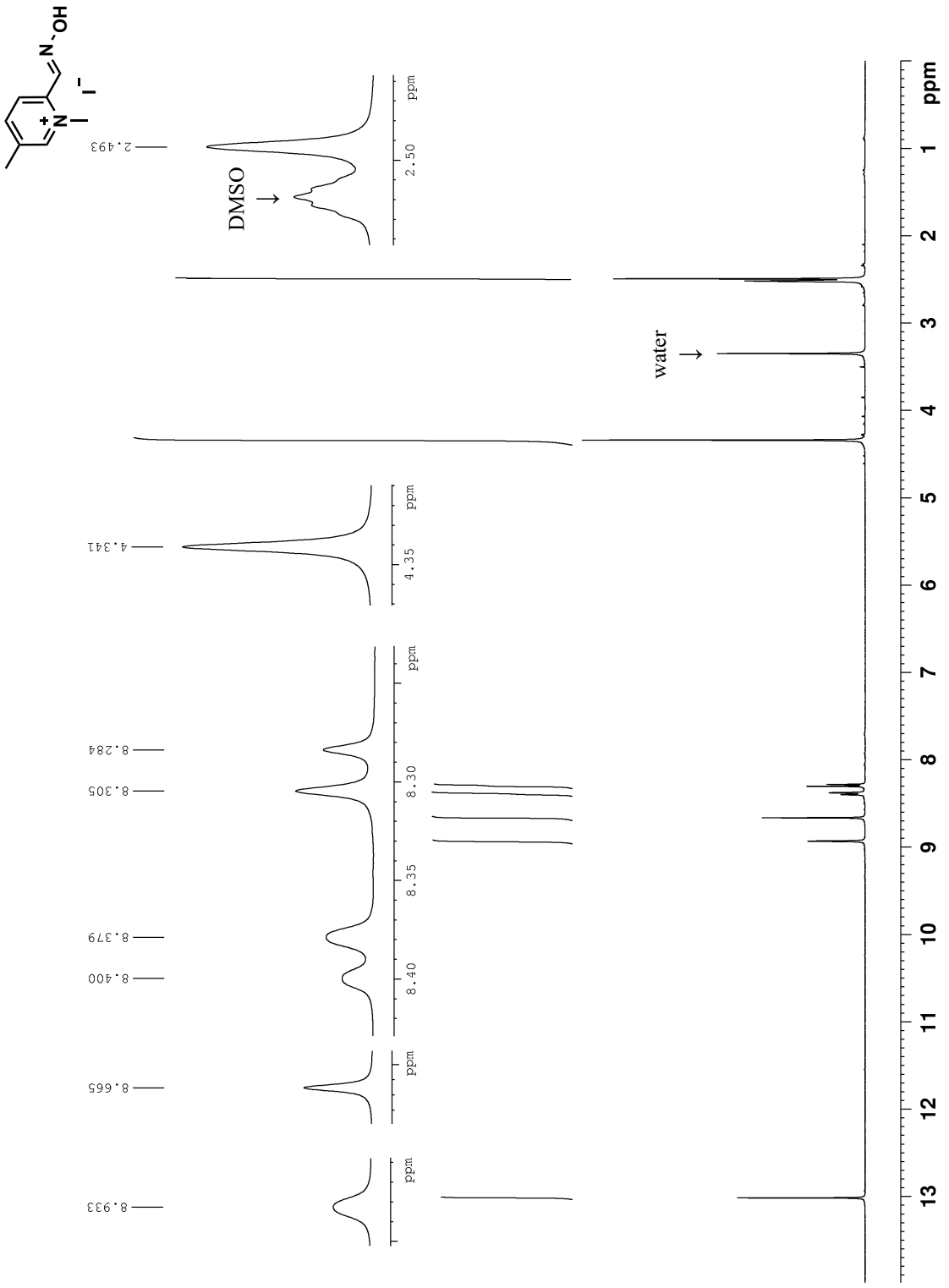

Spectrum 33. [1]H NMR spectrum of (E)-2-((hydroxyimino)methyl)-1,5-dimethylpyridin-1-ium iodide (400 MHz, DMSO-d_6, 293K).

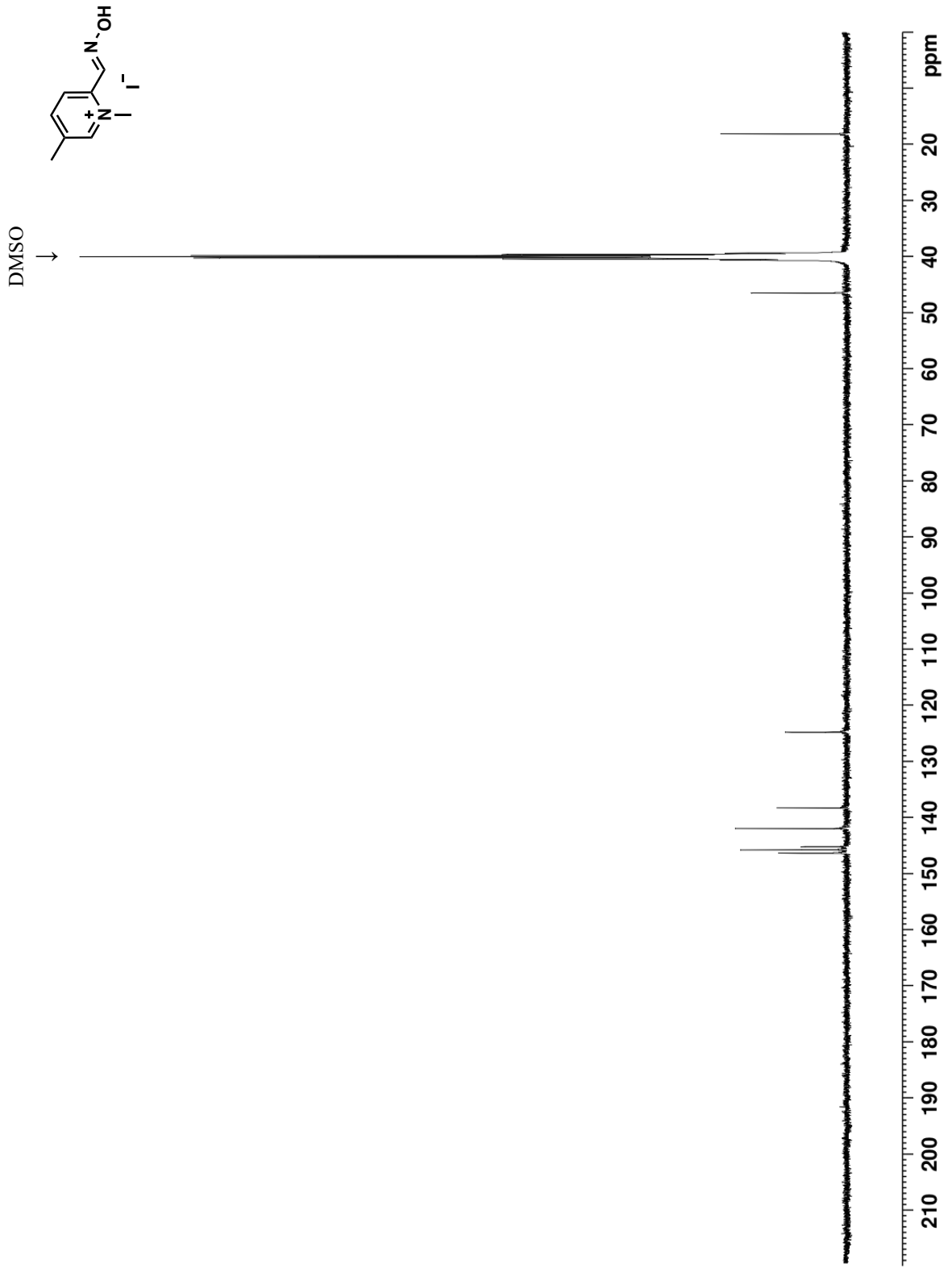

Spectrum 34. ^{13}C NMR spectrum of (E)-2-((hydroxyimino)methyl)-1,5-dimethylpyridin-1-ium iodide (100 MHz, DMSO-d_6, 293K).

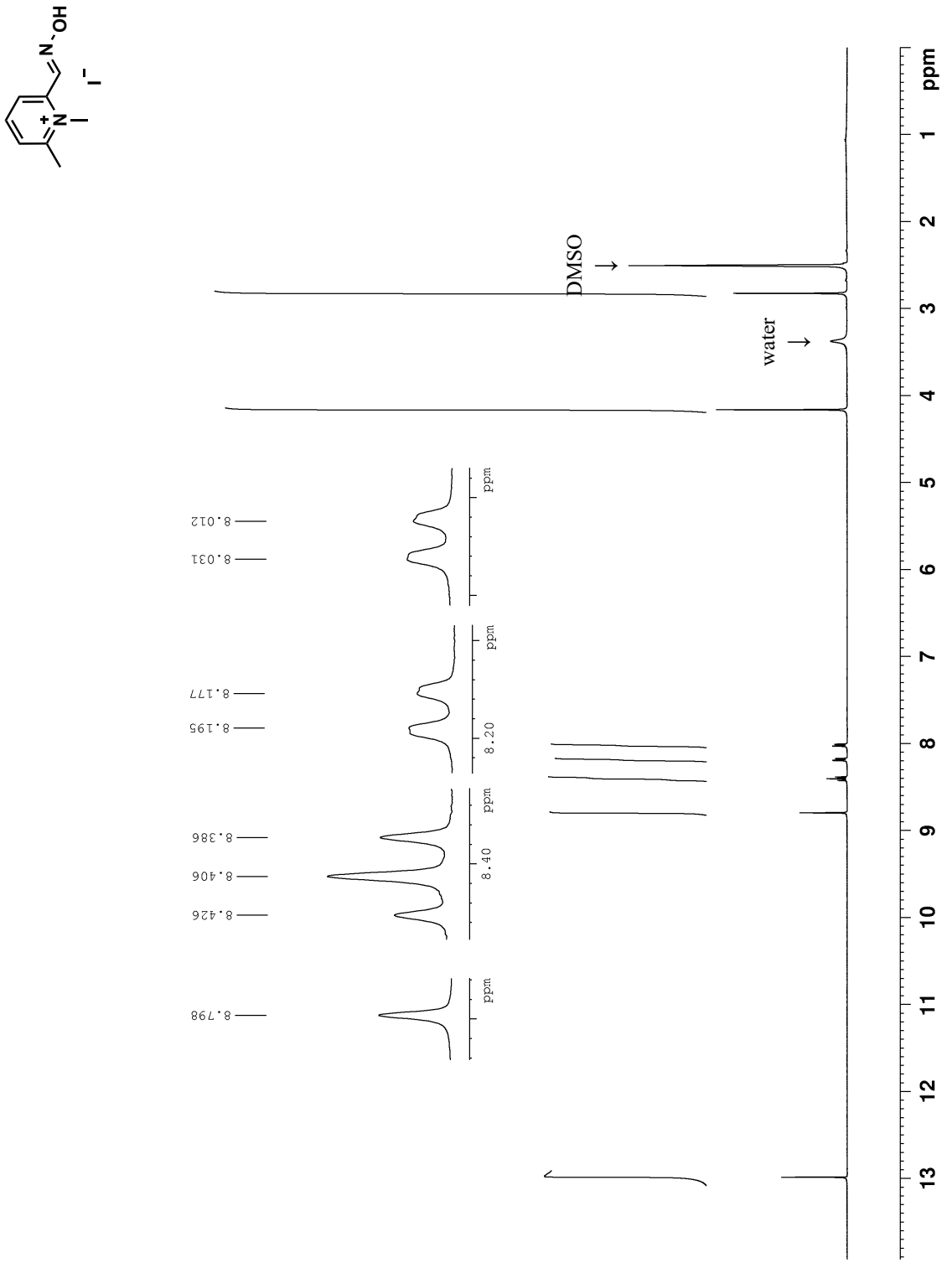

Spectrum 35. ^{1}H NMR spectrum of (E)-2-((hydroxyimino)methyl)-1,6-dimethylpyridin-1-ium iodide (400 MHz, DMSO-d_6, 293K).

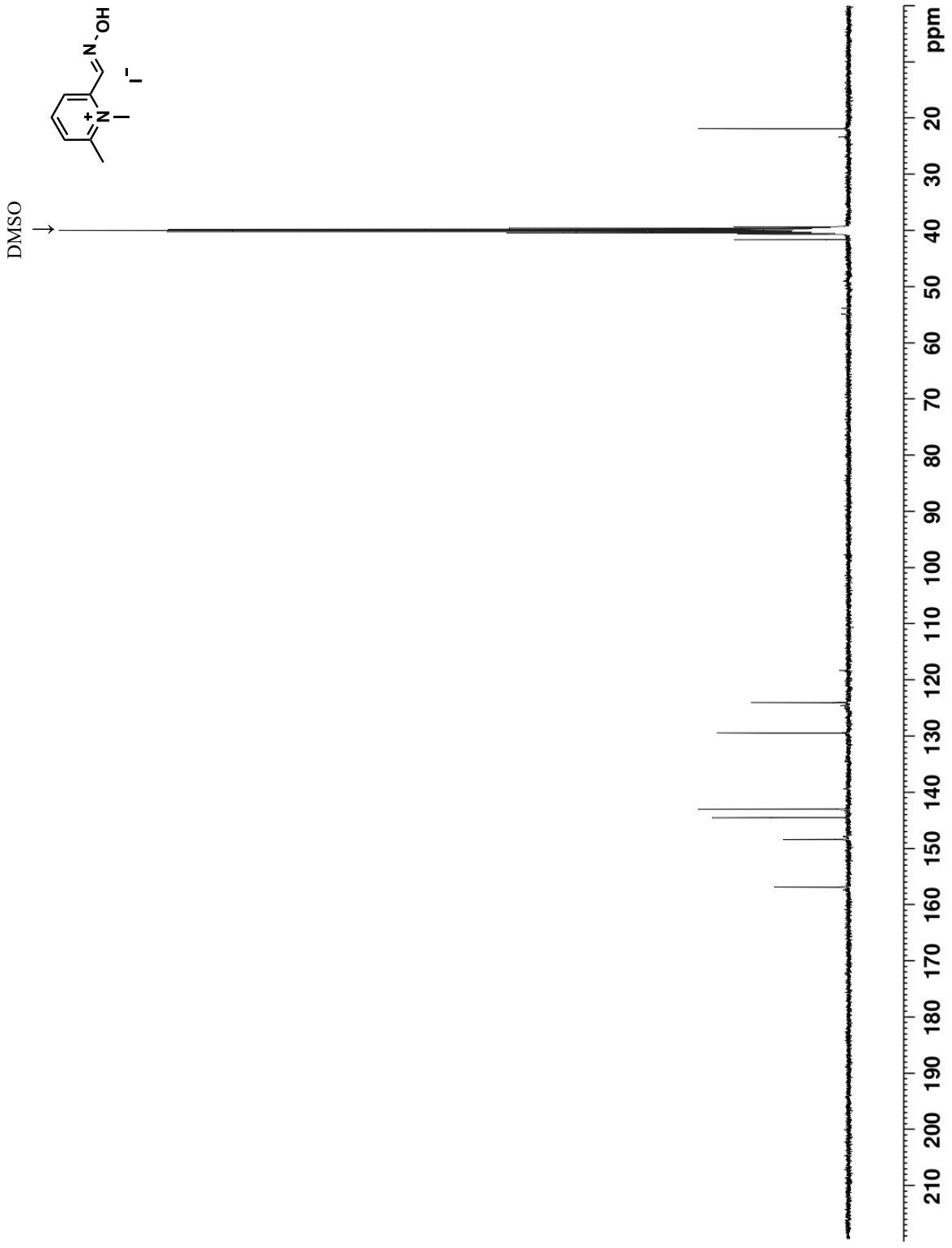

Spectrum 36. ^{13}C NMR spectrum of (E)-2-((hydroxyimino)methyl)-1,6-dimethylpyridin-1-ium iodide (100 MHz, DMSO-d_6, 293K).